Endochondral Ossification – Towards a Clinical Translation

Inauguraldissertation

zur
Erlangung der Würde eines Doktors der Philosophie
vorgelegt der
Philosophisch-Naturwissenschaftlichen Fakultät
der Universität Basel

von

Atanas Todorov

aus Bettingen, Basel-Stadt

Originaldokument gespeichert auf dem Dokumentenserver der Universität Basel **edoc.unibas.ch**

Basel, 2015

Genehmigt von der Philosophisch-Naturwissenschaftlichen Fakultät

auf Antrag von

Prof. Ivan Martin, PhD
Prof. Markus Affolter, PhD
PD Dr. Arnaud Scherberich, PhD

Basel, den 8.12.2015

Prof. Dr. Jörg Schibler
Dekan

Acknowledgement

I thank all my friends and colleagues that supported me throughout the creation of this work and kept me company in the best and worst of times. I thank my parents for their loving care and for regularly cheering me up.

Index

Chapter 1

Introduction

Introduction

The Structure of Bone

Bone is a rigid mineralized organ and forms part of the human skeleton. It provides support and protection for sensitive internal organs and allows limb movement and locomotion. It also plays an important role in the metabolism of minerals such as calcium and phosphate, and harbors the blood-forming bone marrow. Morphologically there are flat bones of the skull, long bones and short bones of the limbs, and irregularly shaped bones of the spine and pelvis. Macroscopically one can separate compact from cancelous or spongy bone. The compact bone forms the outer surface of bones and the diaphysis in long bones. Cancelous or spongy bone is a loose network of trabecular structures, which fills the metaphysis and epiphysis of long bones and enables the transmission and distribution of forces(1) (Figure 1). In between the trabecular structures and inside the central cavity formed by the compact bone resides the bone marrow, a loose tissue comprised of blood sinusoids and haematopoietic cells providing most of the cellular blood components. This arrangement of supportive structures and loose internal tissue allows bones to be very strong and very light at the same time.

In microscopic appearance, the rapidly formed and unorganized woven bone can be distinguished from the highly organized and mature lamellar bone. Osteons, the organizational units of lamellar bone, consist of a central vessel surrounded by concentric circles of osteoid matrix(2). The osteoid matrix consists mainly of collagen and provides flexibility and elasticity(1), whereas highly structured deposits of calciumphosphate called hydroxyapatite(1, 3) impart rigidity and compressive strength. Specialized cells, the osteocytes (Figure 1), are encased in regular intervals in the osteoid matrix(4). Osteoblasts secreting new matrix and osteoclasts resorbing

mineralized matrix can be found attached to the surface of this matrix. These cell types are involved in the homeostasis of mature bone.

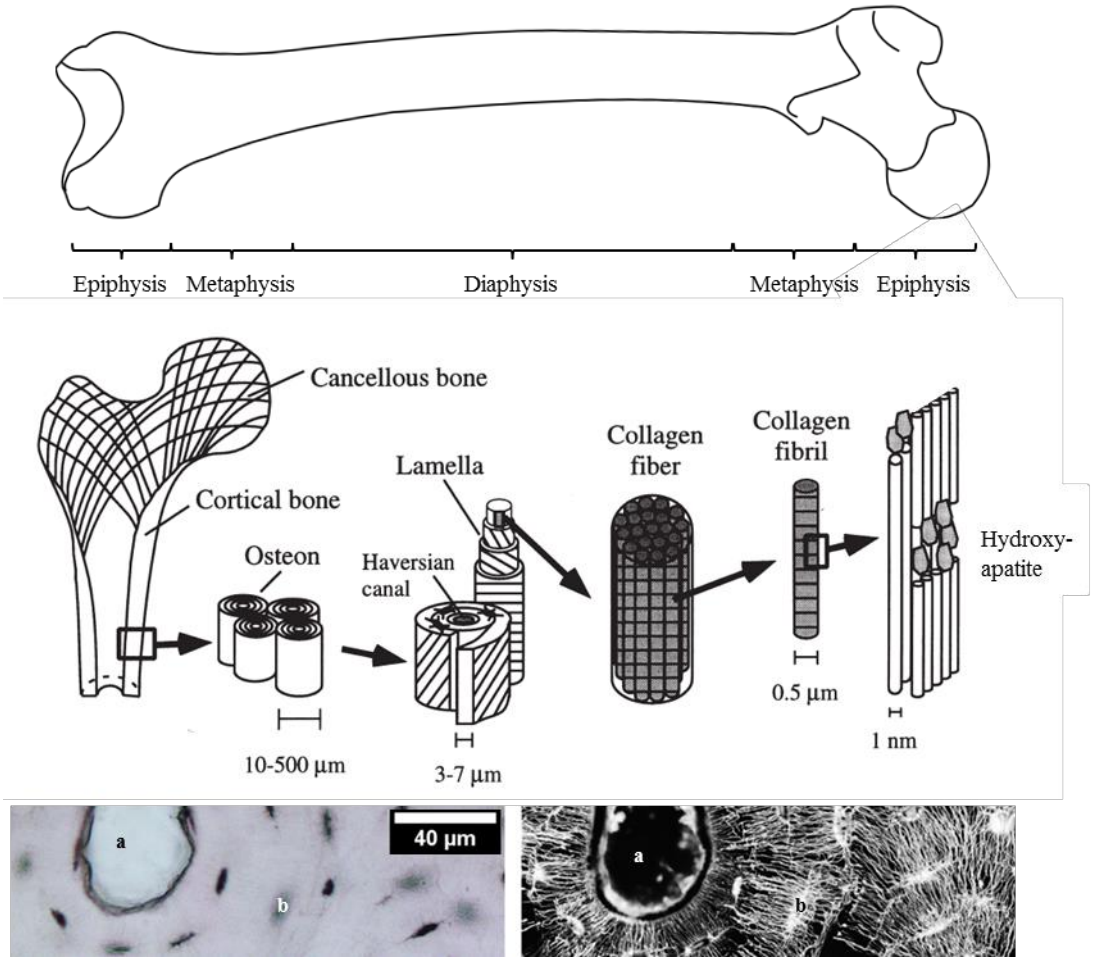

Figure 1: Structure of long bones. Top: General division of long bones. Middle: Microstructure. Bottom: Rhodamine staining of osteon under light microscopy (left) and confocal microscopy (right). Central vessel (a) and embedded osteocytes (b) can be seen. Adapted from Rho et al.(1) and Kerschnitzki et al.(4).

Embryological Development

Bone forming tissues are derived from the mesoderm or a specialized part of the ectoderm named the neuroectoderm(5). The mesenchymal stem cells form bone by two processes called intramembranous and endochondral ossification(6). During intramembranous ossification, mesenchymal stem cells in the connective tissue differentiate into osteoblasts and begin secreting osteoid matrix, which calcifies and becomes lamellar bone. During endochondral ossification (Figure 2) on the other hand,

the cells aggregate and form cartilaginous structures, which are the rudimentary templates for the subsequent bone formation(7), The cartilage then undergoes a maturation process during which the central portion becomes hypertrophic, i.e. the cells expand drastically in volume and modify the matrix around them(7). Mesenchymal stem cells directly adjacent to the hypertrophic matrix form the perichondral bone collar through intramembranous ossification (6, 8). At the same time, vasculature is attracted towards the central portion and begins to invade the hypertrophic cartilage. During this invasion, hypertrophic matrix calcifies and is replaced by woven bone (7, 9). From the center, this process continues towards both proximal and distal ends of the bone rudiment. Near both ends, secondary ossification centers appear and undergo the same process. Where two bones interface, a joint is formed and the bones are capped with hyaline cartilage. This hyaline cartilage appears similar to the rudimentary cartilage template, but evidence suggests that the mesenchymal progenitors and the process of formation are different (10, 11). At birth only a thin layer of cartilage rudiment remains between metaphysis and epiphysis and is responsible for the later bone growth.

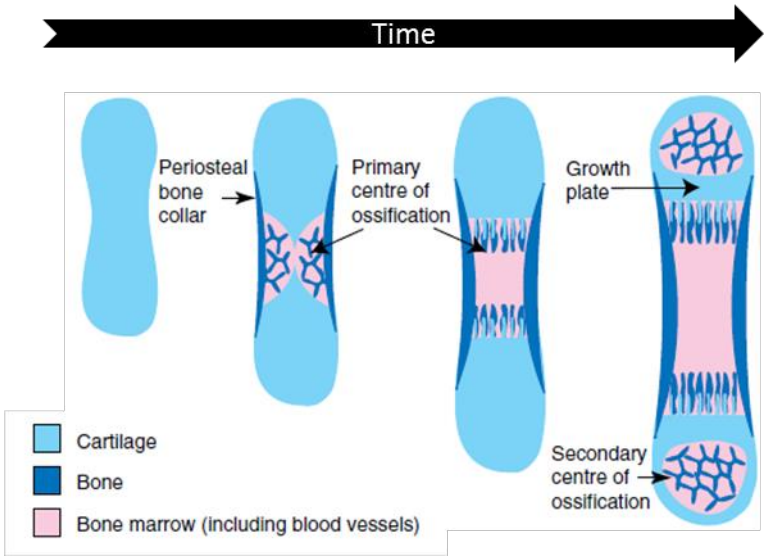

Figure 2: Principle of endochondral ossification. Adapted from Mackie et al.(7)

Growth of Long Bones

The cartilage found in the epiphyseal gap has a defined hierarchical structure (9, 12) (Figure 3). Directly beneath the secondary ossification center of the epiphysis there is a zone of resting cartilage, which resembles the hyaline cartilage found in adult joints and contains few chondrocytes. The next zone contains a higher number of cells and is called the proliferative zone. Next to it is the pre-hypertrophic zone, in which the cells begin to oragnize in distinct columns. In the subsequent hypertrophic zone, cells increase in volume and modify the matrix, effectively elongating bone. In the final zone of remodeling, cells undergo apoptosis and the matrix calcifies, while osteoclasts and vessels invade and remove the calcified matrix from the other side, followed by osteoblasts which deposit osteoid matrix.

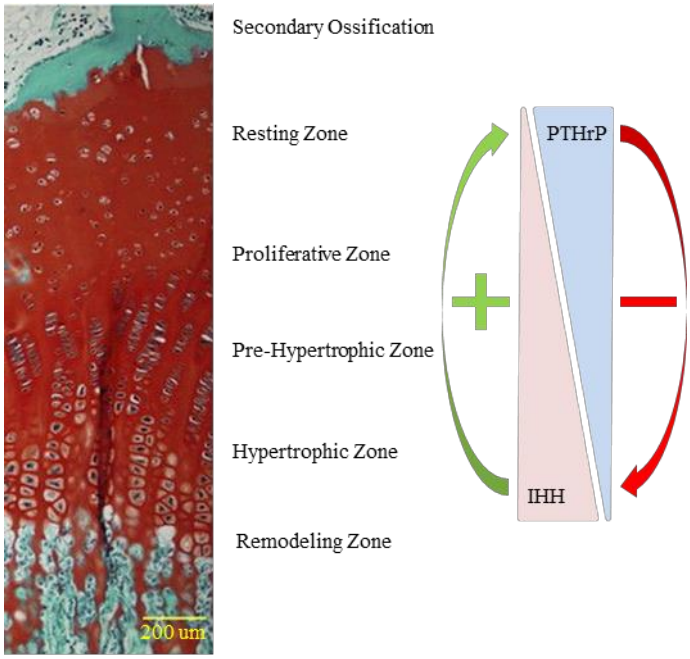

Figure 3: Organization of the growth plate cartilage. Safranin-O staining with fast green counterstaining. Adapted from Kim et al.(13)

It is assumed that the proliferating chondrocytes are similar to stem cells(12) in that one daughter cell continues proliferating while the other differentiates. Proliferation can be guided by both systemic and local signals. For example growth hormone (GH) is

secreted by the hypophysis and stimulates secretion of insulin-like growth factor 1(IGF-1) by liver cells and pre-hypertrophic chondrocytes, which in turn stimulates proliferating chondrocytes(7). Indian hedgehog (IHH) is produced by prehypertrophic chondrocytes and increases proliferation and hypertrophy. On the other hand, parathyroid hormone related peptide (PTHrP) is mainly produced by proliferating chondrocytes and inhibits hypertrophy. IHH can induce expression of PTHrP, whereas PTHrP suppresses IHH expression(14). In this way a negative feedback loop is formed (Figure 3), which minutely controls the maturation of the growth plate(15). Other signals such as Wingless/Int (Wnt) or bone morphogenic proteins (BMP) can promote chondrocyte proliferation, whereas fibroblast growth factor (FGF) can repress it(7). In the latter case achondroplasia, the most frequent disease leading to dwarfism, results from an overactivation of the FGF pathway(16).

The chondrocytes secrete extracellular matrix which consists of aggrecan, glycosaminoglycans and collagen type II. Other proteins are found in lower concentrations and mainly aid the assembly of the matrix and its interconnections(7). Expression of these matrix components is absolutely dependent on Sox9 (sex determining region Y box 9)(6, 7) and can be stimulated by tumor growth factor beta (TGFb) superfamily members (TGFb-1, BMP-2) and FGF.

Once the chondrocytes become hypertrophic through expression of Runt-related transcription factor 2 (Runx2)(9), they increase production of collagen type X, matrix metalloproteinase 13 (MMP-13), alkaline phosphatase (ALP) and IHH(14). Their volume increases up to 10 fold(17), though they do not necessarily degrade the ECM to make space(7). Thyroxin is the most important systemic regulator of hypertrophy(18) and its local effect is most likely transmitted by Wnt signaling(19).

The hypertrophic chondrocytes induce matrix mineralization through secretion of matrix vesicles, which contain akaline phosphatase and are able to nucleate

hydroxyapatite crystals (7, 20). They can actively communicate with the subsequently invading cells, for example by expressing vascular endothelial growth factor (VEGF) to attract endothelial cells(21), receptor aktivator of NF-kB ligand (RANKL) to attract and differentiate osteoclasts(22), and IHH / Wnt to induce osteoblast differentiation of attracted mesenchymal stem cells(6). At the end of hypertrophy, most hypertrophic chondrocytes undergo apoptosis(7) and few transdifferentiate towards osteoblasts and osteocytes(23).

The hypertrophic matrix is degraded by apoptotic hypertrophic chondrocytes and osteoclasts (24, 25) through secretion of MMP-13 and MMP-9 respectively (21, 26). Endothelial cells(7) or macrophages(27) can aid matrix degradation and may increase MMP-9 expression if MMP-13 is absent(28). The degradation of the matrix releases factors which attract additional osteoclasts, endothelial cells and mesenchymal progenitors(29).

When the bone growth finishes during young adulthood, the growth plate closes due to the influence of oestrogens, which deplete the pool of proliferating chondrocytes (7, 30).

Homeostasis of Mature Bone

According to Wolff's law bone tissue adapts to the mechanical stresses it is exposed to(31). This is possible through a constant buildup and degradation of bone by osteoblasts, osteocytes and osteoclasts (Figure 4).

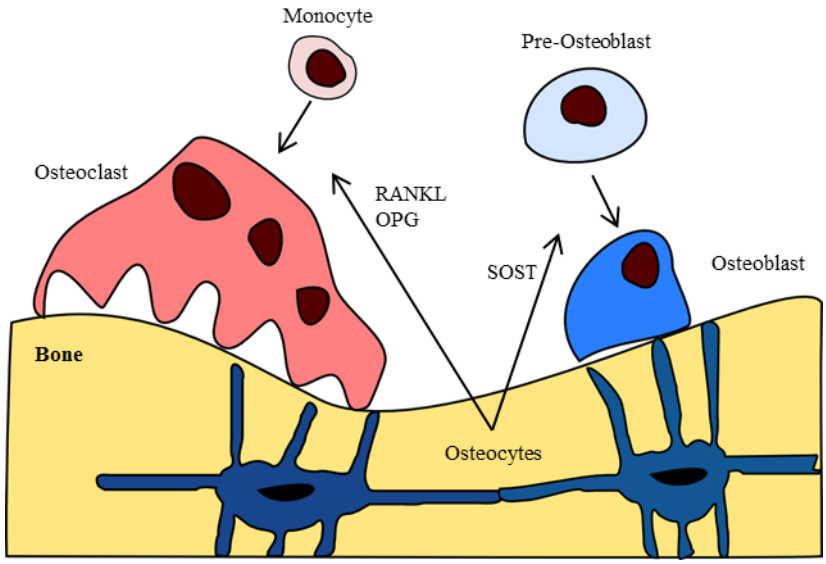

Figure 4: Bone homeostasis. RANKL = receptor activator of NF-kB ligand. OPG = Osteoprotegerin. SOST = sclerostin.

Osteoblasts are derived from mesenchymal stem cells and normally found as a cuboid eptihelium attached to bone(6). They begin differentiating by transiently expressing Sox9, followed by upregulation of Runx2, osterix (OSX) and finally activating transcription factor 4 (ATF4). These stages of development are regulated by Hedgehog, Notch, Wnt, BMP and FGF signaling(6). Sclerostin (SOST) can inhibit osteoblast formation(6). Osteoblasts secrete large amounts of collagen type I as well as a variety of extracellular matrix proteins(32). They also produce matrix vesicles containing alkaline phosphatase(33), which catalyzes the formation of hydroxyapatite and plays a crucial role during calcification (33, 34). The final product of osteoblasts is a regular wall of hydroxyapatite «bricks » surrounded by and connected with fibres of extracellular matrix creating a robust and at the same time flexible material. The osteoblasts may either undergo apoptosis, become bone lining cells or differentiate further into osteocytes(6).

Osteocytes are the main regulators of bone turnover(35). They are found in lacunae inside the osteoid matrix and express a similar range of proteins compared to osteoblasts(35) which may enable them to locally repair the matrix. A more important

regulatory mechanism involves multiple osteocytes, connected to each other and to the extracellular space outside the bone matrix through a manifold of small channels called the canalicular network. Through this network, thin cellular appendages of each osteocyte connect to others by gap junctions and exchange signals about the general well-being of bone. Mechanical stresses are transferred to the single osteocytes through fluid displacements inside the canalicular network (36, 37). The fluid displacements lead to changes in levels of SOST, RANKL, osteoprotegerin (OPG) and other factors(35), resulting in bone deposition or resorption. Apoptosis of osteocytes due to estrogen deprivation, physical inactivity, old age or just loss of contact with other osteocytes can lead to bone loss due to excessive release of RANKL(35).

Bone is resorbed by osteoclasts, giant multinucleated cells which share a common progenitor with macrophages, dendritic cells and giant foreign body cells (38, 39). When the right signals such as macrophage colony stimulating factor (M-CSF) and RANKL are present(40), mononcytes coming from the bone marrow, periost or peripheral blood migrate towards the chemoattractive gradient and fuse together. The new multinucleated cell attaches firmly to the bone surface and seals off a small space. In this space it will pump H+ ions and enzymes such as tartrate resistant acid phosphatase(TRAP) or cathepsin K, which are capable of dissolving hydroxyapatite and also the underlying collagenous extracellular matrix (41, 42). MMPs have a very minor role in this bone resorption(43). The products of the resorption are released by the osteoclast into the extracellular fluid and may directly couple resorption to the bone formation of osteoblasts(44). For example TGFb-1, which is stored in a latent form in the bone matrix, is released and activated through the osteoclasts to attract osteoblasts (45, 46). Osteoclasts themselves also produce factors such as BMP-6, Wnt-10b, sphingosine-1-phosphate (S1P)(44) and collagen triple helix repeat containing protein 1 (CTHRC1)(47) which stimulate bone matrix deposition by osteoblasts. Osteoblasts and

osteocytes can inhibit osteoclast resorption through release of OPG, a decoy receptor for RANKL(48).

Fracture Healing

Bone is the only tissue of the human body which can completely heal without any scar formation. However, this is only possible if conditions are just right. Two distinct processes of fracture healing can occur. If there is a clean break, the two fragments are not separated by more than 0.01mm and no movement occurs, new osteons will form at both ends and continue the process of homeostasis detailed above(49). The fracture will thus be bridged by many new osteoid laminae.

If the fracture is complex, separated by a large gap or subjected to much movement, a process similar to endochondral ossification begins (49, 50). In the first stage, the fracture gap is filled by blood from the ruptured vessels and bone marrow cavity. The blood coagulates and stabilizes the fracture site. The blood clot is rapidly invaded by a wave of neutrophils(51) followed by macrophages and mesenchymal stem cells. The latter begin differentiating to chondrocytes and form a type of disorganized fibrocartilage which represents the soft fracture callus (Figure 5). This tissue has better mechanical properties than the blood clot and is able to stabilize the fracture(52). Intriguingly, instead of disorganized tissue, a peculiar type of growth plate may sometimes form and help to realign the fracture fragments(53). The fibrocartilage becomes hypertrophic and undergoes endochondral ossification as detailed above. The tissue calcifies, is invaded by vessels and replaced by osteoid matrix. In particular, the outside shell is replaced by cortical bone, whereas the interior of the callus is replaced with bone marrow and trabecular structures (Figure 5). After the callus has ossified, the process of bone homeostasis will reshape it according to the mechanical loads and stresses, until an approximately ideal shape is reached. The final shape depends on the

previous alignment of the fracture fragments and on the age of the person and may take several years to be fully reached(49).

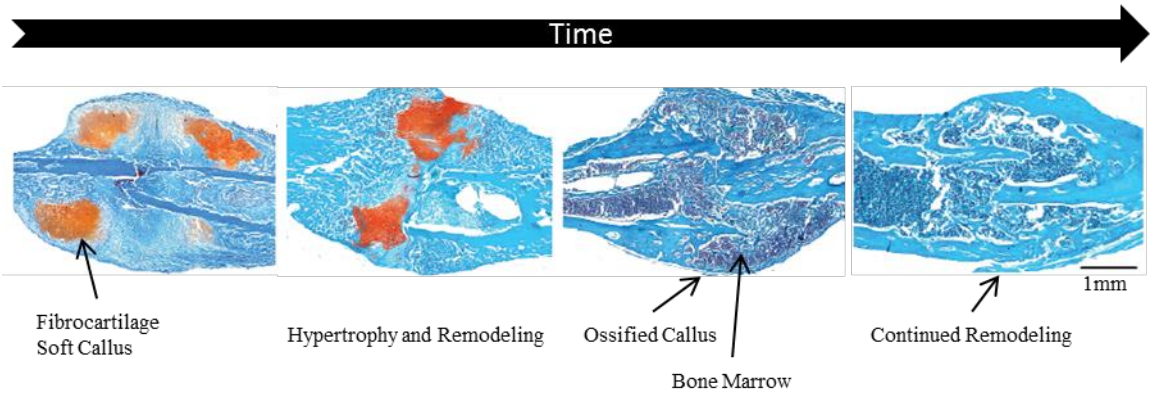

Figure 5: Fracture healing through endochondral ossification, safranin-O and fast green staining. Modified from Ai-Aql et al.(54)

Enhancing Bone Regeneration

Clinical Procedures in Fracture Repair

In realistical clinical situations, bone regeneration is often not possible without additional outside help. Fractures, bone loss or osteotomies after tumor removal can often be treated through stabilization and supportive management. Surgeons first need to adapt the fragments to replicate the correct alignment. They can then stabilize the fracture either by a cast or by applying internal or external fixation. Internal fixation can be performed by inserting a nail in the intramedullar cavity or bridging the defect by a combination of screws and plates. External fixation involves placing screws through the skin and connecting them with plates outside the body(55-57). However, not every defect in every patient can be anatomically adapted using only these tools.

If a large bone volume is missing, other techniques of bone generation have to be applied. Distraction osteogenesis is one possibility, where fragments are brought together to heal and subsequently distracted slowly with an internal or external device. This approach is very time- and cost-intensive and leads to problems such as secondary

fractures, neurovascular difficulties and psychological stigma(58). Another possibility is the Masquelet technique, for which a cement spacer is inserted into the stabilized bone defect and left until an « induced membrane » with additional vasculature has formed. In a second procedure, the cement is replaced by autologous bone chips(59). This technique requires two surgeries and autologous bone extraction and is often accompanied by infection of the fracture.

If the conditions of fracture healing are not optimal, a non-union can develop. The bone fragments thus never join, either because of insufficient stabilization, insufficient vascularization, inflammatory or infectious processes or metabolic problems(60).

If the patient has an underlying pathology such as osteoporosis, the fracture fixation can already become problematic and require the augmentation of bone volume(61).

Large missing bone volumes, non-unions and treatment of osteoporotic fractures are thus challenging clinical scenarios, for which a suitable bone graft is necessary.

Transplantation of Bones

The currently most suitable bone graft for the above mentioned challenges is autologous bone. It can be used as a bone filling material or prepared together with its blood supply and transplanted. Bone tissue for a fracture augmentation is most commonly taken from the illiac crest, where part of the bone is cut out, crushed and implanted in the fracture site(62). Large segmental defects can be treated with a vascularized bone piece, for example by extracting part of the fibula together with its blood supply and re-attaching it at the fracture site(63). With both approaches, difficulties arise due to limited availability, donor site morbidity and costs. Although transplantation of allogeneic bone from cadavers is possible, it is rarely used due to the difficulty of screening for infections in bone tissue and the necessity to suppress a possible immune response(64, 65).

Bone Substitutes

The drawbacks of bone transplantation have led to the development of a variatey of off-the-shelf bone substitute materials. Three major types of materials are categorized according to their mode of action(66). Osteoconductive materials provide a scaffold on which host derived osteoblasts from the adjacent fracture fragments can migrate and form new bone through stimulation with local factors. Commonly available materials include ceramics such as various forms of calcium phosphate, bioglasses or highly processed allogeneic or xenogeneic bone matrix(66, 67). Osteoinductive grafts provide additional factors, such as the clinically available BMP-2 and BMP-7, which further stimulate bone formation when applied in supraphysiological doses. A stringent requirement for osteoinductive grafts is that they can produce bone upon implantation in an ectopic site without any fracture nearby(66, 68). Finally osteogenic grafts contain both factors and osteoblasts which are directly able to generate bone. Apart from the transplantation of actual bone fragments as detailed above, off-the-shelf osteogenic grafts are an active area of development and still far from regular clinical application.

Although for osteoconductive and osteoinductive grafts there exist commercially available materials(68) (Table 1), they all suffer from significant drawbacks. Osteoconductive materials in general require an othewise healthy environment, since they depend completely on the host signals and cells. They are also limited in size and may form non-unions. Currently available osteoinductive materials either raise concerns because of the supraphysiological use of signaling molecules such as BMP or are generally difficult to produce and standardize, as in the case of demineralized bone matrix(66).

Product Name	Composition	Company	Approved by
Accell TBM(R)	DBM	Integra LifeSciences Holdings Corporation	US FDA
AlloFuse(TM)	Heat sensitive copolymer with DBM in injectable gel and putty form	AlloSource	US FDA
Allomatrix	DBM and cancellous bone chips with calcium sulfate carrier	Wright Medical	US FDA and EU
Collagraft	5% hydroxyapatite, 35% tricalcium phosphate and bovine collagen	Neucoll	US FDA and EU
DBX	DBM in sodium hyaluronate carrier	MTF	US FDA
EquivaBone(R)	DBM and nanocrystalline calcium phosphate	ETEX Corporation	US FDA
Grafton	DBM fibers with glycerol carrier	Osteotech	US FDA and EU
InductOs(R)	BMP-2 in bovine collagen sponge carrier	Wyeth Pharmaceuticals	US FDA and EU
INFUSE(R) Bone Graft	BMP-2 in absorbable collagen sponge	Medtronic	US FDA
InterGro(R) DBM	Demineralized allograft bone in lipid carrier	Interpore Cross International	US FDA
NuBone(TM)	DBM combined with cortical bone gelatin carrier	Globus Medical, Inc.	US FDA
OP-1(TM)	BMP-7 and a collagen carrier	Stryker	US FDA and EU
Opteform(R)	DBM and cortical cancellous chips suspended in gelatin carrier	Exatech	US FDA
Optium DBM(R)	DBM combined with glycerol carrier and gel/putty	Life Net Health	US FDA
OrthoBlast(R) II	DBM	lsoTis OrthoBiologics, Inc.	US FDA and EU
Osteofil(R)	DBM particulate with porcine collagen carrier	Regeneration Technology	US FDA
Pro-Stim Injectable Inductive Graft	Calcium sulfate and calcium phosphate materials with DBM	Wright Medical Group	US FDA
Tutoplast (R)	Allograft bone	Tutogen Medicals	US FDA
Viagraf	DBM combined with glycerol carrier and gel/putty	Smith & Nephew	US FDA
Vitoss(R)	100% b-TCP, 80% b-TCP/20% collagen, 70% b-TCP/ 20% collagen/ bioactive glass	Orthovita	US FDA

Table 1: Commercially available osteoinductive bone substitutes. One product per company is listed. DBM = Demineralized Bone Matrix. BMP = Bone Morphogenic Protein. US FDA = United States Food and Drug Administration. EU = European Union. Adapted from Miron et al.(68) and Liu et al.(67)

Tissue Engineering of Bone

The development of bone substitutes in general and osteogenic grafts in particular is a form of tissue engineering. Classically, this includes the selection of appropriate bone

forming cells, a supportive scaffold, appropriate culture conditions, some form of quality control and the testing of grafts in an animal model.

Cell Source

Osteoblasts, osteocytes and osteoclasts involved in normal bone formation and homeostasis are terminally differentiated cells which are very difficult to cultivate in vitro and are therefore not used directly. Instead, progenitors or even stem cell are used because of their better availability, easier cultivation and plasticity.

For differentiation of osteoblasts and osteocytes, the discovery of the adult mesenchymal stromal cell (MSC) in bone marrow has been a major mile stone(69, 70). Although currently induced pluripotent stem cells(71) and embryonic stem cells(72) are also being used for bone generation, adult MSC offer many advantages. They can be applied autologously, are relatively easy to isolate and expand(73) and have found approval for clinical trials(74). A minimal set of criteria for the identification of MSC has been proposed(75):

1. Adherence to plastic when maintained in standard culture conditions.
2. Expression of CD105, CD73 and CD90; no expression of CD45, CD34, CD14 or CD11b, CD79α or CD19 and HLA-DR on the surface
3. Differentiation to osteoblasts, adipocytes and chondroblasts *in vitro*.

Sources such as muscle, fat or synovium have also been proposed for adult MSC, with subtle differences in differentiation kinetics(76, 77). In some cases genetic modification of these cells has been performed to add production of osteoinductive factors such as BMPs(78).

CD14-positive monocytes from peripheral human blood are precursors for both osteoclasts and macrophages(38, 39). They can be easily collected, purified and

immediately stimulated with RANKL and M-CSF(40) to yield multinucleated osteoclasts, which are fully functional(79, 80).

An intriguing source of several cell populations is the stromal vascular fraction(SVF) of adult human fat tissue(81) (Figure 6). The contained MSC, monocytes and endothelial cells could have the potential to differentiate into osteoblasts, osteoclasts and capillaries in a suitable environment.

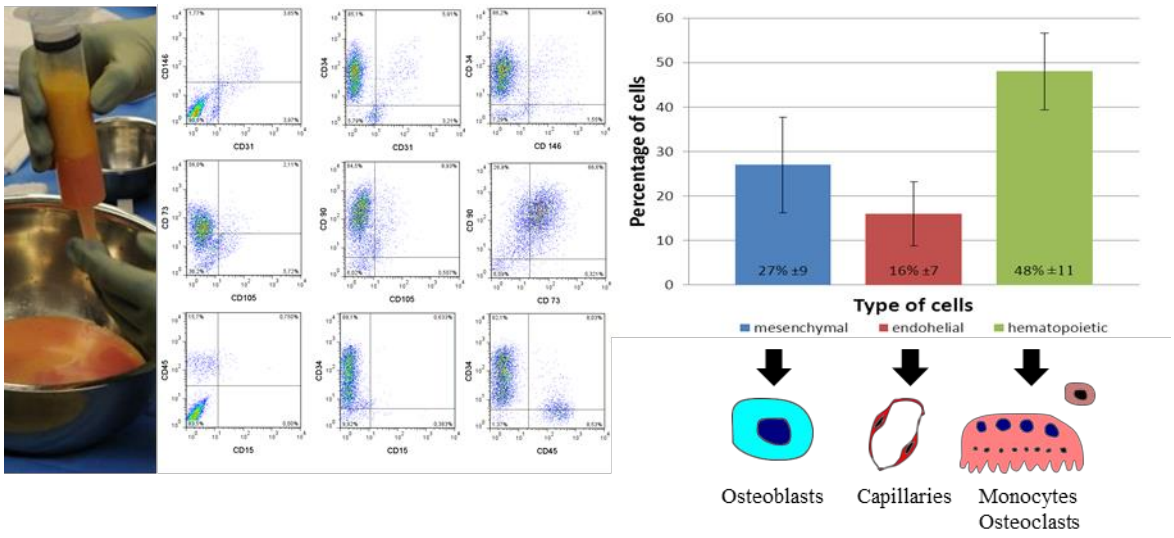

Figure 6: SVF cells as a viable source of MSC, endothelial cells and monocytes, which can become osteoblasts, capillaries and osteoclasts respectively.

Scaffold Material

Most commonly, MSC are seeded and differentiated on suitable biomaterials mimicking in their composition, porosity and biomechanics the physiological bone(82). This biomimicry has been achieved trough the use of ceramics, polymers of natural (e.g. collagen) or synthetic origin, bioglasses or composites (67, 82). The biomaterials should support the adhesion, proliferation and differentiation of cells(67, 73). As a consequence of their use as implantable devices they should also be biocompatible and biodegradable(67), ensuring that no overwhelming inflammation or toxicity arises and complete bone regeneration occurs. Addition of metal ions as a means of improving both

biomechanics and osteoinductive properties of the scaffolds has been investigated(67). For better invasion of host vasculature after implantation, pore sizes of 150-500um and interconnected geometries have been proposed(67). However, the role of pore size in osteogenicity is not well understood and manufacturing of standardized architectures can be challenging(83). In hydrogel systems the addition of peptides and signaling molecules has been used to improve osteoinductivity (84, 85). Most commonly, calcium phosphate in one or several crystalline structures such as hydroxyapatite, bicalcium phosphate or tricalcium phosphate is used(86).

Culture Conditions

To use a cell-seeded biomaterial as an actual osteogenic graft, in vitro culture allowing the differentiation of cells and tissue formation may be necessary. However, a valid consideration for clinical application is the regulatory complexity when dealing with extensive pre-differentiation as opposed to a direct use of cells(87). Therefore, a variety of culture protocols have been used, ranging from intraoperative seeding and implantation to extensive in vitro culture in a dedicated bioreactor system.

Intraoperative application of cells either in isolation (88, 89) or mixed with scaffold materials and osteoinductive peptides(90) have been investigated. Additionally, the approach of ectopic implantation as an in vivo « bioreactor » has been developed, in which the graft would develop both bone and vasculature before final orthotopic transfer (91-94). As a drawback, these strategies depend on vascularization by the host and are not well controlled in terms of homogenous bone formation.

In vitro culture allows the targeted modification of the graft to manufacture homogenous and functional tissue. It is important to control basic parameters such as oxygen supply (95-98), culture medium pH(99) and waste removal. As described above, stimulation with several signaling molecules may be necessary to differentiate MSC into osteoblasts, for example by exposure to Wnt, Hedgehog, Nell1, BMP or IGF(100).

Mechanical stimulation of the osteogenic pathway using fluid shear stress could be benefitial(101). In addition, culture of 3D volumes as opposed to flat sheets of cells increases the complexity and poses the problem of mass transfer.

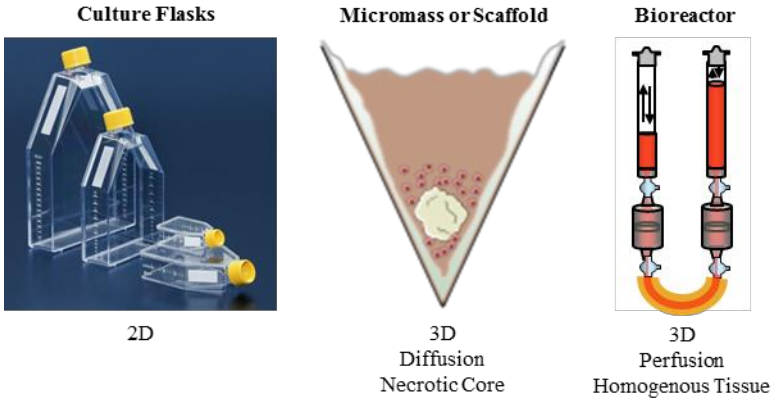

Figure 7: Possibilities of in vitro culture.

3D cultures with controlled parameters may be best achieved with the use of dedicated bioreactors (83, 102) (Figure 7). They can guarantee homogenous cell distribution during seeding and a homogenous supply of nutrients, oxygen and signaling molecules as well as application of shear stresses (83, 102). Improved in vivo bone formation after seeding and pre-culture using these systems has been reported(102-106).

Quality Control

For clinical applications, quality control will be necesssary during graft production (83, 102). Invasive monitoring is desctructive and tissue biopsies may not be representative, whereas tissue replicates may be misleading because of residual variability. The non-invasive monitoring of actual tissue formation could address these issues, yet it is still very challenging both in standard cultures and in bioreactors. Monitoring of glycosaminoglycan or collagen content in supernatants using high resolution nuclear magnetic resonance (NMR) as well as monitoring of the differentiation status of MSC using high resolution imaging have been proposed(107) but are expensive and

technically demanding. In addition, the relevance of these parameters has to be proven for specific culture systems and tissue types.

Animal Models

Models of ectopic bone formation are an important testing ground for bone substitute materials(68). Implantations have been performed in skeletal muscle, kidney capsule and also subcutaneously(87). Both skeletal muscle and the kidney capsule offer immediate blood supply and the presence host MSC, making them less suitable as models of clinical bone regeneration(87). Subcutaneous implantations represent a much more challenging environment and are used most frequently.

To go forward in clinical translation it is necessary to develop various orthotopic models in large animals(102, 108, 109). These models may include calvarial or iliacal round defects without any load bearing as well as segmental defects of the long bones with varying degrees of load. As an option before going into expensive large animal trials with sheep, goats or pigs(110-112), rabbit models can be used as a cost-effective alternative(109) with a clinically relevant size(113). The use of species-specific cells may be required since the animals are immunocompetent and immunosuppression may interfere significantly with inflammatory pathways important for fracture healing.

Developmental Engineering

All of the above presented strategies for the creation of osteogenic grafts rely on the close resemblance of materials and cells to normal bone. MSC differentiation directly into osteoblasts has been described as a corner stone of osteoinductivity and osteogenicity(68). The grafts thus follow the process of intramembraneous ossification and require immediate vascularization (91, 113-115) after implantation. The resulting bone is highly dependent on the chosen differentiation pathways(100) and culture conditions(83).

A novel approach, developmental egnineering aims to design a process which mimics the embryological development of a given tissue(116). The principle is that stem cells can replicate a developmental program given the right trigger without relying on further external cues(116). This approach offers several advantages : it is robust and stable, multiple stages allow observation and quality control, every stage of tissue formation is only dependent on the previous stage and the tissue is self-organized(116). Endochondral ossification is a prime example of such a process(116), especially because all stages of the tissue can be present at the same time and regulate each other through the IHH/PTHrP feedback loop, as described above. In addition to robust tissue formation, the signaling allows several smaller modules of tissue to self-organize into larger entities (116, 117). However, to be even more biomimetic, co-cultures with different other cell types may be required(116).

The described principles have lead to the development of engineered hypertrophic cartilage as a bone substitute (118-122), which displays advantageous properties such as resistance to hypoxia (122-124) and gradual vascular invasion(125). This type of graft has been used in orthotopic models such as calvarial(126) or femoral segmental defects (127, 128) and with strategies as diverse as monolithic constructs (125, 126, 128), pellets between 1-3mm in diameter (127, 129) or complex modified structures (125, 130). Generation of greater tissue volumes has been proposed using bioreactor systems(131, 132). As a next biomimetic step, co-cultures of hypertrophic cartilage with endothelial cells have been performed to improve mineralization(133). For clinical applications of engineered hypertrophic cartilage, a remaining drawback is the use of autologous MSC to form the graft. Although necessary to prevent immunologic rejection, autologous MSC use means additional extraction and a significant time-delay. The interdonor variability encountered with MSC (127, 134) may also lead to unpredictable outcomes.

Devitalization of Tissues

The use of allogeneic hypertrophic cartilage of high quality would be possible if immunologic rejection could be prevented. This could be achieved through removal of cells, since matrix constituents are hihgly conserved and may even prevent an adaptive immune response(135). Indeed, the extracellular matrix itself may hold sufficient cues to instruct cell function and identity(136). Moreover, in the case of hypertrophic cartilage, apoptosis of hypertrophic chondrocytes(7) and the release of matrix bound signals such as VEGF through MMP-mediated matrix degradation(21) are part of the natural developmental and growth processes. Thus devitalization of allogeneic hypertrophic cartilage by chemical or physical means or induction of apoptosis(137) can be an alternative to the use of patient derived grafts. Yet, even though devitalized hypertrophic cartilage may form complete bone organs(138), it seems to be remodeled much slower than the living matrix(130, 139).

Re-activation of Devitalized Matrix

To improve the remodeling efficiency of devitalized matrix, an additional step before implantation may be necessary. Following the natural process of endochondral ossification detailed above, diverse cell types such as endothelial cells, osteoclasts, macrophages and mesenchymal stem cells need to be present during the late stages of matrix remodeling. In terms of developmental engineering, the addition of a subsequent module(117) through co-culture with the appropriate cell types(116) could be required. As mentioned above, peripheral blood can be used to derive osteoclasts and the stromal vascular fraction of fat is a rich source of MSC and endothelial progenitors. This opens the possibility of « re-activating » the devitalized hypertrophic cartilage intraoperatively before implantation. Using this approach would allow the generation of an off-the-shelf product, which could be used in a defined procedure as a bone substitute for various applications (Figure 8).

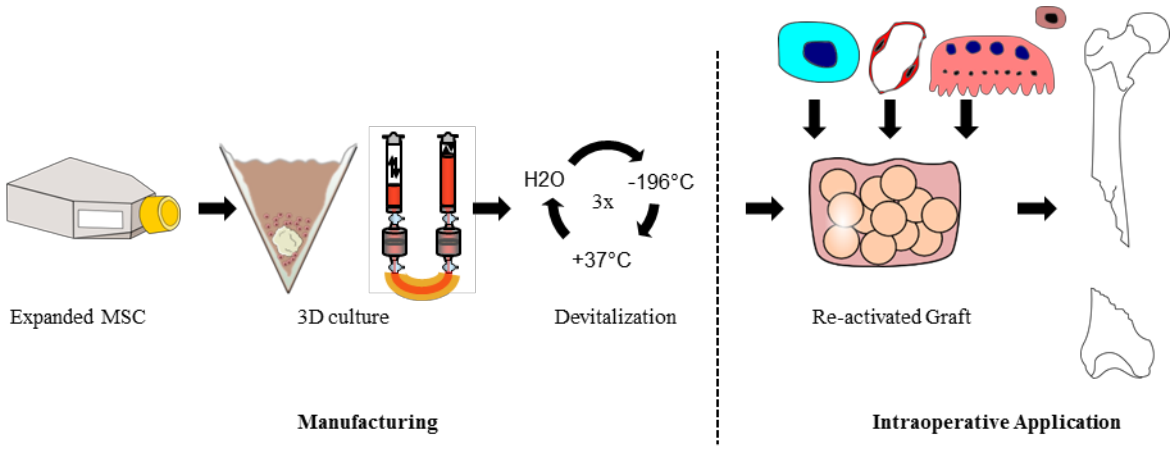

Figure 8: Devitalized hypertrophic cartilage as an off-the-shelf material, which is "re-activated" before use.

General Aim of the Thesis

Based on the introduced concepts of endochondral ossification, developmental engineering, devitalization and reactivation, the aim of my thesis is to validate possible applications of engineered hypertrophic cartilage. Two main pathways could lead to a rapid clinical translation (Figure 9). First, the engineering of hypertrophic cartilage by autologous bone marrow derived mesenchymal stromal cells could be directly used. This requires suitable production methods for large graft generation and a way of monitoring and assuring the quality of resulting grafts. Second, engineered hypertrophic grafts could be pre-produced of from allogeneic sources, subsequently devitalized and re-activated with different cell types.

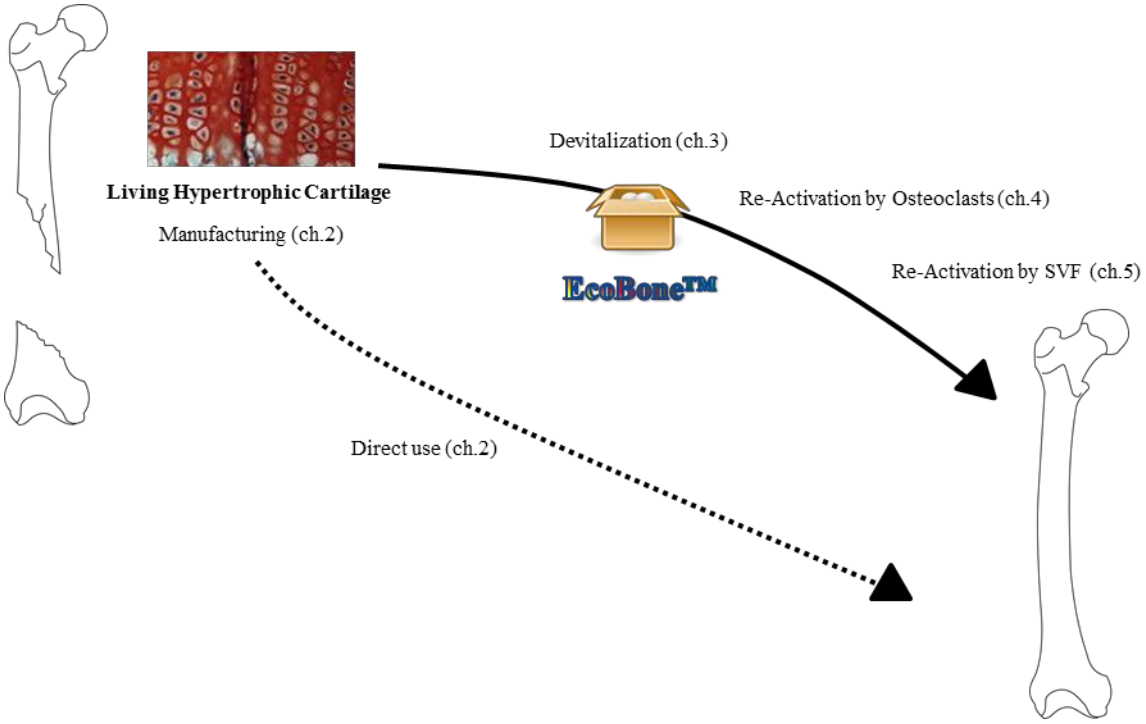

Figure 9: Two pathways for the use of engineered hypertrophic cartilage as a bone substitute.

Specific Aims of the Chapters

The scientific work is presented in the form of four scientific publications.

Chapter 2 « Monitoring perfusion-based bioreactor cultures of engineered hypertrophic cartilage towards clinically oriented production of bone grafts »

This chapter deals with the generation of hypertrophic cartilage in a perfusion bioreactor system, monitoring of culture parameters and the correlation of monitoring parameters and in vivo bone formation. The hypothesis is that glycosaminoglycan and alkaline phosphatase content in culture supernatants are relevant for endochondral ossification and therefore correlate with tissue integrity and maturity. Rabbit bone marrow derived mesenchymal stem cells are used in order to generate protocols and guidelines for a future pre-clinical trial in a rabbit orthotopic model.

Chapter 3 « Osteoinductivity of engineered cartilaginous templates devitalized by inducible apoptosis »

This chapter aims to characterize the effect of different modes of devitalization on the engineered hypertrophic matrix. The hypothesis is that a soft devitalization method better preserves growth factors and components of the extracellular matrix and consequently enhances osteoinductivity compared to a harsh method. Morphological appearance, content of specific morphogens and ultimately, bone formation capacity in vivo are analyzed(140).

Chapter 4 « Interaction of CD14+ monocytes and engineered hypertrophic cartilage during end-stage endochondral ossification »

This chapter investigates the interaction of living and devitalized hypertrophic cartilage with peripheral blood derived monocytes. The hypothesis is that primed osteoclastogenic monocytes seeded in vitro on the hypertrophic matrix can degrade the tissue, release chemoattractant factors and ultimately improve bone formation. In vitro, the formation of osteoclasts, the secretion of factors in supernatants, the attraction of monocytes, endothelial cells or mesenchymal stem cells and the differentiation of mesenchymal stem cells in the presence of secreted factors are analyzed. In vivo, the presence of osteoclasts, macrophages, endothelial cells and mesenchymal stem cells is described at an early time point, as well as the bone formation at a late time point.

Chapter 5 « Fat-derived stromal vascular fraction cells enhance the bone forming capacity of devitalized engineered hypertrophic cartilage matrix »

This chapter explores the regenerative potential of devitalized hypertrophic cartilage re-activated by stromal vascular fraction (SVF) cells from human adipose tissue. The hypothesis is that the presence of multiple progenitor lineages in the SVF can enhance bone formation. Multiple pellets of devitalized matrix are combined together with different amounts of SVF and implanted subcutaneously. The contribution of SVF to

the bone formation, vascularization and bone resorption are analyzed. The system is then tested in an orthotopic model in the rat calvarium.

References

1. Rho JY, Kuhn-Spearing L, & Zioupos P (1998) Mechanical properties and the hierarchical structure of bone. *Medical engineering & physics* 20(2):92-102.
2. Pazzaglia UE, Bonaspetti G, Rodella LF, Ranchetti F, & Azzola F (2007) Design, morphometry and development of the secondary osteonal system in the femoral shaft of the rabbit. *Journal of anatomy* 211(3):303-312.
3. Weiner S & Traub W (1986) Organization of hydroxyapatite crystals within collagen fibrils. *FEBS letters* 206(2):262-266.
4. Kerschnitzki M*, et al.* (2011) The organization of the osteocyte network mirrors the extracellular matrix orientation in bone. *Journal of structural biology* 173(2):303-311.
5. Reichert JC, Gohlke J, Friis TE, Quent VM, & Hutmacher DW (2013) Mesodermal and neural crest derived ovine tibial and mandibular osteoblasts display distinct molecular differences. *Gene* 525(1):99-106.
6. Long F (2012) Building strong bones: molecular regulation of the osteoblast lineage. *Nature reviews. Molecular cell biology* 13(1):27-38.
7. Mackie EJ, Tatarczuch L, & Mirams M (2011) The skeleton: a multi-functional complex organ: the growth plate chondrocyte and endochondral ossification. *The Journal of endocrinology* 211(2):109-121.
8. Riminucci M*, et al.* (1998) Vis-a-vis cells and the priming of bone formation. *Journal of bone and mineral research : the official journal of the American Society for Bone and Mineral Research* 13(12):1852-1861.
9. Mackie EJ, Ahmed YA, Tatarczuch L, Chen KS, & Mirams M (2008) Endochondral ossification: how cartilage is converted into bone in the developing skeleton. *The international journal of biochemistry & cell biology* 40(1):46-62.
10. Hyde G, Dover S, Aszodi A, Wallis GA, & Boot-Handford RP (2007) Lineage tracing using matrilin-1 gene expression reveals that articular chondrocytes exist as the joint interzone forms. *Developmental biology* 304(2):825-833.
11. Fosang AJ & Beier F (2011) Emerging Frontiers in cartilage and chondrocyte biology. *Best practice & research. Clinical rheumatology* 25(6):751-766.
12. Abad V*, et al.* (2002) The role of the resting zone in growth plate chondrogenesis. *Endocrinology* 143(5):1851-1857.
13. Kim HK, Stephenson N, Garces A, Aya-ay J, & Bian H (2009) Effects of disruption of epiphyseal vasculature on the proximal femoral growth plate. *J Bone Joint Surg Am* 91(5):1149-1158.
14. Studer D, Millan C, Ozturk E, Maniura-Weber K, & Zenobi-Wong M (2012) Molecular and biophysical mechanisms regulating hypertrophic differentiation in chondrocytes and mesenchymal stem cells. *European cells & materials* 24:118-135; discussion 135.
15. van Donkelaar CC & Huiskes R (2007) The PTHrP-Ihh feedback loop in the embryonic growth plate allows PTHrP to control hypertrophy and Ihh to regulate proliferation. *Biomechanics and modeling in mechanobiology* 6(1-2):55-62.
16. Shiang R*, et al.* (1994) Mutations in the transmembrane domain of FGFR3 cause the most common genetic form of dwarfism, achondroplasia. *Cell* 78(2):335-342.

17. Bush PG, Parisinos CA, & Hall AC (2008) The osmotic sensitivity of rat growth plate chondrocytes in situ; clarifying the mechanisms of hypertrophy. *J Cell Physiol* 214(3):621-629.
18. Shao YY, Wang L, & Ballock RT (2006) Thyroid hormone and the growth plate. *Reviews in endocrine & metabolic disorders* 7(4):265-271.
19. Wang L, Shao YY, & Ballock RT (2007) Thyroid hormone interacts with the Wnt/beta-catenin signaling pathway in the terminal differentiation of growth plate chondrocytes. *Journal of bone and mineral research : the official journal of the American Society for Bone and Mineral Research* 22(12):1988-1995.
20. Yadav MC, *et al.* (2011) Loss of skeletal mineralization by the simultaneous ablation of PHOSPHO1 and alkaline phosphatase function: a unified model of the mechanisms of initiation of skeletal calcification. *Journal of bone and mineral research : the official journal of the American Society for Bone and Mineral Research* 26(2):286-297.
21. Ortega N, Wang K, Ferrara N, Werb Z, & Vu TH (2010) Complementary interplay between matrix metalloproteinase-9, vascular endothelial growth factor and osteoclast function drives endochondral bone formation. *Disease models & mechanisms* 3(3-4):224-235.
22. Boyce BF & Xing L (2008) Functions of RANKL/RANK/OPG in bone modeling and remodeling. *Archives of biochemistry and biophysics* 473(2):139-146.
23. Yang L, Tsang KY, Tang HC, Chan D, & Cheah KS (2014) Hypertrophic chondrocytes can become osteoblasts and osteocytes in endochondral bone formation. *Proceedings of the National Academy of Sciences of the United States of America* 111(33):12097-12102.
24. Deckers MM, *et al.* (2002) Dissociation of angiogenesis and osteoclastogenesis during endochondral bone formation in neonatal mice. *Journal of bone and mineral research : the official journal of the American Society for Bone and Mineral Research* 17(6):998-1007.
25. Knowles HJ, *et al.* (2012) Chondroclasts are mature osteoclasts which are capable of cartilage matrix resorption. *Virchows Archiv : an international journal of pathology* 461(2):205-210.
26. Ortega N, Behonick D, Stickens D, & Werb Z (2003) How proteases regulate bone morphogenesis. *Annals of the New York Academy of Sciences* 995:109-116.
27. Blumer MJ, Longato S, & Fritsch H (2008) Localization of tartrate-resistant acid phosphatase (TRAP), membrane type-1 matrix metalloproteinases (MT1-MMP) and macrophages during early endochondral bone formation. *Journal of anatomy* 213(4):431-441.
28. Inada M, *et al.* (2004) Critical roles for collagenase-3 (Mmp13) in development of growth plate cartilage and in endochondral ossification. *Proceedings of the National Academy of Sciences of the United States of America* 101(49):17192-17197.
29. Gerber HP, *et al.* (1999) VEGF couples hypertrophic cartilage remodeling, ossification and angiogenesis during endochondral bone formation. *Nature medicine* 5(6):623-628.
30. Weise M, *et al.* (2001) Effects of estrogen on growth plate senescence and epiphyseal fusion. *Proceedings of the National Academy of Sciences of the United States of America* 98(12):6871-6876.
31. Frost HM (1987) Bone "mass" and the "mechanostat": a proposal. *The Anatomical record* 219(1):1-9.
32. Romanello M, *et al.* (2014) Osteoblastic cell secretome: a novel role for progranulin during risedronate treatment. *Bone* 58:81-91.
33. Hessle L, *et al.* (2002) Tissue-nonspecific alkaline phosphatase and plasma cell membrane glycoprotein-1 are central antagonistic regulators of bone

mineralization. *Proceedings of the National Academy of Sciences of the United States of America* 99(14):9445-9449.
34. Sharma U, Pal D, & Prasad R (2014) Alkaline phosphatase: an overview. *Indian journal of clinical biochemistry : IJCB* 29(3):269-278.
35. Bellido T (2014) Osteocyte-driven bone remodeling. *Calcified tissue international* 94(1):25-34.
36. Weinbaum S, Cowin SC, & Zeng Y (1994) A model for the excitation of osteocytes by mechanical loading-induced bone fluid shear stresses. *J Biomech* 27(3):339-360.
37. Kamioka H*, et al.* (2006) Fluid shear stress induces less calcium response in a single primary osteocyte than in a single osteoblast: implication of different focal adhesion formation. *Journal of bone and mineral research : the official journal of the American Society for Bone and Mineral Research* 21(7):1012-1021.
38. Teitelbaum SL & Ross FP (2003) Genetic regulation of osteoclast development and function. *Nature reviews. Genetics* 4(8):638-649.
39. Sorensen MG*, et al.* (2007) Characterization of osteoclasts derived from CD14+ monocytes isolated from peripheral blood. *Journal of bone and mineral metabolism* 25(1):36-45.
40. Quinn JM, Elliott J, Gillespie MT, & Martin TJ (1998) A combination of osteoclast differentiation factor and macrophage-colony stimulating factor is sufficient for both human and mouse osteoclast formation in vitro. *Endocrinology* 139(10):4424-4427.
41. Teitelbaum SL (2000) Bone resorption by osteoclasts. *Science* 289(5484):1504-1508.
42. Soe K, Merrild DM, & Delaisse JM (2013) Steering the osteoclast through the demineralization-collagenolysis balance. *Bone* 56(1):191-198.
43. Fuller K, Kirstein B, & Chambers TJ (2007) Regulation and enzymatic basis of bone resorption by human osteoclasts. *Clinical science* 112(11):567-575.
44. Henriksen K, Karsdal MA, & Martin TJ (2014) Osteoclast-derived coupling factors in bone remodeling. *Calcified tissue international* 94(1):88-97.
45. Tang Y*, et al.* (2009) TGF-beta1-induced migration of bone mesenchymal stem cells couples bone resorption with formation. *Nature medicine* 15(7):757-765.
46. Iqbal J, Sun L, & Zaidi M (2009) Coupling bone degradation to formation. *Nature medicine* 15(7):729-731.
47. Takeshita S*, et al.* (2013) Osteoclast-secreted CTHRC1 in the coupling of bone resorption to formation. *The Journal of clinical investigation* 123(9):3914-3924.
48. Baud'huin M*, et al.* (2013) Osteoprotegerin: multiple partners for multiple functions. *Cytokine & growth factor reviews* 24(5):401-409.
49. Marsell R & Einhorn TA (2011) The biology of fracture healing. *Injury* 42(6):551-555.
50. Schindeler A, McDonald MM, Bokko P, & Little DG (2008) Bone remodeling during fracture repair: The cellular picture. *Seminars in cell & developmental biology* 19(5):459-466.
51. Mori G, D'Amelio P, Faccio R, & Brunetti G (2013) The Interplay between the bone and the immune system. *Clinical & developmental immunology* 2013:720504.
52. Shefelbine SJ*, et al.* (2005) Prediction of fracture callus mechanical properties using micro-CT images and voxel-based finite element analysis. *Bone* 36(3):480-488.
53. Rot C, Stern T, Blecher R, Friesem B, & Zelzer E (2014) A mechanical Jack-like Mechanism drives spontaneous fracture healing in neonatal mice. *Developmental cell* 31(2):159-170.

54. Ai-Aql ZS, Alagl AS, Graves DT, Gerstenfeld LC, & Einhorn TA (2008) Molecular mechanisms controlling bone formation during fracture healing and distraction osteogenesis. *Journal of dental research* 87(2):107-118.
55. Gustilo RB, Merkow RL, & Templeman D (1990) The management of open fractures. *J Bone Joint Surg Am* 72(2):299-304.
56. Helfet DL*, et al.* (2003) AO philosophy and principles of fracture management-its evolution and evaluation. *J Bone Joint Surg Am* 85-A(6):1156-1160.
57. Ruedi TP, Sommer C, & Leutenegger A (1998) New techniques in indirect reduction of long bone fractures. *Clin Orthop Relat Res* (347):27-34.
58. Papakostidis C, Bhandari M, & Giannoudis PV (2013) Distraction osteogenesis in the treatment of long bone defects of the lower limbs: effectiveness, complications and clinical results; a systematic review and meta-analysis. *The bone & joint journal* 95-B(12):1673-1680.
59. Giannoudis PV, Faour O, Goff T, Kanakaris N, & Dimitriou R (2011) Masquelet technique for the treatment of bone defects: tips-tricks and future directions. *Injury* 42(6):591-598.
60. Panteli M, Pountos I, Jones E, & Giannoudis PV (2015) Biological and molecular profile of fracture non-union tissue: current insights. *Journal of cellular and molecular medicine* 19(4):685-713.
61. Konstantinidis L*, et al.* (2013) Failure after osteosynthesis of trochanteric fractures. Where is the limit of osteoporosis? *Osteoporosis international : a journal established as result of cooperation between the European Foundation for Osteoporosis and the National Osteoporosis Foundation of the USA* 24(10):2701-2706.
62. Ahlmann E, Patzakis M, Roidis N, Shepherd L, & Holtom P (2002) Comparison of anterior and posterior iliac crest bone grafts in terms of harvest-site morbidity and functional outcomes. *J Bone Joint Surg Am* 84-A(5):716-720.
63. Korompilias AV*, et al.* (2011) Recent updates of surgical techniques and applications of free vascularized fibular graft in extremity and trunk reconstruction. *Microsurgery* 31(3):171-175.
64. Bolano L & Kopta JA (1991) The immunology of bone and cartilage transplantation. *Orthopedics* 14(9):987-996.
65. Hernigou P (2015) Bone transplantation and tissue engineering, part III: allografts, bone grafting and bone banking in the twentieth century. *Int Orthop* 39(3):577-587.
66. De Long WG, Jr.*, et al.* (2007) Bone grafts and bone graft substitutes in orthopaedic trauma surgery. A critical analysis. *J Bone Joint Surg Am* 89(3):649-658.
67. Liu Y, Lim J, & Teoh SH (2013) Review: development of clinically relevant scaffolds for vascularised bone tissue engineering. *Biotechnology advances* 31(5):688-705.
68. Miron RJ & Zhang YF (2012) Osteoinduction: a review of old concepts with new standards. *Journal of dental research* 91(8):736-744.
69. Friedenstein AJ, Chailakhyan RK, & Gerasimov UV (1987) Bone marrow osteogenic stem cells: in vitro cultivation and transplantation in diffusion chambers. *Cell and tissue kinetics* 20(3):263-272.
70. Pittenger MF*, et al.* (1999) Multilineage potential of adult human mesenchymal stem cells. *Science* 284(5411):143-147.
71. de Peppo GM*, et al.* (2013) Engineering bone tissue substitutes from human induced pluripotent stem cells. *Proceedings of the National Academy of Sciences of the United States of America* 110(21):8680-8685.
72. Kuznetsov SA, Cherman N, & Robey PG (2011) In vivo bone formation by progeny of human embryonic stem cells. *Stem cells and development* 20(2):269-287.

73. Pountos I, Corscadden D, Emery P, & Giannoudis PV (2007) Mesenchymal stem cell tissue engineering: techniques for isolation, expansion and application. *Injury* 38 Suppl 4:S23-33.
74. Grayson WL, *et al.* (2015) Stromal cells and stem cells in clinical bone regeneration. *Nature reviews. Endocrinology* 11(3):140-150.
75. Dominici M, *et al.* (2006) Minimal criteria for defining multipotent mesenchymal stromal cells. The International Society for Cellular Therapy position statement. *Cytotherapy* 8(4):315-317.
76. Rebelatto CK, *et al.* (2008) Dissimilar differentiation of mesenchymal stem cells from bone marrow, umbilical cord blood, and adipose tissue. *Experimental biology and medicine* 233(7):901-913.
77. Boeuf S & Richter W (2010) Chondrogenesis of mesenchymal stem cells: role of tissue source and inducing factors. *Stem cell research & therapy* 1(4):31.
78. Leo AJ & Grande DA (2006) Mesenchymal stem cells in tissue engineering. *Cells, tissues, organs* 183(3):112-122.
79. Seta N, Okazaki Y, & Kuwana M (2008) Human circulating monocytes can express receptor activator of nuclear factor-kappaB ligand and differentiate into functional osteoclasts without exogenous stimulation. *Immunology and cell biology* 86(5):453-459.
80. Hemingway F, *et al.* (2011) In vitro generation of mature human osteoclasts. *Calcified tissue international* 89(5):389-395.
81. Riordan NH, *et al.* (2009) Non-expanded adipose stromal vascular fraction cell therapy for multiple sclerosis. *Journal of translational medicine* 7:29.
82. Hutmacher DW, Schantz JT, Lam CX, Tan KC, & Lim TC (2007) State of the art and future directions of scaffold-based bone engineering from a biomaterials perspective. *Journal of tissue engineering and regenerative medicine* 1(4):245-260.
83. Bouet G, Marchat D, Cruel M, Malaval L, & Vico L (2015) In vitro three-dimensional bone tissue models: from cells to controlled and dynamic environment. *Tissue Eng Part B Rev* 21(1):133-156.
84. Lienemann PS, Lutolf MP, & Ehrbar M (2012) Biomimetic hydrogels for controlled biomolecule delivery to augment bone regeneration. *Advanced drug delivery reviews* 64(12):1078-1089.
85. Martino MM, Briquez PS, Maruyama K, & Hubbell JA (2015) Extracellular matrix-inspired growth factor delivery systems for bone regeneration. *Advanced drug delivery reviews*.
86. LeGeros RZ (2008) Calcium phosphate-based osteoinductive materials. *Chemical reviews* 108(11):4742-4753.
87. Scott MA, *et al.* (2012) Brief review of models of ectopic bone formation. *Stem cells and development* 21(5):655-667.
88. Coelho MB, Cabral JM, & Karp JM (2012) Intraoperative stem cell therapy. *Annual review of biomedical engineering* 14:325-349.
89. Wang X, *et al.* (2013) Role of mesenchymal stem cells in bone regeneration and fracture repair: a review. *Int Orthop* 37(12):2491-2498.
90. Mehrkens A, *et al.* (2012) Intraoperative engineering of osteogenic grafts combining freshly harvested, human adipose-derived cells and physiological doses of bone morphogenetic protein-2. *European cells & materials* 24:308-319.
91. Warnke PH, *et al.* (2004) Growth and transplantation of a custom vascularised bone graft in a man. *Lancet* 364(9436):766-770.
92. Stevens MM, *et al.* (2005) In vivo engineering of organs: the bone bioreactor. *Proceedings of the National Academy of Sciences of the United States of America* 102(32):11450-11455.

93. Han D & Dai K (2013) Prefabrication of a vascularized bone graft with Beta tricalcium phosphate using an in vivo bioreactor. *Artificial organs* 37(10):884-893.
94. Liu Y, Moller B, Wiltfang J, Warnke PH, & Terheyden H (2014) Tissue engineering of a vascularized bone graft of critical size with an osteogenic and angiogenic factor-based in vivo bioreactor. *Tissue engineering. Part A* 20(23-24):3189-3197.
95. Markway BD, *et al.* (2010) Enhanced chondrogenic differentiation of human bone marrow-derived mesenchymal stem cells in low oxygen environment micropellet cultures. *Cell transplantation* 19(1):29-42.
96. Sammarco MC, *et al.* (2014) Endogenous bone regeneration is dependent upon a dynamic oxygen event. *Journal of bone and mineral research : the official journal of the American Society for Bone and Mineral Research* 29(11):2336-2345.
97. Salim A, Nacamuli RP, Morgan EF, Giaccia AJ, & Longaker MT (2004) Transient changes in oxygen tension inhibit osteogenic differentiation and Runx2 expression in osteoblasts. *J Biol Chem* 279(38):40007-40016.
98. Fehrer C, *et al.* (2007) Reduced oxygen tension attenuates differentiation capacity of human mesenchymal stem cells and prolongs their lifespan. *Aging cell* 6(6):745-757.
99. Kato K & Matsushita M (2014) Proton concentrations can be a major contributor to the modification of osteoclast and osteoblast differentiation, working independently of extracellular bicarbonate ions. *Journal of bone and mineral metabolism* 32(1):17-28.
100. James AW (2013) Review of Signaling Pathways Governing MSC Osteogenic and Adipogenic Differentiation. *Scientifica* 2013:684736.
101. McCoy RJ & O'Brien FJ (2010) Influence of shear stress in perfusion bioreactor cultures for the development of three-dimensional bone tissue constructs: a review. *Tissue Eng Part B Rev* 16(6):587-601.
102. Gardel LS, Serra LA, Reis RL, & Gomes ME (2014) Use of perfusion bioreactors and large animal models for long bone tissue engineering. *Tissue Eng Part B Rev* 20(2):126-146.
103. Braccini A, *et al.* (2005) Three-dimensional perfusion culture of human bone marrow cells and generation of osteoinductive grafts. *Stem cells* 23(8):1066-1072.
104. Guven S, *et al.* (2012) Validation of an automated procedure to isolate human adipose tissue-derived cells by using the Sepax(R) technology. *Tissue engineering. Part C, Methods* 18(8):575-582.
105. Li D, *et al.* (2014) Tissue-engineered bone constructed in a bioreactor for repairing critical-sized bone defects in sheep. *Int Orthop* 38(11):2399-2406.
106. Ding M, Henriksen SS, Wendt D, & Overgaard S (2015) An automated perfusion bioreactor for the streamlined production of engineered osteogenic grafts. *Journal of biomedical materials research. Part B, Applied biomaterials*.
107. Schulz RM & Bader A (2007) Cartilage tissue engineering and bioreactor systems for the cultivation and stimulation of chondrocytes. *European biophysics journal : EBJ* 36(4-5):539-568.
108. Cancedda R, Giannoni P, & Mastrogiacomo M (2007) A tissue engineering approach to bone repair in large animal models and in clinical practice. *Biomaterials* 28(29):4240-4250.
109. Horner EA, *et al.* (2010) Long bone defect models for tissue engineering applications: criteria for choice. *Tissue Eng Part B Rev* 16(2):263-271.
110. Thomson RC, *et al.* (1999) Guided tissue fabrication from periosteum using preformed biodegradable polymer scaffolds. *Biomaterials* 20(21):2007-2018.
111. Bensaid W, *et al.* (2005) De novo reconstruction of functional bone by tissue engineering in the metatarsal sheep model. *Tissue engineering* 11(5-6):814-824.

112. Brey EM, *et al.* (2007) Comparison of guided bone formation from periosteum and muscle fascia. *Plast Reconstr Surg* 119(4):1216-1222.
113. Kaempfen A, *et al.* (2015) Engraftment of Prevascularized, Tissue Engineered Constructs in a Novel Rabbit Segmental Bone Defect Model. *International journal of molecular sciences* 16(6):12616-12630.
114. Scheufler O, *et al.* (2008) Spatial and temporal patterns of bone formation in ectopically pre-fabricated, autologous cell-based engineered bone flaps in rabbits. *Journal of cellular and molecular medicine* 12(4):1238-1249.
115. Warnke PH, *et al.* (2006) Man as living bioreactor: fate of an exogenously prepared customized tissue-engineered mandible. *Biomaterials* 27(17):3163-3167.
116. Lenas P, Moos M, & Luyten FP (2009) Developmental engineering: a new paradigm for the design and manufacturing of cell-based products. Part I: from three-dimensional cell growth to biomimetics of in vivo development. *Tissue Eng Part B Rev* 15(4):381-394.
117. Lenas P, Luyten FP, Doblare M, Nicodemou-Lena E, & Lanzara AE (2011) Modularity in developmental biology and artificial organs: a missing concept in tissue engineering. *Artificial organs* 35(6):656-662.
118. Chang SC, Tai CL, Chung HY, Lin TM, & Jeng LB (2009) Bone marrow mesenchymal stem cells form ectopic woven bone in vivo through endochondral bone formation. *Artificial organs* 33(4):301-308.
119. Scotti C, *et al.* (2010) Recapitulation of endochondral bone formation using human adult mesenchymal stem cells as a paradigm for developmental engineering. *Proceedings of the National Academy of Sciences of the United States of America* 107(16):7251-7256.
120. Janicki P, Kasten P, Kleinschmidt K, Luginbuehl R, & Richter W (2010) Chondrogenic pre-induction of human mesenchymal stem cells on beta-TCP: enhanced bone quality by endochondral heterotopic bone formation. *Acta biomaterialia* 6(8):3292-3301.
121. Farrell E, *et al.* (2011) In-vivo generation of bone via endochondral ossification by in-vitro chondrogenic priming of adult human and rat mesenchymal stem cells. *BMC musculoskeletal disorders* 12:31.
122. Sheehy EJ, Vinardell T, Buckley CT, & Kelly DJ (2013) Engineering osteochondral constructs through spatial regulation of endochondral ossification. *Acta biomaterialia* 9(3):5484-5492.
123. Grimshaw MJ & Mason RM (2000) Bovine articular chondrocyte function in vitro depends upon oxygen tension. *Osteoarthritis and cartilage / OARS, Osteoarthritis Research Society* 8(5):386-392.
124. Sheehy EJ, Buckley CT, & Kelly DJ (2012) Oxygen tension regulates the osteogenic, chondrogenic and endochondral phenotype of bone marrow derived mesenchymal stem cells. *Biochem Biophys Res Commun* 417(1):305-310.
125. Sheehy EJ, *et al.* (2015) Tissue Engineering Whole Bones Through Endochondral Ossification: Regenerating the Distal Phalanx. *BioResearch open access* 4(1):229-241.
126. Kuhn LT, *et al.* (2014) Developmental-like bone regeneration by human embryonic stem cell-derived mesenchymal cells. *Tissue engineering. Part A* 20(1-2):365-377.
127. van der Stok J, *et al.* (2014) Chondrogenically differentiated mesenchymal stromal cell pellets stimulate endochondral bone regeneration in critical-sized bone defects. *European cells & materials* 27:137-148; discussion 148.
128. Harada N, *et al.* (2014) Bone regeneration in a massive rat femur defect through endochondral ossification achieved with chondrogenically differentiated MSCs in a degradable scaffold. *Biomaterials* 35(27):7800-7810.

129. Bahney CS, *et al.* (2014) Stem cell-derived endochondral cartilage stimulates bone healing by tissue transformation. *Journal of bone and mineral research : the official journal of the American Society for Bone and Mineral Research* 29(5):1269-1282.
130. Cunniffe GM, *et al.* (2015) Porous decellularized tissue engineered hypertrophic cartilage as a scaffold for large bone defect healing. *Acta biomaterialia* 23:82-90.
131. Kock LM, Malda J, Dhert WJ, Ito K, & Gawlitta D (2014) Flow-perfusion interferes with chondrogenic and hypertrophic matrix production by mesenchymal stem cells. *J Biomech* 47(9):2122-2129.
132. Hoffmann W, Feliciano S, Martin I, de Wild M, & Wendt D (2015) Novel Perfused Compression Bioreactor System as an in vitro Model to Investigate Fracture Healing. *Frontiers in bioengineering and biotechnology* 3:10.
133. Freeman FE, Haugh MG, & McNamara LM (2015) An in vitro bone tissue regeneration strategy combining chondrogenic and vascular priming enhances the mineralization potential of mesenchymal stem cells in vitro while also allowing for vessel formation. *Tissue engineering. Part A* 21(7-8):1320-1332.
134. Solchaga LA, Penick KJ, & Welter JF (2011) Chondrogenic differentiation of bone marrow-derived mesenchymal stem cells: tips and tricks. *Methods in molecular biology* 698:253-278.
135. Bollyky PL, *et al.* (2009) Intact extracellular matrix and the maintenance of immune tolerance: high molecular weight hyaluronan promotes persistence of induced CD4+CD25+ regulatory T cells. *Journal of leukocyte biology* 86(3):567-572.
136. Crapo PM, Gilbert TW, & Badylak SF (2011) An overview of tissue and whole organ decellularization processes. *Biomaterials* 32(12):3233-3243.
137. Bourgine PE, Pippenger BE, Todorov A, Jr., Tchang L, & Martin I (2013) Tissue decellularization by activation of programmed cell death. *Biomaterials* 34(26):6099-6108.
138. Bridges JB & Pritchard JJ (1958) Bone and cartilage induction in the rabbit. *Journal of anatomy* 92(1):28-38.
139. Gawlitta D, *et al.* (2015) Decellularized cartilage-derived matrix as substrate for endochondral bone regeneration. *Tissue engineering. Part A* 21(3-4):694-703.
140. Bourgine PE, *et al.* (2014) Osteoinductivity of engineered cartilaginous templates devitalized by inducible apoptosis. *Proceedings of the National Academy of Sciences of the United States of America* 111(49):17426-17431.

Chapter 2

Monitoring perfusion-based bioreactor cultures of engineered hypertrophic cartilage towards clinically oriented production of bone grafts

Monitoring perfusion-based bioreactor cultures of engineered hypertrophic cartilage towards clinically oriented production of bone grafts

Atanas Todorov[1], Adelaide Asnaghi[1], Celeste Scotti[1,2], Andrea Barbero[1], Adam Papadimitropoulos[1], Ivan Martin[1]

1 Departments of Surgery and Biomedicine, University Hospital Basel, Hebelstrasse 20, CH-4031 Basel, Switzerland

2 Orthopaedic Institute I.R.C.C.S. Galeazzi, Via R. Galeazzi 4, 20161 Milan, Italy

Abstract

In vitro engineered hypertrophic cartilage is a promising bone substitute material. However, tissue with a thickness of more than 3mm can develop central core necrosis due to limited mass transport during culture. To address this issue, perfusion-based bioreactors have been used, yet effective monitoring and predictive parameters for tissue formation and in vivo performance have not been investigated in detail. In this study we cultured 6x3mm hypertrophic cartilage constructs derived from rabbit bone marrow mesenchymal stromal cells in a perfusion bioreactor. Monitoring of glycosaminoglycans (GAG) and alkaline phosphatase (ALP) in the supernatants was performed during 3 weeks of chondrogenesis and 2 weeks of hypertrophy. Tissues with typical morphological and molecular traits of hypertrophic cartilage formed after a total of 5 weeks bioreactor culture. GAG and ALP in supernatants positively correlated with GAG accumulated in the matrix. In some cultures non-homogenous tissue formed, possibly due to metalloproteinase-mediated cartilage digestion by residual CD45+ cells. The levels of released GAG correlated significantly with the percentage of cartilaginous matrix in these tissues. After implantation in nude mice for up to 12 weeks, bone and bone marrow formed by endochondral ossification. Total bone volume correlated significantly with

the levels of GAG and ALP quantified in the supernatants. The findings indicate that quantification of GAG and ALP released during the bioreactor-based culture enable to monitor the quality of the hypertrophic cartilage developing and inform on its osteogenic capacity in vivo. Such measurements can thus be used as non-invasive, in-process quality control for bone grafts.

Introduction

Since the demonstration that hypertrophic cartilage can be engineered in vitro from bone marrow mesenchymal stromal cells and undergoes a process related to endochondral ossification in vivo(1-4), the field of regenerative medicine has rushed to prove the regenerative potential of this material and promote its clinical application. So far this has included implantation of hypertrophic cartilage in orthotopic models such as calvarial(5) or femoral segmental defects(6, 7) and strategies as diverse as monolithic constructs(5, 7, 8), pellets between 1-3mm in diameter(6, 9) and complex modified structures(8, 10). The homogenous tissue generation in constructs with 3mm thickness has been challenging in static culture and unidirectional perfusion(11, 12). Although the use of perfusion bioreactors(13, 14) has been shown as a viable way to improve and upscale production of hypertrophic cartilage(12), the effects of perfusion on construct generation have been controversial(15).

According to Lourenco et al.(16), “Real-time monitoring of bioreactors is now regarded as an essential part of effective bioprocess control that can lead to increased efficiency, productivity, and reproducibility and also to improved quality control [...], thus optimizing overall costs”. Furthermore, as Gardel et al.(17) put it in the context of cartilage tissue engineering, “[...]an advantage in the area would be the development and employment of techniques, which could assess the integrity of the tissue noninvasively.“

Following this reasoning we have strived to identify relevant parameters for an at-line-monitoring during the generation of hypetrophic cartilage in perfusion bioreactors. Although

monitoring of ECM components such as glycosaminoglycans (GAG) or collagens using high resolution NMR as well as monitoring of the differentiation status of MSC using high resolution imaging have been proposed(18), most propositions would require very expensive machinery to be implemented. Monitoring of alkaline phosphatase activity in supernatants from osteogenically differentiating bone marrow mesenchymal stromal cells in bioreactors has been performed(17), but not extensively correlated to tissue formation in vitro or in vivo. Since the culture of hypertrophic cartilage involves chondrogenesis and results in later bone formation, we decided to monitor both GAG and alkaline phosphatase (AP) activity using relatively simple and fast biochemical methods.

Our hypothesis was that we could closely monitor in vitro tissue formation by tracking both parameters. More importantly, we hypothesized that the level of the parameters would inform on the tissue maturity and thus also predict in vivo bone formation.

For the construct generation in this present study, we employed rabbit bone marrow mesenchymal stromal cells. After mouse and rat models, a rabbit calvarial or segmental defect model(19) would be an expected next step for clinical translation. Thus the data resulting from this present study would be highly useful for future pre-clinical trials.

Materials and Methods

Isolation and culture of rabbit BMSC

All rabbit procedures were reviewed and approved by the Swiss Federal Veterinary Office (Permit BS 2080). Bone marrow was extracted from the right iliac crest of 7 female New Zealand White Rabbits (NZW, Charles River Laboratories, Kisslegg, Germany) between 8 and 10 weeks of age. Before the procedure animals were anesthetized with 25mg/kg Ketamin and 2.5 mg / kg Xylazin (Veterinaria AG, Zürich, Switzerland) by subcutaneous injection. Anaesthesia during the procedure was continued with Isoflurane 2.5% in 1l / min O2. Buprenorphin 0.05mg/kg (Temgesic, Essex Chemie AG, Luzern, Switzerland) was given for analgesia during the operation and re-administered 2-3 times daily for the

first 2 weeks. The area over the right illiac crest was shaved, disinfected with Octenisept (Schülke & Mayr AG, Switzerland) and a stab incision to the bone was performed. A bone marrow biopsy needle for children (Jamshidi, CareFusion, Kelberg, Germany) was used and up to 6ml of bone marrow aspirated with a 10ml syringe filled with 1 ml heparin solution (Heparin-Na 5000 IU / ml, B. Braun Medical AG, Emmenbrücke, Switzerland). The wound was closed with a single stitch suture (Prolene 5/0, Ethicon, Somerville, NJ, USA) and the animals allowed to recover under infrared light.

Nucleated cells in the bone marrow aspirates were counted and 100'000 cells /cm^2 were seeded on tissue culture flasks with complete medium (alpha-MEM, 10% fetal bovine serum, 1% penicillin-streptomycin-glutamate, 10 mM HEPES, 1mM sodium pyruvate, all from Gibco, Invitrogen, Basel, Switzerland) and 5 ng/ml FGF-2 (R&D Systems, Wiesbaden, Germany). After reaching confluency, cells were washed with PBS, detached with 0.5 mg/ml trypsin (Gibco, Basel, Switzerland) and frozen in 90% FBS and 10% DMSO. Before use in a bioreactor, 3000 cells /cm^2 were seeded with complete medium and 5 ng/ml FGF-2 and expanded until passage three.

Bioreactor culture

The oscillatory perfusion bioreactor system described by Wendt et al(13) was used for this study. Collagen type I based scaffolds (Ultrafoam, Davol Inc., USA) were soaked in phosphate butter solution (PBS) for at least 20 minutes and cylinders of 8 mm diameter and 3 mm height were punched out. The scaffolds were placed on a plastic grid and clamped using a 1 mm wide teflon ring with an inner diameter of 6 mm, ensuring perfusion of a 6 x 3 mm volume of scaffold. As published previously(11, 12), 2.5 - 3 million cells per scaffold were seeded using chondrogenic medium consisting of serum free medium (DMEM, 1.25 mg/ml human serum albumin, 10 mM HEPES, 1 mM sodium pyruvate, 1% penicillin-streptomycin-glutamate and 1% ITS-1, all from Gibco, Switzerland), 10 ng/ml TGFβ3 (Novartis, Basel, Switzerland), 10^{-7} M dexamethasone and 0.1 mM ascorbate-2-phosphate (both from Sigma Aldrich). Seeding was performed using a perfusion speed of 3 ml/min overnight, while 0. 3ml/min were used for subsequent culture. Static culture was performed as

described previously(11). Briefly, 6 x 3 mm scaffolds were manually seeded with 3 million cells in 60 μl chondrogenic medium and cultured in agarose coated plates with 1 ml medium. Medium changes were performed manually twice per week. After 21 days, hypertrophic medium consisting of serum free medium, 0.05 μM L-thyroxin, 10^{-6} M dexamethasone, 10 mM β-glycerophosphate and 0.1 mM ascorbate-2-phosphate was used instead of chondrogenic medium for additional 14 days. For metalloproteinase inhibition, 15 nM Merimastat (Sigma Aldrich) was added to the culture media both during chondrogenesis and hypertrophy.

Monitoring of GAG and ALP

Supernatants of each medium change were analysed for glycosaminoglycan content and alkaline phosphatase activity. For GAG, the method of Barbosa et al(20) was employed. Briefly, 250 μl of supernatant were incubated with approximately 1 ml of DMMB solution (16 mg/l DMMB, 6 mM sodium formate, 200 mM GuHCL, all from Sigma Aldrich) on a shaker at room temperature for 30 minutes. Precipitated DMMB-GAG complexes were centrifuged and supernatants were discarded. Complexes were dissolved in decomplexion solution (4 M GuHCL, 50 mM Na-Acetate, 10% Propan-1-ol, all from Sigma Aldrich), absorption was measured at 656 nm and GAG concentrations were calculated using a standard curve.

For ALP, the method of Burstone(21) with adaptations was employed. Briefly, 50 μl supernatant was incubated with 50 μl buffer (5 mg/ml p-nitro-phenyl phosphate, 200 mM TRIS, 1 mM $MgCl_2$, pH9.5) at 37°C in triplicate. Adding 50 μl of 1 M NaOH stopped the reaction, absorption was measured at 405 nm and ALP activity was calculated using a standard curve.

GAG and DNA content

For measurements of the GAG and DNA accumulated in the matrix at the end of the culture, samples were digested overnight with Proteinase K solution (1 mg/ml Proteinase K in 50 mM Tris pH 7.6, 1 mM EDTA, 1 mM Iodoacetamide, 10 μg/ml Pepstatin, all from Sigma Aldrich). GAG measurements were performed as described above. DNA measurements were performed with the

CyQuant kit (Thermo Fisher Scientific, Zug, Switzerland) according to the protocol of the manufacturer.

Implantations

All mouse procedures were reviewed and approved by the Swiss Federal Veterinary Office (BS 1797). Female nude mice 6 - 8 weeks of age were anesthetized using isoflurane 2% in 1 l / min O_2. The skin on the back was disinfected and cut along the midline for maximally 8mm. Subcutaneous pockets were prepared on both sides by blunt dissection and samples were inserted. The skin was closed with surgical staples and the mice were allowed to recover under red light. They were subsequently kept according to the animal husbandry guidelines of the University Hospital Basel, had free access to food and water and were regularly checked for signs of pain, infection or wound opening. Staples were removed after 7 - 10 days. After 8 or 12 weeks, mice were euthanized using CO_2 in a dedicated chamber and the implants removed and stored immediately in 1.5% PFA for further processing. Several femurs were extracted for additional microtomographic measurements.

Microtomography

Microtomography was performed using a tungsten x-ray source at 70 kV and 260 μA with an aluminium filter of 0.5 mm (Nanotome, GE). Transmission images were acquired for 360° with an incremental step size of 0.25°. Volumes were reconstructed using a modified Feldkamp algorithm (software supplied by manufacturer) at a voxel size of 2.5 – 3 μm. Thresholding, segmentation and 3D measurements were performed using the Image(22)J software with the BoneJ(23) and 3D Shape(24) additions.

Histology

Samples were embedded in paraffin and sections of 5 μm thickness prepared using a microtome. Safranin-O, Alizarin red, hematoxylin/eosin and Masson tri-chrome staining were performed as published previously(11). Quantification of cartilaginous area percentage was performed on 4 representative Safranin-O stained sections per sample. Primary antibodies for CD45 (MCA808GA,

AbD Serotec), DIPEN (1042002, MDBiosciences, USA), collagen type II (ab34712), collagen type X (ab49945), MMP-9 (ab38898) and MMP-13 (ab39012, Abcam, UK) were used. After washing and incubation with an appropriate biotinylated secondary antibody (Dako, Denmark), the stainings were developed with the Vectastain ABC kit (Vector Laboratories, USA) according to the manufacturer's protocols.

Statistical Analysis

Data was analysed by t-test, ANOVA and Pearson correlation using the GraphPad Prism v2.2 software. A significance level alpha of 0.05 was set. Average values and standard deviations are reported.

Results

Generation of hypertrophic cartilaginous matrix in a 3D perfusion bioreactor system

Measurement of GAG content and ALP activity in supernatants was feasible at each medium change and resulted in curves of a characteristic shape (Figure 1A and B). Medium from replicate bioreactor cultures showed some variability, mostly in ALP activity. The highest values for each measurement were observed at the second medium change after 7 days of culture. GAG content in the tissues as well as GAG/DNA ratio positively correlated with the GAG and ALP measurements, though only the correlation of GAG/DNA with GAG in supernatants reached statistical significance ($r = 0.96$, $p = 0.04$, Figure 1C). For subsequent in vitro cultures, only GAG was used to assess tissue formation.

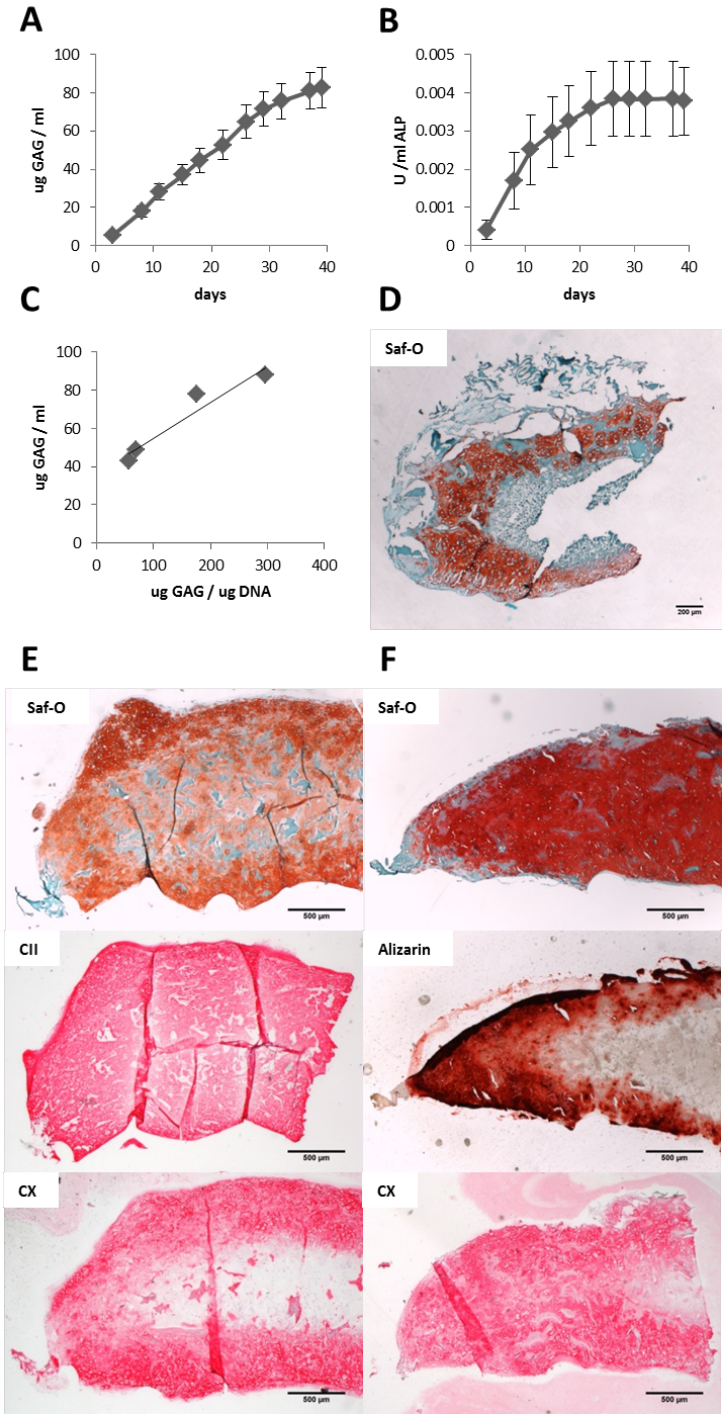

Figure 1: Generation of hypertrophic cartilagineous matrix in a 3D perfusion system. Donor R11. A: Cumulative secretion of glycosaminoglycans in supernatants of perfusion culture. B: Cumulative ALP activity in supernatants of perfusion culture. C: Correlation of secreted GAG and GAG / DNA ratio of the matrix. r = 0.96, P = 0.04. D: Safranin-O staining of 5 weeks static culture displaying typical central necrosis. Black bar represents 200 µm. G: Formation of pre-hypertrophic matrix after 3 weeks of culture. CII = collagen type 2 staining, CX = collagen type X staining. The peripheral presence of collagen type X suggests that the matrix is becoming hypertrophic. Black bar represents 500 µm. H: Hypertrophic matrix after 5 weeks of culture. Alizarin red staining shows peripheral calcification. Collagen type X staining is present throughout the matrix. Black bar represents 500µm.

The presence of central core necrosis was confirmed in static cultures of the same volume and cell number (Figure 1D). Histological analysis of perfusion cultures showed homogenous tissue formation without central core necrosis or fibrosis both in the chondrogenic and hypertrophic phases (Figure G and H). Already during the chondrogenic phase, deposition of both collagen type II and collagen type X could be observed, suggesting that the tissue already acquired hypertrophic traits. However, collagen type X was only found in the periphery of the constructs. After the hypertrophic phase, collagen type X was homogenously distributed and a calcified outer part was observed with Alizarin red staining. Even though the samples displayed dense matrix and calcification, perfusion did not seem to be affected during bioreactor culture.

Monitoring in non-homogenous cultures

Cultures with unsatisfactory secretion of GAG were stopped at different time points to analyse the formation of cartilaginous tissue (Figure 2A). The tissues in these cultures were found to be non-homogenous and the relative area of Safranin-O positive cartilaginous matrix was significantly correlated with the amount of GAG secretion ($P = 0.04$, Figure 2B and C). The non-homogenous tissue formation was connected to CD45 positive cells - possibly bone marrow-derived macrophages - which were present even after 3 passages on 2D plastic (Figure 2D). The number of CD45 positive cells was at least 2-fold higher in cultures where non-homogenous tissue had formed as opposed to cultures where homogenous tissue had formed ($P < 0.01$, Figure 2E). Indeed, histological analysis of non-homogenous tissue also revealed the presence of CD45 positive cells, as opposed to their complete absence in homogenous tissue (data not shown).

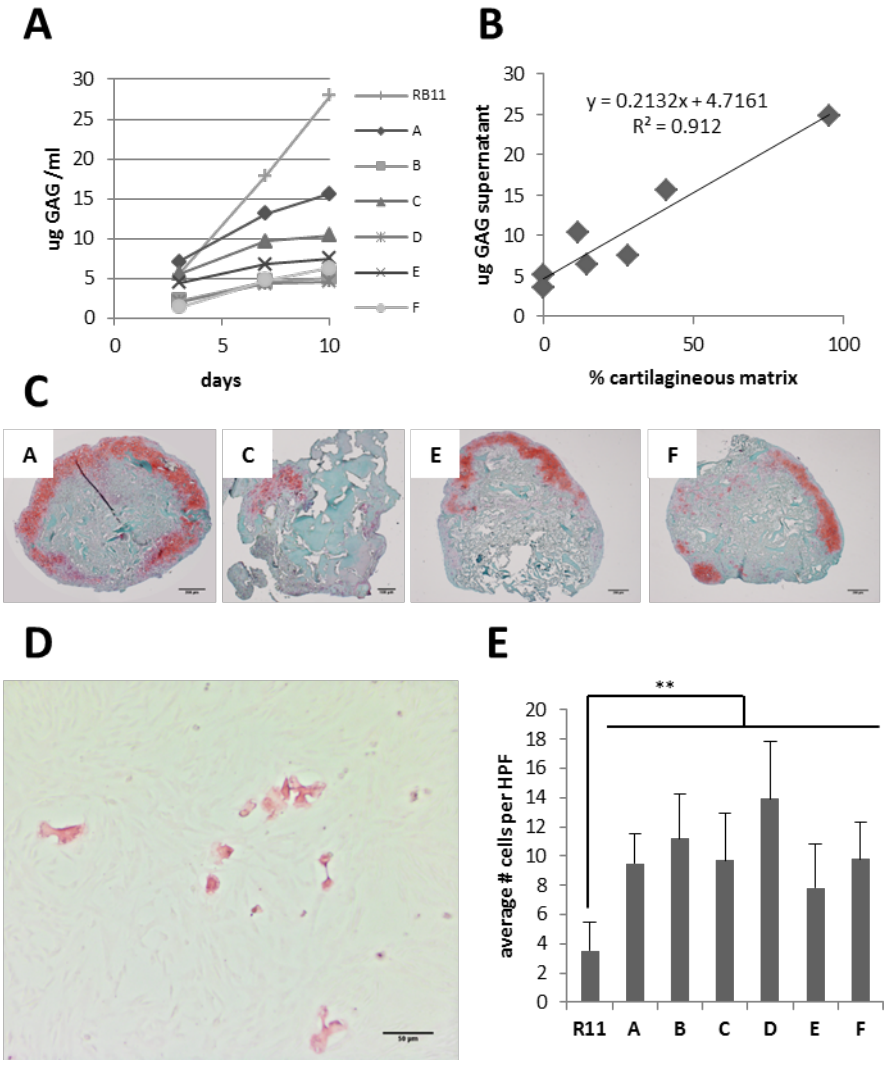

Figure 2: Monitoring in non-homogenous cultures. A: Representative GAG secretion for each donor, labelled A-F. Cultures were stopped at different times to evaluate cartilagineous matrix formation. B: Correlation of GAG secretion at 10 days an percenteage cartilaginous matrix. Each dot represents one donor. C: Representative Safranin-O stainings for each donor tested. The black bars represent 200µm in A, 100µm in C, 200µm in E, 200µm in F. D: Representative CD45 staining in a confluent rabbit BMSC culture at passage 3. Black bar represents 50µm. E: Quantification of CD45 positive cells in confluent cultures of rabbit BMSC donors. Average of 10 high-power fields (HPF, 40x magnification) for each donor. (**=P<0.01)

In vivo remodeling of hypertrophic cartilage from perfusion bioreactor cultures with best parameters

Implantation of hypertrophic cartilage with the best in vitro monitoring parameters lead to modest bone and bone marrow formation already after 8 weeks (Figure 3A). Large portions of the cartilaginous matrix were still present, even though they were no longer positive for GAG, suggesting

an on-going digestion and remodelling process. Indeed, staining for DIPEN, the cryptic epitope of aggrecan, which is exposed during cartilage remodelling, showed active areas of matrix breakdown. The same areas were also positive for MMP-9 and MMP-13, which are active during endochondral ossification.

After 12 weeks in vivo, the hypertrophic cartilage had nearly disappeared and been replaced by a vast bone marrow cavity, a thin surrounding bone lamina and few trabecular structures and calcified remnants of cartilage (Figure 3B). Again DIPEN staining displayed areas of ongoing cartilage degradation, which were however considerably reduced compared to 8 weeks. MMP-9 staining was much weaker and no MMP-13 staining was detected at this time point.

Microtomographic analysis also showed a significantly increased amount of bone after 12 weeks compared to 8 weeks ($p = 0.05$, Figure 3C). Due to the high resolution and tissue geometry, it was possible to separate bone lamina, calcified hypertrophic cartilage remnants and bone marrow cavity (Figure 3D). A comparison with normal mouse femurs showed that although bone volume by itself was modest, bone marrow volume was comparable to the bone marrow volume of the femur diaphysis (Figure 3E).

Figure 3: In vivo remodeling of hypertrophic cartilage from perfusion cultures with best parameters. Donor R11. A: Representative histological sections after 8 weeks in vivo. Large remaining volume of cartilagineous tissue depleeted of glycosaminoglycans is visible. HE = Haematoxylin & Eosin, Saf-O = Safranin-O staining, Masson = Masson tri-chrome staining, DIPEN = cryptic epitope of aggrecan staining. Black bars represent 500µm. B: Representative histological sections after 12 weeks in vivo. Thin bone lamina and some cartilagineous remnants surround large bone marrow space. C: Bone volume measured by microtomography after 8 and 12 weeks in vivo. (*=P<0.05) D: Microtomographical reconstruction displaying threshold for bone volume. Red pixels were counted as bone, grey and white pixels were counted as calcified cartilagineous remnants, black pixels enclosed in the convex volume defined by red pixels were counted as bone marrow. E: Bone volume (BV), bone marrow volume (BMV), residual volume (RV) compared to the bone volume and bone marrow volume (diaphysis only) of a normal mouse femur.

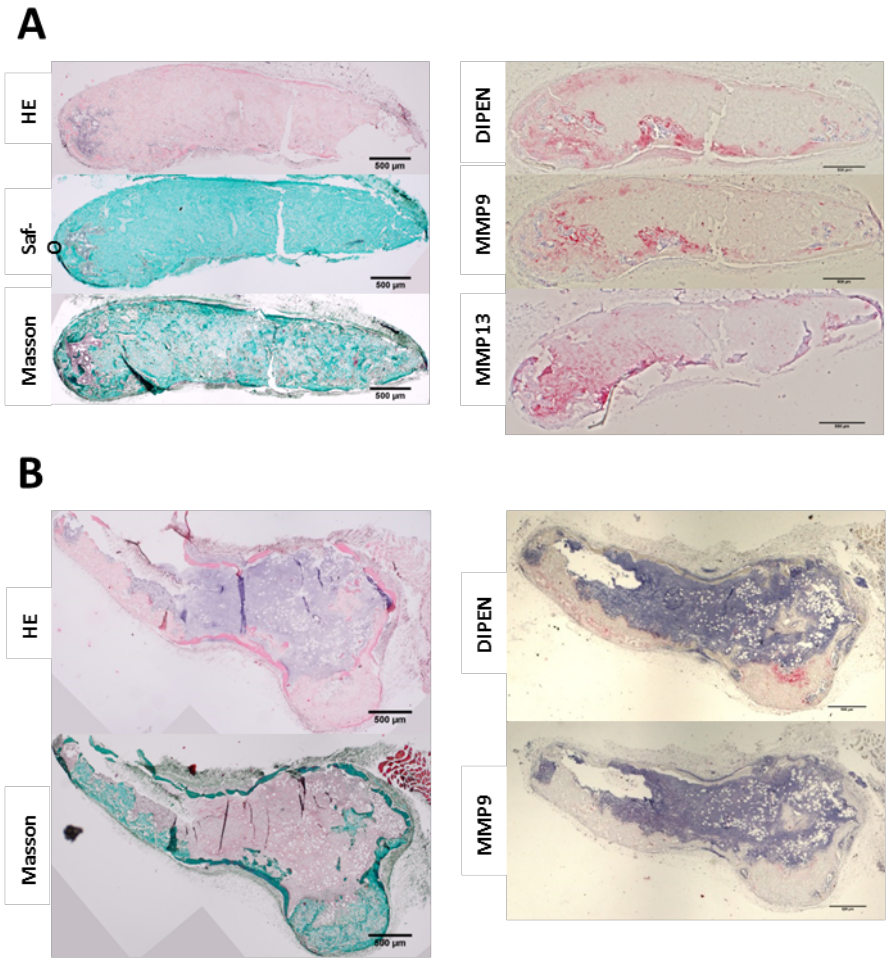
A
HE
Saf-O
Masson
DIPEN
MMP9
MMP13
B
HE
Masson
DIPEN
MMP9
C
mm3
3
2.5
2
1.5
1
0.5
0
*
8 weeks
12 weeks
D
0.5 mm
E
mm3
40
35
30
25
20
15
10
5
0
BV
BMV
RV
BV
BMV
Graft
Mouse Femur

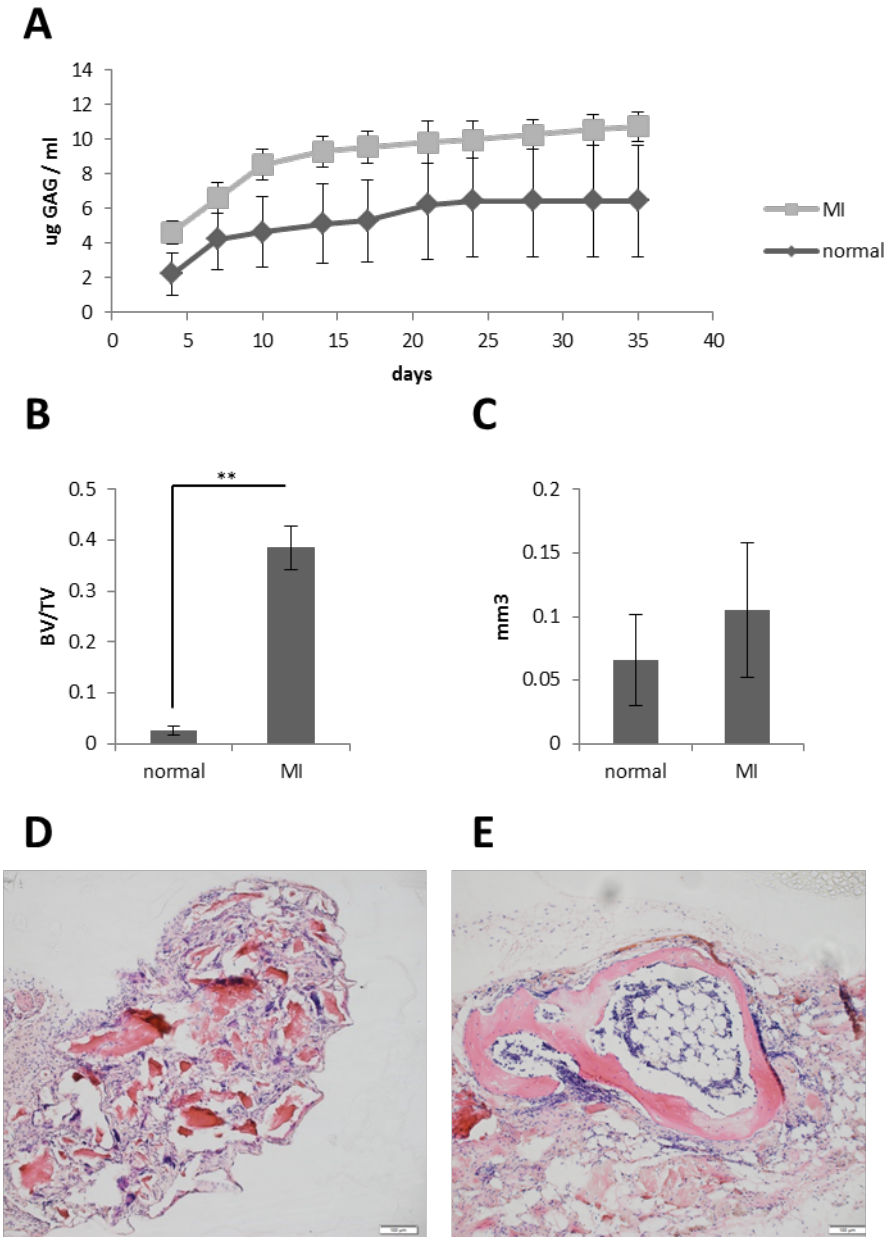

Figure 4: Cultures with worst parameters show improvement in vitro and in vivo with metalloproteinase inhibition. Donors A, E and F. A: Average GAG secretion is significantly higher and shows significantly less variation with Merimastat (MI) compared to normal culture. 3 donors with 3 replicates each were used. B: Bone volume fraction is significantly higher in samples cultured with MI. (**=P<0.01) C: Bone volume does not show a significant difference, though trend is higher. E: Representative HE staining of sample without MI. White bar represents 100µm. F: Representative HE staining of sample with MI. White bar represents 100µm.

Cultures with worst parameters show improvement in vitro and in vivo with metalloproteinase inhibition

We hypothesized that the CD45+ cells could represent bone marrow derived macrophages, which may secrete metalloproteinases to digest cartilage(25). Therefore, to improve tissue

formation, a general metalloproteinase inhibitor was added to the culture medium. Although GAG secretion in the supernatants did not reach the level of the best cultures, MMP inhibition did lead to a significant increase ($P<0.01$ for each time point) as well as decreased variability between replicates (Figure 4A). After 12 weeks in vivo, Bone volume fraction was significantly greater ($P<0.01$) in samples cultured under MMP inhibition, though absolute bone volume was not significantly different (Figure 4B and C). Histological evaluation showed that although in both conditions dense eosin-positive tissue formed, only MMP inhibition lead to bone marrow formation (Figure 4D and E).

Correlation of in vitro parameters with in vivo bone volume

Finally, GAG and ALP content in supernatants during the culture period were correlated to the bone volume after 12 weeks in vivo as measured by microtomography in mm^3. For both parameters, the sum over all time points and single peak values after 7 days of culture significantly correlated with bone volume (Table 1).

	total GAG	7 day GAG	total ALP	7 day ALP
rho	0.93	0.92	0.83	0.91
R2	0.87	0.85	0.69	0.82
P	<0.0001	<0.0001	<0.0001	<0.0001

Table 1: Correlation of in vitro parameters with in vivo bone volume. Absolute bone volumes (in mm3) measured by microtomogrpahy were correlated to in vitro paramter of 4 donors with 3-4 replicates each (Donors R11, A, E, F).

Discussion

In this study we have showed that perfusion bioreactor based culture of rabbit BMSC on a collagen type I scaffold can lead to formation of homogenous hypertrophic cartilage. Measurement of glycosaminoglycans and alkaline phosphatase during medium change allows at-line-monitoring and can be correlated to the GAG content and percentage of cartilage area of the resulting tissue.

More importantly, we could correlate our monitoring parameters with in vivo bone formation after 12 weeks.

In view of the principles proposed by Lourenco et al(16) and Gardel et al(17) we have shown that relevant real-time monitoring is possible in perfusion culture of engineered hypertrophic cartilage. Since the parameters involve sampling of the supernatant, they cannot be considered as “online”, although it is possible to develop sensors for actual online measurement(18). However, both proposed parameters can be measured in less than 2 hours and accumulate gradually in between medium changes. Based on this, one can rapidly judge the wellbeing of the culture by using measurements before each medium change. Other proposed parameters such as alamar blue for cell growth and viability(26), O_2 and $CO_{2(27)}$ or pH(28) would also allow culture monitoring. In our specific bioprocess however, the function of hypertrophic cartilage crucially depends on the amount and quality of extracellular matrix(29-31) and features the apoptosis of hypertrophic chondrocytes at later maturity stages(29, 32). It is therefore not possible to rely on cell metabolism alone in order to predict the outcome of the culture.

In the context of bioreactors both glycosaminoglycan content as a surrogate for cartilage formation(18) and alkaline phosphatase as a surrogate for ossification(17) have been measured in the tissues at the end of culture. In both cases, the aim has been to show that perfusion cultures can improve these parameters compared to static cultures. However, the same parameters have not been up to now used in supernatants to non-invasively monitor cultures and predict in vivo performance. Glycosaminoglycans are crucial components of the cartilage matrix, giving it mechanical stability due to the Donnan ion distribution law(18) and thus being intimately tied to the size of the wet tissue. However, they also bind diverse signaling molecules such as FGF(33), Wnt, BMP, Ihh and others(34-36) and could represent a surrogate measure for the content of these molecules in the matrix. Alkaline phosphatase is found in several tissues(37). It exerts one of its main functions in bone, where it guides mineralization in a membrane bound form both on osteoblasts

and on small vesicles(38). Already Kato et al(39) could show that micromass cultures of rabbit growth plate chondrocytes forming hypertrophic cartilage display alkaline phosphatase activity that correlates with collagen type X production. The enzyme is accepted as a crucial part of the endochondral ossification process during cartilage matrix calcification(29).

The use of rabbit cells in our study was motivated by the necessity for a future pre-clinical model. Although orthotopic implantation of engineered hypertrophic cartilage has been performed in rats and mice, larger animal models such as rabbits, sheep, goats or pigs are required. Rabbits are the least expensive and easiest to handle and allow a variety of clinically relevant set-ups including very challenging segmental defects(19). Also rabbit bone marrow stromal cells are known to form cartilaginous tissue without the requirement to sort specific sub-populations(40). To our knowledge, this is the first description of bone formation from hypertrophic cartilage produced in a bioreactor by rabbit MSC. The variability of cartilage formation with different rabbit donors is in line with observations in human MSCs(6). Although in principle xenogenic tissue can be used in clinics, for future studies we aim to verify our monitoring parameters in human cultures as well. Based on the similarity of hypertrophic cartilage and in vivo bone formation, we expect a high transferability.

The detection of GAG was significantly correlated with final tissue GAG/DNA ratio and percentage of cartilaginous area in non-homogenous cultures. This opens the possibility to obtain information on the quality of the tissues in a perfusion bioreactor culture in a non-destructive manner. 6 of the 7 donors we analysed did not form completely homogenous tissue, which could be explained by the presence of CD45+ bone marrow derived macrophages, which are known for metalloproteinase-mediated cartilage digestion(25). Thus, the inhibition of metalloproteinases(41) improved GAG secretion and in vivo performance of the bioreactor cultures. It has not been shown that CD45+ cells from rabbit bone marrow can be co-cultured with MSC and extensively passaged under the conditions chosen in this study. Although CD45 is a pan hematopoietic marker, the most likely candidate cells, which can attach to culture plastic and are found in MSC cultures of other

species, are macrophages(42). However, no CD45+ cells have been described in expanded human MSC using similar conditions.

Most intriguingly, both GAG and ALP were strongly correlated with the in vivo bone formation. One has to keep in mind that the process of endochondral ossification requires the complete remodelling of hypertrophic cartilage(29). Therefore, our proposed monitoring parameters give insight not only into the integrity of the culture, but also into further tissue maturation and remodelling in vivo. To our knowledge, this is the first work showing this type of correlation and providing surrogate measures to judge final in vivo performance.

Future application of hypertrophic cartilage as a bone substitute material will require large-scale production to meet clinical demands. Bioreactor-based production could offer many advantages such as an increased tissue size, improved reproducibility and easier handling. Monitoring will allow identification of the tissues (from different donors and/or experimental replicates) capable to efficiently induce bone formation. Consequently, the otherwise extensive in vivo testing could be significantly reduced.

Conclusion

This present study identified and analyzed two monitoring parameters, GAG and ALP, in the supernatants of perfusion bioreactor based cultures of engineered hypertrophic cartilage. A correlation of the monitoring parameters to tissue quality and also to in vivo bone formation was presented. The results of this study can be used to improve the future efficiency, productivity, reproducibility and most importantly quality of this type of culture.

Acknowledgement

The AO Foundation (AO S-11-13P) and the Swiss National Science Fund (Grant 310030_133110) supported this study. We thank Waldemar Hoffmann, Ralph Dühr and David Wendt for their technical support.

References

1. Chang SC, Tai CL, Chung HY, Lin TM, & Jeng LB (2009) Bone marrow mesenchymal stem cells form ectopic woven bone in vivo through endochondral bone formation. *Artificial organs* 33(4):301-308.
2. Scotti C*, et al.* (2010) Recapitulation of endochondral bone formation using human adult mesenchymal stem cells as a paradigm for developmental engineering. *Proceedings of the National Academy of Sciences of the United States of America* 107(16):7251-7256.
3. Janicki P, Kasten P, Kleinschmidt K, Luginbuehl R, & Richter W (2010) Chondrogenic pre-induction of human mesenchymal stem cells on beta-TCP: enhanced bone quality by endochondral heterotopic bone formation. *Acta biomaterialia* 6(8):3292-3301.
4. Farrell E*, et al.* (2011) In-vivo generation of bone via endochondral ossification by in-vitro chondrogenic priming of adult human and rat mesenchymal stem cells. *BMC musculoskeletal disorders* 12:31.
5. Kuhn LT*, et al.* (2014) Developmental-like bone regeneration by human embryonic stem cell-derived mesenchymal cells. *Tissue engineering. Part A* 20(1-2):365-377.
6. van der Stok J*, et al.* (2014) Chondrogenically differentiated mesenchymal stromal cell pellets stimulate endochondral bone regeneration in critical-sized bone defects. *European cells & materials* 27:137-148; discussion 148.
7. Harada N*, et al.* (2014) Bone regeneration in a massive rat femur defect through endochondral ossification achieved with chondrogenically differentiated MSCs in a degradable scaffold. *Biomaterials* 35(27):7800-7810.
8. Sheehy EJ*, et al.* (2015) Tissue Engineering Whole Bones Through Endochondral Ossification: Regenerating the Distal Phalanx. *BioResearch open access* 4(1):229-241.
9. Bahney CS*, et al.* (2014) Stem cell-derived endochondral cartilage stimulates bone healing by tissue transformation. *Journal of bone and mineral research : the official journal of the American Society for Bone and Mineral Research* 29(5):1269-1282.
10. Cunniffe GM*, et al.* (2015) Porous decellularized tissue engineered hypertrophic cartilage as a scaffold for large bone defect healing. *Acta biomaterialia* 23:82-90.
11. Scotti C*, et al.* (2013) Engineering of a functional bone organ through endochondral ossification. *Proceedings of the National Academy of Sciences of the United States of America* 110(10):3997-4002.
12. Hoffmann W, Feliciano S, Martin I, de Wild M, & Wendt D (2015) Novel Perfused Compression Bioreactor System as an in vitro Model to Investigate Fracture Healing. *Frontiers in bioengineering and biotechnology* 3:10.
13. Wendt D, Marsano A, Jakob M, Heberer M, & Martin I (2003) Oscillating perfusion of cell suspensions through three-dimensional scaffolds enhances cell seeding efficiency and uniformity. *Biotechnology and bioengineering* 84(2):205-214.
14. Wendt D, Stroebel S, Jakob M, John GT, & Martin I (2006) Uniform tissues engineered by seeding and culturing cells in 3D scaffolds under perfusion at defined oxygen tensions. *Biorheology* 43(3-4):481-488.
15. Kock LM, Malda J, Dhert WJ, Ito K, & Gawlitta D (2014) Flow-perfusion interferes with chondrogenic and hypertrophic matrix production by mesenchymal stem cells. *J Biomech* 47(9):2122-2129.
16. Lourenco ND, Lopes JA, Almeida CF, Sarraguca MC, & Pinheiro HM (2012) Bioreactor monitoring with spectroscopy and chemometrics: a review. *Analytical and bioanalytical chemistry* 404(4):1211-1237.

17. Gardel LS, Serra LA, Reis RL, & Gomes ME (2014) Use of perfusion bioreactors and large animal models for long bone tissue engineering. *Tissue Eng Part B Rev* 20(2):126-146.
18. Schulz RM & Bader A (2007) Cartilage tissue engineering and bioreactor systems for the cultivation and stimulation of chondrocytes. *European biophysics journal : EBJ* 36(4-5):539-568.
19. Kaempfen A*, et al.* (2015) Engraftment of Prevascularized, Tissue Engineered Constructs in a Novel Rabbit Segmental Bone Defect Model. *International journal of molecular sciences* 16(6):12616-12630.
20. Barbosa I*, et al.* (2003) Improved and simple micro assay for sulfated glycosaminoglycans quantification in biological extracts and its use in skin and muscle tissue studies. *Glycobiology* 13(9):647-653.
21. Burstone MS (1958) Histochemical demonstration of acid phosphatases with naphthol AS-phosphates. *Journal of the National Cancer Institute* 21(3):523-539.
22. Schneider CA, Rasband WS, & Eliceiri KW (2012) NIH Image to ImageJ: 25 years of image analysis. *Nature methods* 9(7):671-675.
23. Doube M*, et al.* (2010) BoneJ: Free and extensible bone image analysis in ImageJ. *Bone* 47(6):1076-1079.
24. Sheets KG*, et al.* (2013) Microglial ramification and redistribution concomitant with the attenuation of choroidal neovascularization by neuroprotectin D1. *Molecular vision* 19:1747-1759.
25. Hauser P & Vaes G (1978) Degradation of cartilage proteoglycans by a neutral proteinase secreted by rabbit bone-marrow macrophages in culture. *The Biochemical journal* 172(2):275-284.
26. Gloeckner H, Jonuleit T, & Lemke HD (2001) Monitoring of cell viability and cell growth in a hollow-fiber bioreactor by use of the dye Alamar Blue. *Journal of immunological methods* 252(1-2):131-138.
27. Kamen AA, Bedard C, Tom R, Perret S, & Jardin B (1996) On-line monitoring of respiration in recombinant-baculovirus infected and uninfected insect cell bioreactor cultures. *Biotechnology and bioengineering* 50(1):36-48.
28. Jeevarajan AS, Vani S, Taylor TD, & Anderson MM (2002) Continuous pH monitoring in a perfused bioreactor system using an optical pH sensor. *Biotechnology and bioengineering* 78(4):467-472.
29. Mackie EJ, Ahmed YA, Tatarczuch L, Chen KS, & Mirams M (2008) Endochondral ossification: how cartilage is converted into bone in the developing skeleton. *The international journal of biochemistry & cell biology* 40(1):46-62.
30. Ortega N, Wang K, Ferrara N, Werb Z, & Vu TH (2010) Complementary interplay between matrix metalloproteinase-9, vascular endothelial growth factor and osteoclast function drives endochondral bone formation. *Disease models & mechanisms* 3(3-4):224-235.
31. Bourgine PE*, et al.* (2014) Osteoinductivity of engineered cartilaginous templates devitalized by inducible apoptosis. *Proceedings of the National Academy of Sciences of the United States of America* 111(49):17426-17431.
32. Mackie EJ, Tatarczuch L, & Mirams M (2011) The skeleton: a multi-functional complex organ: the growth plate chondrocyte and endochondral ossification. *The Journal of endocrinology* 211(2):109-121.
33. Gandhi NS & Mancera RL (2008) The structure of glycosaminoglycans and their interactions with proteins. *Chemical biology & drug design* 72(6):455-482.
34. Lin X (2004) Functions of heparan sulfate proteoglycans in cell signaling during development. *Development* 131(24):6009-6021.
35. Cuellar A & Reddi AH (2013) Cell biology of osteochondromas: bone morphogenic protein signalling and heparan sulphates. *Int Orthop* 37(8):1591-1596.
36. Jochmann K, Bachvarova V, & Vortkamp A (2014) Heparan sulfate as a regulator of endochondral ossification and osteochondroma development. *Matrix Biol* 34:55-63.

37. Sharma U, Pal D, & Prasad R (2014) Alkaline phosphatase: an overview. *Indian journal of clinical biochemistry : IJCB* 29(3):269-278.
38. Hessle L*, et al.* (2002) Tissue-nonspecific alkaline phosphatase and plasma cell membrane glycoprotein-1 are central antagonistic regulators of bone mineralization. *Proceedings of the National Academy of Sciences of the United States of America* 99(14):9445-9449.
39. Kato Y, Iwamoto M, Koike T, Suzuki F, & Takano Y (1988) Terminal differentiation and calcification in rabbit chondrocyte cultures grown in centrifuge tubes: regulation by transforming growth factor beta and serum factors. *Proceedings of the National Academy of Sciences of the United States of America* 85(24):9552-9556.
40. Koga H*, et al.* (2008) Comparison of mesenchymal tissues-derived stem cells for in vivo chondrogenesis: suitable conditions for cell therapy of cartilage defects in rabbit. *Cell and tissue research* 333(2):207-215.
41. Sinno M*, et al.* (2013) The matrix metalloproteinase inhibitor marimastat promotes neural progenitor cell differentiation into neurons by gelatinase-independent TIMP-2-dependent mechanisms. *Stem cells and development* 22(3):345-358.
42. Eslaminejad MB, Nikmahzar A, Taghiyar L, Nadri S, & Massumi M (2006) Murine mesenchymal stem cells isolated by low density primary culture system. *Development, growth & differentiation* 48(6):361-370.

Chapter 3

Osteoinductivity of engineered cartilaginous templates devitalized by inducible apoptosis

PDF of the paper published 2014 in PNAS 111(49):17426-17431

Osteoinductivity of engineered cartilaginous templates devitalized by inducible apoptosis

Paul E. Bourgine[a,b], Celeste Scotti[a,b,c], Sebastien Pigeot[a,b], Laurent A. Tchang[a,b], Atanas Todorov[a,b], and Ivan Martin[a,b,1]

[a]Department of Surgery and [b]Department of Biomedicine, University Hospital Basel, University of Basel, 4031 Basel, Switzerland; and [c]IRCCS Istituto Ortopedico Galeazzi, via R. Galeazzi 4, 20161 Milano, Italy

Edited by Robert Langer, Massachusetts Institute of Technology, Cambridge, MA, and approved October 30, 2014 (received for review July 1, 2014)

The role of cell-free extracellular matrix (ECM) in triggering tissue and organ regeneration has gained increased recognition, yet current approaches are predominantly based on the use of ECM from fully developed native tissues at nonhomologous sites. We describe a strategy to generate customized ECM, designed to activate endogenous regenerative programs by recapitulating tissue-specific developmental processes. The paradigm was exemplified in the context of the skeletal system by testing the osteoinductive capacity of engineered and devitalized hypertrophic cartilage, which is the primordial template for the development of most bones. ECM was engineered by inducing chondrogenesis of human mesenchymal stromal cells and devitalized by the implementation of a death-inducible genetic device, leading to cell apoptosis on activation and matrix protein preservation. The resulting hypertrophic cartilage ECM, tested in a stringent ectopic implantation model, efficiently remodeled to form de novo bone tissue of host origin, including mature vasculature and a hematopoietic compartment. Importantly, cartilage ECM could not generate frank bone tissue if devitalized by standard "freeze & thaw" (F&T) cycles, associated with a significant loss of glycosaminoglycans, mineral content, and ECM-bound cytokines critically involved in inflammatory, vascularization, and remodeling processes. These results support the utility of engineered ECM-based devices as off-the-shelf regenerative niches capable of recruiting and instructing resident cells toward the formation of a specific tissue.

developmental engineering | endochondral | osteoinductive | extracellular matrix | hematopoisesis

The clinical gold standard solution to critical bone defects consists of autologous bone transplantation. However, it is associated with severe donor site morbidity, risks for infection, and limited availability of the material (1, 2). Off-the-shelf synthetic or naturally derived bone substitute materials (e.g., ceramics, collagen) allow bypassing of these issues (3) but have reduced regenerative potency, especially in challenging scenarios (e.g., atrophic nonunions, comminuted fractures, large substance loss, compromised environment). Cell-based approaches could introduce a superior biological functionality, but their clinical use remains rather limited (4), predominantly because of their nonpredictable effectiveness combined with their economic, logistic, and interpatient variability issues (5, 6).

Modern approaches to bone tissue engineering aim at triggering regenerative processes by matching the corresponding developmental program and thus recapitulating the embryonic stages of bone tissue development (7). During embryonic development, long bones typically develop by endochondral ossification, a process involving the formation and subsequent remodeling of a hypertrophic cartilage template (8). Following the principles of "developmental engineering," the process of endochondral ossification has been successfully reproduced using embryonic stem cells (9) and human mesenchymal stromal cells (hMSCs) (10–12). A further step was achieved with the upscaling of the graft size, leading not only to the successful formation of large bone tissue but also to the development of a mature organ that includes a fully mature hematopoietic compartment (13).

The increased recognition of the potency of the extracellular matrix (ECM)-derived materials in regenerative processes (14) led us to investigate whether a living cell compartment is strictly required or whether the endochondral route could be initiated by a cell-free ECM, represented by a devitalized hypertrophic template. Addressing this question may lead to a better understanding of the elements regulating the endochondral ossification process and to the generation of cell-based but cell-free off-the-shelf materials capable of instructing host osteoprogenitors toward bone formation. A devitalized approach to endochondral ossification has been envisioned from the beginning of the research in this field (9, 10), as it would bypass the complexity of delivering living cells of possibly autologous origin, but it has never been realized to date.

Existing studies converge on the importance of preserving ECM integrity to elicit the desired regenerative effect (15–17). This implies the use of a devitalization strategy reducing alterations in the composition and architecture of the generated template to mimic both the physiologic regenerative milieu and the 3D structure of the fracture callus. Toward this objective, a devitalization approach has been proposed via the induction of apoptosis (18). In particular, an inducible genetic system (19) can be incorporated into primary hMSCs to specifically induce their apoptosis on exposure to a clinical-grade chemical compound. This strategy offers the possibility to generate hypertrophic cartilage templates that can be subsequently devitalized with, theoretically, minimal changes in the ECM.

Significance

It has been previously reported that hypertrophic cartilage tissues engineered from human mesenchymal stromal cells can efficiently remodel in vivo into bone organs, recapitulating developmental steps of endochondral ossification. We have here demonstrated that the extracellular matrix (ECM) of such engineered cartilage, even in the absence of a living cell component, retains frankly osteoinductive properties. The use of an apoptosis-driven devitalization technique revealed the importance of preserving the ECM integrity and, in particular, the embedded factors to trigger the regenerative process. Although exemplified in a skeletal context, our work outlines the general paradigm of cell-based but cell-free off-the-shelf materials capable of activating endogenous cells toward the formation of specific tissues.

Author contributions: P.E.B., C.S., and I.M. designed research; P.E.B., C.S., S.P., L.A.T., and A.T. performed research; P.E.B. contributed new reagents/analytic tools; P.E.B., C.S., S.P., and A.T. analyzed data; and P.E.B. and I.M. wrote the paper.

The authors declare no conflict of interest.

This article is a PNAS Direct Submission.

[1]To whom correspondence should be addressed. Email: ivan.martin@usb.ch.

This article contains supporting information online at www.pnas.org/lookup/suppl/doi:10.1073/pnas.1411975111/-/DCSupplemental.

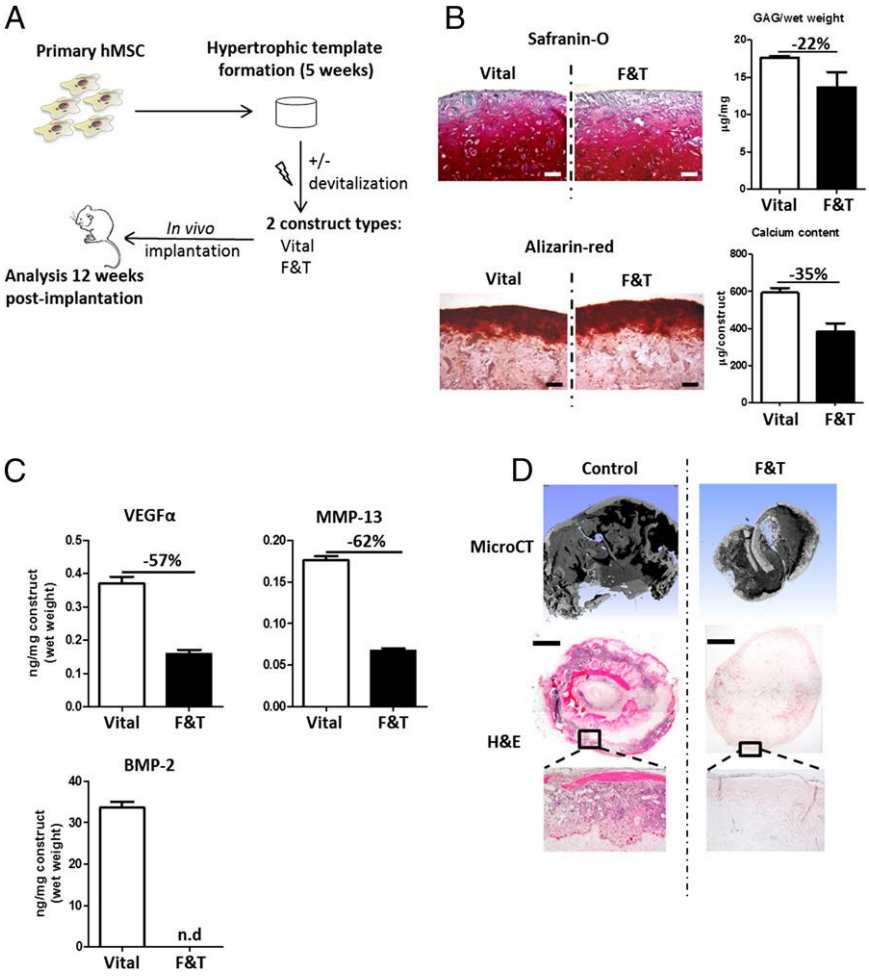

Fig. 1. Assessment of the osteoinductive properties of living (*Vital*) and F&T (*F&T*) devitalized engineered hypertrophic cartilage constructs. (*A*) Experimental scheme for the generation of hypertrophic tissues starting from hMSCs, devitalized and subsequently implanted in nude mice. (*B*) Representative sections of in vitro (5 wk) generated hypertrophic cartilage samples and the effect of the F&T treatment on the GAGs and calcium content ($n = 3$). (Scale bars, 100 µm.) (*C*) Effect of the F&T devitalization on the content of VEGF-α, BMP-2, and MMP-13 protein. (*D*) 3D reconstruction of microtomographic images (MicroCT) and hematoxylin and eosin (H&E) stained representative sections of samples retrieved 12 wk after ectopic implantation in nude mice ($n = 3$). (Scale bars, 1 mm.) Error bars represent SEMs of $n = 3$ measurements.

In this study, we aimed to induce de novo bone organ formation, using cell-free hypertrophic cartilage templates devitalized by apoptotic induction. We hypothesized that the preservation of the ECM integrity, serving as a reservoir of multiple growth factors at physiological levels, is a key prerequisite to recruiting and instructing endogenous progenitors to initiate bone regeneration.

Results

Assessment of the Osteoinductive Properties of Freeze & Thaw Devitalized Constructs. As a first attempt, we tested whether hypertrophic cartilage templates, engineered according to a previously established protocol (13) and devitalized by standard "freeze & thaw" (F&T) treatment, are capable of inducing bone formation (Fig. 1*A*). F&T is a well-established physical devitalization method efficiently leading to cell bursting and limited ECM alteration (20, 21). Primary hMSCs were then seeded at high density on cylindrical collagen meshes (8 mm diameter, 4 mm thickness) and cultured for 3 wk in chondrogenic medium, followed by 2 wk of hypertrophic medium. The resulting grafts successfully displayed the typical pattern of a hypertrophic cartilaginous tissue, consisting of a glycosaminoglycan (GAG)-rich core surrounded by a mineralized ring (*Vital*; Fig. 1*B*). Some constructs were subsequently devitalized, using a recognized method consisting of three F&T cycles followed by a bath in hypertonic solution (*F&T*) (22), leading to the absence of human living cells after implantation (Fig. S1*A*). The *F&T* constructs were still positively stained for GAG and mineral deposits, but quantitative assessments indicated a marked reduction in the wet weight percentage of GAG (−22%) and mineral content (−35%) (Fig. 1*B*). The F&T treatment also reduced the amount of growth factors that are known to play a critical role in hypertrophic cartilage remodeling into bone, including VEGFα (−57%), matrix metalloproteinase 13 (MMP-13; −62%), and bone morphogenetic protein 2 (BMP-2; below detection level; Fig. 1*C*).

On ectopic implantation in nude mice for 12 wk, *Vital* samples were macroscopically colonized by blood cells, in contrast to *F&T* tissues (Fig. S1*B*). *Vital* samples were extensively remodeled, resulting in interconnected mineralized bone trabeculae embedding bone marrow elements (Fig. 1*D*), with minimal cartilage residuals (Fig. S1*B*). In contrast, the retrieved *F&T* samples maintained an outer shell of calcified matrix and abundant remnants of devitalized cartilage, with no evidences of bone or bone marrow formation (Fig. 1*D* and Fig. S1*B*). The failure of *F&T* devitalized hypertrophic constructs to remodel and induce bone formation could be attributed to the absence of living cells within the implanted graft and/or the effect of the devitalization process, leading to a loss of osteoinductive (e.g., BMP-2), angiogenic (e.g., VEGFα), and remodeling (e.g., MMP-13) factors.

Generation of Hypertrophic Constructs Using Death-Inducible hMSCs. To assess whether a better-preserved devitalized hypertrophic ECM can induce endochondral bone formation, we introduced the strategy of devitalization by apoptosis induction (Fig. S2), which was previously proposed to target the living cell fraction with minimal changes in the ECM components (18). Primary hMSCs were thus retrovirally transduced with a death system based on the inducible dimerization of modified caspase 9 (iDS; Fig. S2*A*). To ensure the maximum cell death on induction, the

population was purified on the basis of the expression of the CD19 reporter surface marker (Fig. 2*A*). This allowed for the generation of hMSC-iDS capable of being efficiently induced toward apoptosis in 2D culture (>97%; Fig. 2*B*) by adding the soluble inducer in the culture media. hMSC-iDS could generate hypertrophic cartilage tissues similar to the untransduced cells, as assessed by histological stainings (Fig. 2*C*) and gene expression analysis showing successful induction of chondrogenic and hypertrophic genes (Fig. 2*D*). Hence, the gain of the inducible-apoptosis function did not impair the chondrogenic differentiation and subsequent hypertrophy of hMSC-iDS. Importantly, hMSC-iDS hypertrophic templates continued to express the iDS, as revealed by CD19 immunostaining (Fig. 2*C*), suggesting the possibility of devitalizing the engineered graft by activation of the system.

Devitalization by Apoptosis Induction of Hypertrophic Cartilaginous Templates. Treatment of hypertrophic constructs by *F&T* or apoptosis induction (*Apoptized*) allowed for an effective devitalization, leading to, respectively, 91% and 93% cell killing efficiency, as assessed by flow cytometry measurement of propidium iodide (PI) and annexin V staining (Fig. 3*A*). Conversely, most of the cells from the *Vital* group remained viable (16% of annexin V/PI positivity; Fig. 3*A*). Because the assay measures the apoptosis-driven extracellular translocation of annexin V, the measured cell death is not biased by the reported natural expression of annexin V by chondrocytes (23); in particular, during their mineralization phase (24). Histologic analyses indicated the successful activation of the apoptotic pathway, with clear morphologic evidence of cell and nuclear fragmentation (late stage of apoptosis) throughout *Apoptized* and *F&T* constructs, further confirmed by the presence of cleaved caspase 3 in nucleated cells (Fig. 3*B*). In the *Vital* group, apoptotic cells were mainly found within the hypertrophic outer ring. Luminex-based analysis showed, in *Apoptized* samples, the overall maintenance of factors involved in inflammation [monocyte chemoattractant protein-1 (MCP-1), macrophage colony-stimulating factor (M-CSF), IL-8], angiogenesis (VEGFα), and remodeling [MMP-13, osteoprotegerin (OPG)] processes, with levels similar to those of the *Vital* group. Instead, *F&T* treatment resulted in a severe impairment of ECM composition, with a significant loss in IL-8 (64.9%; $P < 0.0001$), MCP-1 (49.4%; $P = 0.0388$), OPG (37%; $P = 0.0015$), VEGFα (58.7%; $P < 0.0001$), and MMP-13 (32.1%; $P = 0.0307$) compared with the protein content in the *Vital* constructs. Thus, although the two devitalization methods led to a similar killing of the cells, the induction of apoptosis allowed for a better preservation of representative ECM components.

In Vivo Assessment of Hypertrophic Cartilaginous Templates. To assess whether a better-preserved acellular ECM is sufficient to induce vascularization and endochondral bone formation, *Apoptized*, *F&T*, and *Vital* templates were implanted ectopically in immunodeficient mice. On retrieval, samples displayed distinct morphologic patterns. Colonization by host blood cells was evident in *Vital* samples and, to a lower extent, in *Apoptized* ones, whereas *F&T* samples did not display macroscopic evidence of vascularization (Fig. 4*A*). Confocal microscopy confirmed these macroscopic observations, as *Vital* and *Apoptized* samples showed the presence of a mature vasculature characterized by CD31+ vessels stabilized by pericytic cells (NG2 staining; Fig. 4*B* and Fig. S3*A*). In contrast, *F&T* samples were marked by the absence of either cells or blood vessels within the constructs. Collectively, these data indicate the successful recruitment of the host vasculature by *Apoptized*, but not by *F&T* constructs, a prerequisite for the recapitulation of the endochondral ossification route.

Samples were further processed to investigate the presence of bone, cartilage, and bone marrow tissue. Remarkably, *Vital* and *Apoptized* samples, in strong contrast to *F&T* constructs, underwent

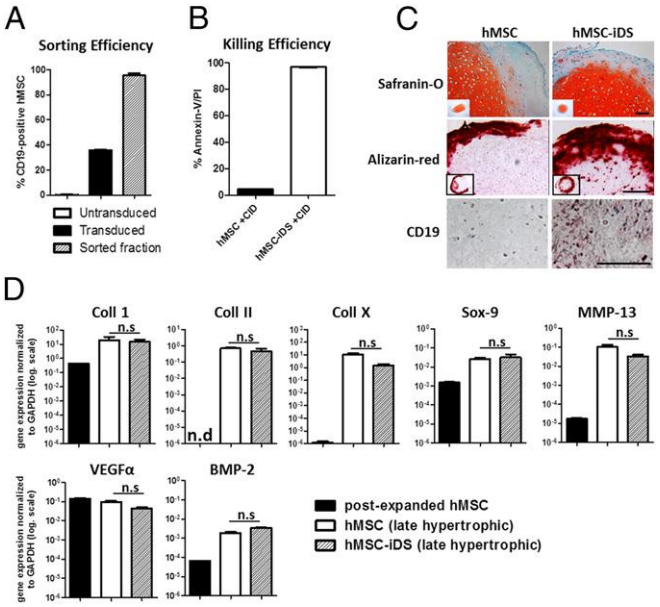

Fig. 2. Generation of hypertrophic constructs using death-inducible hMSCs. (*A*) Flow cytometry measurements of the CD19 (iDS reporter marker) expression by primary hMSC (Untransduced) after iDS retroviral transduction (Transduced) and subsequent enrichment using magnetic beads (Sorted fraction, hMSC-iDS) ($n = 5$). (*B*) Assessment of the efficiency of hMSC-iDS apoptosis induction in 2D culture on overnight exposure to the soluble inducer (+chemical inducer of dimerization) ($n = 4$). (*C*) Histologic sections of in vitro constructs (5 wk) generated by primary untransduced hMSCs and hMSC-iDS displayed a similar hypertrophic cartilage pattern (Safranin-O and Alizarin-red stainings). (Scale bars = 100 μm.) Only the hMSC-iDS expressed the iDS (CD19 immunostaining). (Scale bar = 50 μm.) (*D*) Gene expression analysis of hypertrophic templates generated by hMSCs and hMSC-iDS. Error bars represent SEMs of $n \geq 4$ measurements.

intense remodeling, giving rise after 12 wk to bone structures, including bone marrow spaces (Fig. 5*A*). Interestingly, although cortical external structures were observed in *Vital* and *Apoptized* groups, only *Vital* specimens displayed inner bone trabeculae (Fig. S3 *B* and *C*). The amount of mineralized tissue quantified after segmentation of micro-computerized tomography images was highest in the *Vital* specimens, followed by the *Apoptized* ones (Fig. S3*D*). However, as this technique does not allow discriminating between calcified cartilage and frank bone tissue, more specific quantification of the tissue types in the different groups was carried out, using histological sections. Histomorphometric analysis indicated in *Vital* samples the predominant formation of bone and bone marrow tissues (respectively, 24.9% and 32%), whereas cartilaginous regions were negligible (2%; Fig. 5*B*). *Apoptized* samples displayed a significantly higher bone (14.8%) and bone marrow formation (5.7%) than *F&T* samples (1.5% bone, 0.2% marrow). The latter, in turn, contained the highest percentage of cartilage remnants, confirming the limited efficiency of the remodeling process (Fig. 5*B*).

Ossicles of *Vital* and *Apoptized* constructs were characterized by the presence of osterix and tartrate-resistant-acid-phosphatase-expressing cells, respectively, representing osteoblastic and osteoclastic lineages (Fig. 5*C*). Those cells were predominantly lining the edges of the bone marrow regions, suggesting their involvement in tissue remodeling for marrow colonization. In *Vital* constructs, human cells participated in the bone formation, as assessed by the presence of cells positive for human Alu repeats among nucleated cells (Fig. 5*C*). In contrast, no human cells could be detected within *Apoptized* samples, so the formation of perichondral bone could only be attributed to host osteoprogenitors. *F&T* samples were also

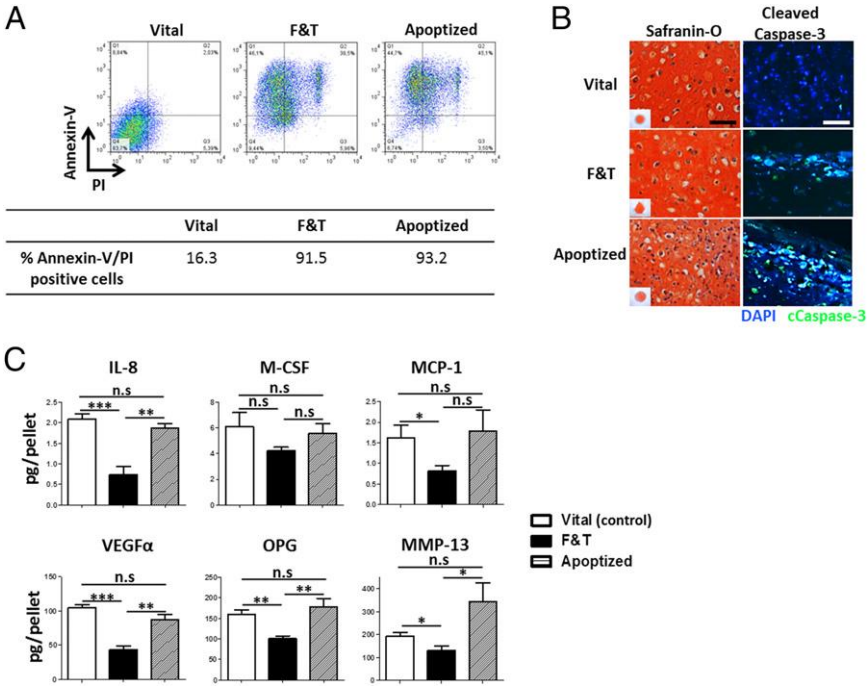

Fig. 3. Devitalization of hypertrophic cartilaginous templates. (*A*) Annexin V/PI flow cytometric analysis of cells retrieved from nondevitalized (*Vital*) or devitalized hypertrophic constructs, based on F&T cycles (F&T) or apoptosis induction (*Apoptized*). Both methods led to efficient tissue devitalization, with a killing efficiency superior to 90%. (*B*) Biochemical (Safranin-O) and immunofluorescence (Cleaved caspase-3) stainings of *Vital* and devitalized constructs. The devitalization processes efficiently induce cell death within the constructs. (Scale bars, 50 μm.) (*C*) Quantitative measurement of ECM proteins loss on devitalization of hypertrophic cartilage. Although the apoptotic method led to a minimal protein loss, the F&T treatment dramatically affected the ECM content. Error bars represent SEMs of $n = 6$ measurements. $^{*}P \leq 0.05$; $^{**}P \leq 0.005$; $^{***}P \leq 0.0005$.

marked by the absence of human cells, but with no evidence of frank bone structures or osteoblastic/osteoclastic cells (Fig. 5*C*).

Discussion

The present study demonstrates the hitherto unreported capacity of devitalized hypertrophic cartilage templates to induce de novo the formation of bone, including a mature vasculature and the presence of a bone marrow compartment, as well as the strict dependency of the regenerative process on the preservation of the ECM matrix and the growth factors and chemokines bound to it. In fact, the formation of heterotopic bone and bone marrow could be achieved only through the implementation of a devitalization strategy minimally affecting ECM integrity.

The deliberate activation of the apoptotic pathway allowed for the preservation of key embedded factors identified as being involved in inflammation (IL-8, MCP-1, M-CSF), vasculature recruitment (VEGFα), and bone remodeling processes (OPG, MMP-13). The initiation of the stage-specific cartilage template remodeling is known to require digestion of the engineered ECM through the identified factors, leading to the attraction of blood vessels via the release of entrapped VEGFα. The ingrowing blood vessels could subsequently deliver osteoblastic, osteoclastic, and hematopoietic precursors, completing cartilage resorption and directing formation of bone and associated stromal sinusoids, and in turn providing the microenvironment for hematopoiesis. Conversely, the use of the F&T as a "crude" devitalization technique led to the dramatic loss of those proteins, resulting in negligible vasculature, host cell recruitment, and tissue remodeling on implantation. These observations provide important information on the nature of the signals to be delivered to initiate endogenous formation of bone tissue and also warrant further investigation to identify the complete set of factors necessary and sufficient to instruct an efficient de novo formation of bone and bone marrow. In particular, our work highlights the paramount role played by the growth factors and chemokines embedded within the MSC-deposited ECM in triggering the tissue regeneration process. The potent biological role of the MSC secretome, appropriately bound to the ECM, is also in line with the recent view of MSCs as an "injury drugstore" and emphasizes the trophic effect of MSCs over their direct participation to the tissue formation (25).

In our study, the induced apoptosis of human hypertrophic chondrocytes is compliant with the physiological apoptosis of hypertrophic chondrocytes occurring during endochondral ossification. However, recent studies indicate that endochondral bone formation necessitates the presence of living hypertrophic chondrocytes, part of which directly contributes to the formation of trabecular structures (13) or the stromal niche for hematopoietic cells (26). As a consequence, despite the use of a cartilage intermediate, bone formation induced by devitalized ECM cannot be defined as being of canonical endochondral origin. Indeed, because the deposited bone tissue was predominantly

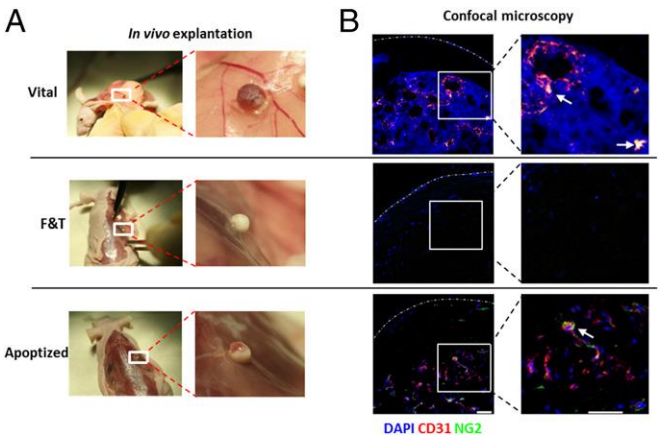

Fig. 4. Vascularization assessment of implanted hypertrophic cartilage tissues. (*A*) Macroscopic view of the samples at the time of explantation. *Vital* and *Apoptized* constructs displayed signs of blood cell colonization, in contrast to *F&T* samples. (*B*) Fluorescence microscopy of representative sections of explanted tissues. *Vital* and *Apoptized* constructs contained sinusoid-like vascular structures, positively stained for CD31 and stabilized by NG2+ pericytes. *F&T* devitalized constructs did not display evidences of vessel formation. (Scale bars, 50 μm.)

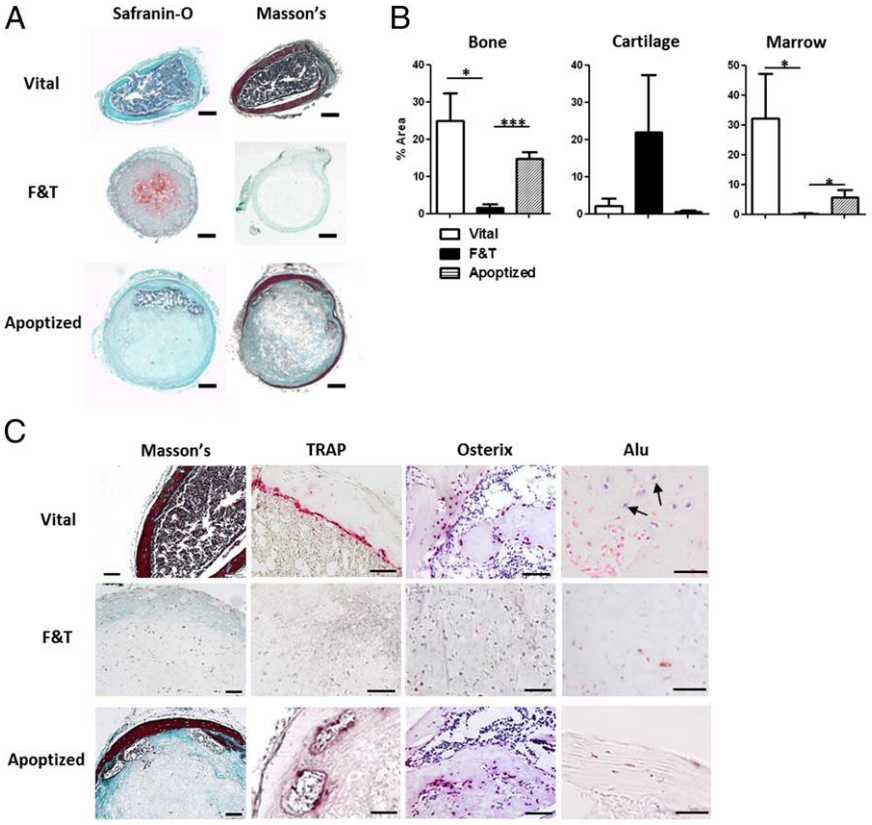

Fig. 5. Endochondral bone formation assessment of implanted hypertrophic cartilage tissues. (*A*) Safranin-O and Masson's Trichrome stainings of constructs retrieved 12 wk after implantation. *Vital* constructs underwent a full remodeling into bone, whereas *F&T* samples resembled an immature collagenous matrix with abundant cartilage remnants. *Apoptized* samples displayed evidence of perichondral bone formation, embedding a hematopoietic compartment. (Scale bars, 200 μm.) (*B*) Histologic quantification of bone, cartilage, and marrow tissue areas in sections of explanted living and devitalized constructs. (*C*) Masson's Trichrome, tartrate-resistant alkaline phosphatase, osterix, and Alu stainings were performed to, respectively, assess the presence of bone tissue, osteoclasts, osteoblasts, and human versus host cells. The presence of host-derived osteoclasts and osteoblasts was detected only in *Vital* and *Apoptized* samples. Human cells were present only in *Vital* constructs (black arrows). (Scale bars, 100 μm.)

perichondral, it could be attributed to the direct ossification of the mineralized cartilage template. A possible strategy to further improve the bone regeneration capacity of *Apoptized* constructs could thus be based on the increase of the surface:volume ratio by manufacturing channeled tissues, as recently described (27), to achieve a higher extent of perichondral bone formation.

Current acellular osteoinductive materials are typically enhanced by the delivery of single growth factors (BMPs). Because of the absence of critical accessory cues and ECM ligands that potentiate their effect, these strategies require supraphysiological doses of the morphogen, raising economic and safety issues (28, 29). Conversely, the osteoinductivity of the devitalized hypertrophic template relies on a mixture of factors accumulated at doses within physiological ranges and presented through a backbone of ECM molecules. Thus, *Apoptized* devitalized hypertrophic cartilage could offer an attractive alternative to currently available off-the-shelf osteoinductive materials, with the potency of cell-based grafts but bypassing both the logistically complex and regulatory costly use of autologous cells and the still-controversial introduction of allogeneic MSCs. As opposed to ECMs derived from native tissues, which are receiving an increased therapeutic interest (30), the present approach offers the opportunity not only to mimic a developmental process to efficiently form bone tissue but also to enrich the engineered templates in targeted proteins. This could be achieved through the overexpression of key identified factors (e.g., BMP-2, VEGFα) during in vitro culture by modified cells, leading to their embedding in the ECM and their preservation by apoptotic induction. The production of "customized" grafts, with an enhanced angiogenic or osteoinductive potency, would be required to target specific classes of patients or compromised environmental conditions at the repair site (e.g., atrophic nonunions requiring extensive vascularization, or simple bone losses requiring only osteoinduction) (31, 32). The ECM-based embedding of different growth factors in a controllable and customizable fashion for specific clinical needs clearly distinguishes the proposed approach from the "smart" ceramic materials, which have been proven to be osteoinductive in large animal models (33).

Obviously, the clinical translation of the proposed system necessitates further development and extensive preclinical studies. In the present work, the apoptosis induction relies on the use of a retroviral vector, leading to the integration of the system in the target cells. Although the approach has been validated for clinical practice (34), the development of alternative nonviral methods capable of efficiently devitalizing hypertrophic cartilaginous templates (e.g., proapoptotic adjuvants) may be preferred. One important issue with clinical implementation of the developed approach is also related to the efficacy in bone formation of *Apoptized* versus *Vital* grafts. At the assessed time, *Apoptized* constructs remained inferior to *Vital* ones, probably because of the lack of donor cells initially contributing to bone formation. Our study thus needs to be extended to a longer time of observation to assess whether this initial difference will be overcome.

The ectopic model used in the present work allows using human cells and investigating the de novo formation of bone tissue independent from osteoconductive events. Therefore, it

represents the most stringent proof of effective osteoinductivity of the devitalized grafts. However, a relevant assessment of the long-term bone-forming capacity of the implanted constructs will require an orthotopic model in immunocompetent animals. This will also allow the study of the regulatory role of osteoprogenitor and inflammatory cells from a bone environment, as well as of mechanical loading parameters.

In conclusion, we demonstrated that engineered hypertrophic cartilaginous matrix, provided a suitable devitalization technique, can deliver the set of factors to induce its remodeling and develop into bone tissue and bone marrow tissue. The findings outline a broader paradigm in regenerative medicine, relying on the engineering of cell-based but cell-free niches capable of recruiting and instructing endogenous cells on the formation of predetermined tissues. The approach can thus be extended to other biological systems to support both innovative translational strategies and fundamental investigations on the role of engineered ECM, decoupled from that of living cells.

Materials and Methods

All human samples were collected with informed consent of the involved individuals, and all mouse experiments were performed in accordance with Swiss law. All studies were approved by the responsible ethics authorities and by the Swiss Federal Veterinary Office.

HMSC-iDS were generated with the use of a retrovirus carrying the inducible death system (iCasp9-ΔCD19) and were purified by magnetic bead sorting based on CD19 expression (35). Cells were expanded for up to four passages (accounting for an average of 15–20 population doubling) to minimize the loss of chondrogenic potential, and were characterized by flow cytometry for putative MSC markers, with results consistent with our previous report (13).

Hypertrophic templates were generated by either the seeding of cells onto type I collagen meshes at a density of 70×10^6 cells/cm^3 (upscaled construct) (13) or using transwell culture seeded at 5×10^5 cells per insert (10). Constructs were cultured in chondrogenic conditions for 3 wk in a serum-free chondrogenic medium, followed by 2 wk in a serum-free hypertrophic medium (13). Samples were devitalized following two different protocols: F&T treatment or apoptosis induction. Samples were implanted in s.c. pouches of nude mice (four samples per mouse) and retrieved after 12 wk. The resulting in vitro and in vivo tissues were analyzed histologically, immunohistochemically, biochemically (glycosaminoglycans, DNA, protein content), by real-time RT-PCR, and by microtomography. Tissue development in vivo was evaluated histologically, immunohistochemically, and by microtomography. The survival and contribution to bone formation by HMSCs was evaluated with in-situ hybridization for human Alu sequences. A more complete and detailed description of the methods is included in *SI Materials and Methods*.

ACKNOWLEDGMENTS. We are grateful to Prof. Stefan Schären for the kind provision of bone marrow aspirates. This work was partially funded by the Swiss National Science Foundation (Grant 310030_133110, to I.M.) and by the Eurostars program (Grant FO132513, to I.M.).

1. Arrington ED, Smith WJ, Chambers HG, Bucknell AL, Davino NA (1996) Complications of iliac crest bone graft harvesting. *Clin Orthop Relat Res* 329:300–309.
2. Boden SD (2000) Biology of lumbar spine fusion and use of bone graft substitutes: Present, future, and next generation. *Tissue Eng* 6(4):383–399.
3. Kolk A, et al. (2012) Current trends and future perspectives of bone substitute materials - from space holders to innovative biomaterials. *J Craniomaxillofac Surg* 40(8): 706–718.
4. Martin I (2014) Engineered tissues as customized organ germs. *Tissue Eng Part A* 20(7-8):1132–1133.
5. Rosset P, Deschaseaux F, Layrolle P (2014) Cell therapy for bone repair. *Orthop Traumatol Surg Res* 100(1, Suppl):S107–S112.
6. Meijer GJ, de Bruijn JD, Koole R, van Blitterswijk CA (2007) Cell-based bone tissue engineering. *PLoS Med* 4(2):e9.
7. Leucht P, Minear S, Ten Berge D, Nusse R, Helms JA (2008) Translating insights from development into regenerative medicine: The function of Wnts in bone biology. *Semin Cell Dev Biol* 19(5):434–443.
8. Kronenberg HM (2003) Developmental regulation of the growth plate. *Nature* 423(6937):332–336.
9. Jukes JM, et al. (2008) Endochondral bone tissue engineering using embryonic stem cells. *Proc Natl Acad Sci USA* 105(19):6840–6845.
10. Scotti C, et al. (2010) Recapitulation of endochondral bone formation using human adult mesenchymal stem cells as a paradigm for developmental engineering. *Proc Natl Acad Sci USA* 107(16):7251–7256.
11. Janicki P, Kasten P, Kleinschmidt K, Luginbuehl R, Richter W (2010) Chondrogenic preinduction of human mesenchymal stem cells on beta-TCP: Enhanced bone quality by endochondral heterotopic bone formation. *Acta Biomater* 6(8):3292–3301.
12. Farrell E, et al. (2011) In-vivo generation of bone via endochondral ossification by in-vitro chondrogenic priming of adult human and rat mesenchymal stem cells. *BMC Musculoskelet Disord* 12:31.
13. Scotti C, et al. (2013) Engineering of a functional bone organ through endochondral ossification. *Proc Natl Acad Sci USA* 110(10):3997–4002.
14. Benders KE, et al. (2013) Extracellular matrix scaffolds for cartilage and bone regeneration. *Trends Biotechnol* 31(3):169–176.
15. Badylak SF (2007) The extracellular matrix as a biologic scaffold material. *Biomaterials* 28(25):3587–3593.
16. Song JJ, Ott HC (2011) Organ engineering based on decellularized matrix scaffolds. *Trends Mol Med* 17(8):424–432.
17. Crapo PM, Gilbert TW, Badylak SF (2011) An overview of tissue and whole organ decellularization processes. *Biomaterials* 32(12):3233–3243.
18. Bourgine PE, Pippenger BE, Todorov A, Jr, Tchang L, Martin I (2013) Tissue decellularization by activation of programmed cell death. *Biomaterials* 34(26):6099–6108.
19. Tey SK, Dotti G, Rooney CM, Heslop HE, Brenner MK (2007) Inducible caspase 9 suicide gene to improve the safety of allodepleted T cells after haploidentical stem cell transplantation. *Biol Blood Marrow Transplant* 13(8):913–924.
20. Burk J, et al. (2014) Freeze-thaw cycles enhance decellularization of large tendons. *Tissue Eng Part C Methods* 20(4):276–284.
21. Lu H, Hoshiba T, Kawazoe N, Chen G (2012) Comparison of decellularization techniques for preparation of extracellular matrix scaffolds derived from three-dimensional cell culture. *J Biomed Mater Res A* 100(9):2507–2516.
22. Sadr N, et al. (2012) Enhancing the biological performance of synthetic polymeric materials by decoration with engineered, decellularized extracellular matrix. *Biomaterials* 33(20):5085–5093.
23. Lucic D, Mollenhauer J, Kilpatrick KE, Cole AA (2003) N-telopeptide of type II collagen interacts with annexin V on human chondrocytes. *Connect Tissue Res* 44(5):225–239.
24. Kirsch T, et al. (1997) Annexin V-mediated calcium flux across membranes is dependent on the lipid composition: Implications for cartilage mineralization. *Biochemistry* 36(11):3359–3367.
25. Caplan AI, Correa D (2011) The MSC: An injury drugstore. *Cell Stem Cell* 9(1):11–15.
26. Serafini M, et al. (2014) Establishment of bone marrow and hematopoietic niches in vivo by reversion of chondrocyte differentiation of human bone marrow stromal cells. *Stem Cell Res (Amst)* 12(3):659–672.
27. Sheehy EJ, Vinardell T, Toner ME, Buckley CT, Kelly DJ (2014) Altering the architecture of tissue engineered hypertrophic cartilaginous grafts facilitates vascularisation and accelerates mineralisation. *PLoS ONE* 9(3):e90716.
28. Garrison KR, et al. (2010) Bone morphogenetic protein (BMP) for fracture healing in adults. *Cochrane Database Syst Rev* 6:CD006950.
29. Woo EJ (2013) Adverse events after recombinant human BMP2 in nonspinal orthopaedic procedures. *Clin Orthop Relat Res* 471(5):1707–1711.
30. Sicari BM, et al. (2014) An acellular biologic scaffold promotes skeletal muscle formation in mice and humans with volumetric muscle loss. *Sci Transl Med* 6(234): 234ra58.
31. Garcia P, et al. (2012) Temporal and spatial vascularization patterns of unions and nonunions: Role of vascular endothelial growth factor and bone morphogenetic proteins. *J Bone Joint Surg Am* 94(1):49–58.
32. Grayson WL, et al. (2010) Engineering anatomically shaped human bone grafts. *Proc Natl Acad Sci USA* 107(8):3299–3304.
33. Yuan H, et al. (2010) Osteoinductive ceramics as a synthetic alternative to autologous bone grafting. *Proc Natl Acad Sci USA* 107(31):13614–13619.
34. Zhou X, et al. (2014) Long-term outcome after haploidentical stem cell transplant and infusion of T cells expressing the inducible caspase 9 safety transgene. *Blood* 123(25): 3895–3905.
35. Bourgine P, et al. (2014) Combination of immortalization and inducible death strategies to generate a human mesenchymal stromal cell line with controlled survival. *Stem Cell Res (Amst)* 12(2):584–598.

Supporting Information

Bourgine et al. 10.1073/pnas.1411975111

SI Materials and Methods

hMSC Isolation, Transduction, in Vitro Culture, and in Vivo Implantation. hMSCs were isolated from bone marrow aspirates and processed as previously described (1). Briefly, marrow aspirates (20 mL volume) were harvested from healthy donors (seven males and one female, 23–49 y old) during routine orthopedic procedures involving exposure of the iliac crest. A bone marrow biopsy needle was inserted through the cortical bone, and the aspirate was immediately transferred into plastic tubes containing 15,000 IU heparin. For hMSC-iDS generation, cells were plated at 6,000 cells/cm^2 in 60-mm dishes the day preceding the transduction. hMSCs were transduced by incubation with retroviral vector (iCasp9-ΔCD19) supernatants supplemented with 8 μg/μL polybrene (Sigma Aldrich) for 5 min at 37 °C and centrifuged at 1,100 × *g* for 30 min at room temperature in the dishes, followed by fresh medium replacement (1). Cells were expanded for up to four passages and seeded onto type I collagen meshes (disks 8 mm in diameter, 2 mm thick; Ultrafoam, Davol) at a density of 70 × 106 cells/cm^3 to generate upscale constructs. Alternatively, smaller hypertrophic templates were generated by seeding in transwell culture at 5 × 10^5 cells per insert cells. Constructs were cultured in chondrogenic conditions for 3 wk in a serum-free chondrogenic medium (2), followed by 2 wk in a serum-free hypertrophic medium, supplemented with 50 nM thyroxine, 7 mM β-glycerophosphate, 10 nM dexamethasone, and 0.25 mM ascorbic acid and IL-1β (50 pg/mL). Samples were implanted in s.c. pouches of nude mice (four samples per mouse) and retrieved after 12 wk.

Real-Time RT-PCR Quantitation of Transcript Levels. Total RNA extraction, cDNA synthesis, and real-time RT-PCR (7300 AB; Applied Biosystems) were performed to quantitate expression levels of the following genes of interest: type I (Coll I; Applied Biosystems, ref. no. Hs00164004_m1), type II (Coll II; Applied Biosystems, ref. no. Hs01060345_m1), or type X collagen (2); Sox-9 (Applied Biosystems, ref. no. Hs00165814_m1); MMP-13 (Applied Biosystems, ref. no. Hs00233992_m1); VEGFα (Applied Biosystems, ref. no. Hs00900055_m1); and BMP2 (Applied Biosystems, ref. no. Hs00154192_m1). GAPDH was used as reference gene to normalize gene expression values (Applied Biosystems, ref. no. Hs02758991_g1).

Histological Stainings, Immunohistochemistry, and in Situ Hybridization for Alu Repeats. After in vitro and in vivo cultures, constructs were fixed in 4% (vol/vol) paraformaldehyde; if necessary, decalcified with 7% (vol/vol) EDTA solution (Sigma); and embedded in paraffin. Sections (5 μm thick) were stained with H&E (Baker), Masson's trichrome, or Alizarin red or for tartrate-resistant acid phosphatase activity by means of the leukocyte acid phosphatase kit (Sigma, ref. no. 387A-1KT). Immunohistochemical analyses were performed to characterize the ECM using the following antibodies: CD19 (AbCam, ref. no. 31947). On rehydratation in ethanol series, sections were treated according to the manufacturer's instructions. The immunobinding was detected with biotinylated secondary antibodies and using the appropriate Vectastain ABC kits. The red signal was developed with the Fast Red kit (Dako Cytomation), and sections were counterstained by hematoxylin. Negative controls were performed during each analysis by omitting the primary antibodies. Chromogenic in situ hybridization (Zytovision kit) to detect human Alu repeat sequences was performed following the manufacturer's instructions, using nuclear fast red (Sigma) as nuclear counterstaining. Histological and immunohistochemical sections were analyzed using an Olympus BX-61 microscope.

Immunofluorescence Images. After in vivo explantation, samples were fixed in 4% (vol/vol) paraformaldehyde (Sigma), decalcified with EDTA (Sigma) solution, embedded in optimal cutting temperature compound, and snap frozen in liquid nitrogen. Sections (20 μm thick) were incubated with the primary antibodies against CD31 (platelet endothelial cell adhesion molecule 1; BD Pharmingen), NG2 (Chemicon International), and α-smooth muscle actin. As appropriate, secondary antibodies labeled with Alexa Fluor 647, Alexa Fluor 488, or Alexa Fluor 546 (Invitrogen) were used, and DAPI was used to stain nuclei. Fluorescence images were acquired using a confocal Zeiss LSM 710 microscope.

Microtomography. Microtomography was performed with in vivo implants. After fixation in formalin and storage in PBS, microcomputerized tomography data were acquired using a Phoenix nanotom m scanner (General Electric) with 0.5 mm aluminum filtered X-rays (applied voltage, 70 kV; current, 260 μA). Transmission images were acquired during a 360° scan rotation with an incremental rotation step size of 0.25°. Reconstruction was made using a modified Feldkamp algorithm at an isotropic voxel size of 2.5 μm. Threshold-based segmentation and 3D measurement analyses (bone mineral density and volume) were performed using the ImageJ software (ImageJ; National Institutes of Health) with the BoneJ (4) and 3D Shape (5) extensions. 3D rendering of the structures was performed using VGStudio MAX 2.2 software (Volume Graphics).

Statistical Analysis. The results of real-time RT-PCR, protein, and tissue quantification are presented as mean ± SEM. Statistical analysis was performed using the unpaired *t* test. *P* values of 0.05 or less were considered statistically significant.

Proteins Quantification. Protein levels were determined in devitalized (F&T and apoptized) and nondevitalized (living) tissue lysates collected from constructs cultured for 5 wk in vitro. Samples were analyzed for their content of a panel of growth factors, chemokines, and metalloproteinases, according to the manufacturer's instructions (Procarta Immunoassay Kit; Panomics).

1. Bourgine P, et al. (2014) Combination of immortalization and inducible death strategies to generate a human mesenchymal stromal cell line with controlled survival. *Stem Cell Res (Amst)* 12(2):584–598.
2. Scotti C, et al. (2010) Recapitulation of endochondral bone formation using human adult mesenchymal stem cells as a paradigm for developmental engineering. *Proc Natl Acad Sci USA* 107(16):7251–7256.
3. Barbero A, Ploegert S, Heberer M, Martin I (2003) Plasticity of clonal populations of dedifferentiated adult human articular chondrocytes. *Arthritis Rheum* 48(5):1315–1325.
4. Doube M, et al. (2010) BoneJ: Free and extensible bone image analysis in ImageJ. *Bone* 47(6):1076–1079.
5. Sheets KG, et al. (2013) Microglial ramification and redistribution concomitant with the attenuation of choroidal neovascularization by neuroprotectin D1. *Mol Vis* 19:1747–1759.

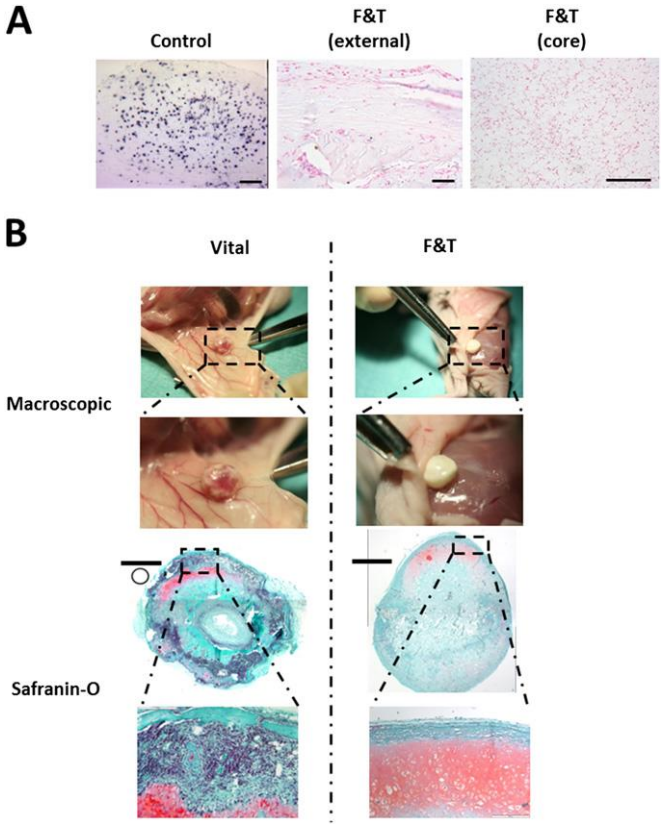

Fig. S1. (*A*) In situ hybridization for Alu repeats. No human cells could be detected in F&T devitalized ossicles 5 wk after in vivo implantation, as demonstrated by the absence of blue positively stained cells in both the external and core part of the ossicle. Purple stained cells (hematoxylin) corresponded to host cell invasion. The control sample consists of an in vitro-generated hypertrophic cartilage template, nondevitalized. (Scale bar, 100 μm.) (*B*) Explantation of non-devitalized (Vital) and F&T devitalized (F&T) ossicles 12 wk after ectopic implantation in nude mice. The Vital ossicles underwent an intense remodeling, giving rise to a mature bone organ with evidence of perichondral and trabecular bone and of a hematopoietic compartment (Safranin-O staining). Conversely, the F&T devitalized ossicles did not showed macroscopic evidences of remodeling and blood cell colonization, as confirmed by histological analysis revealing the absence of bone and bone marrow throughout the samples (Safranin-O). (Scale bar, 1 mm.)

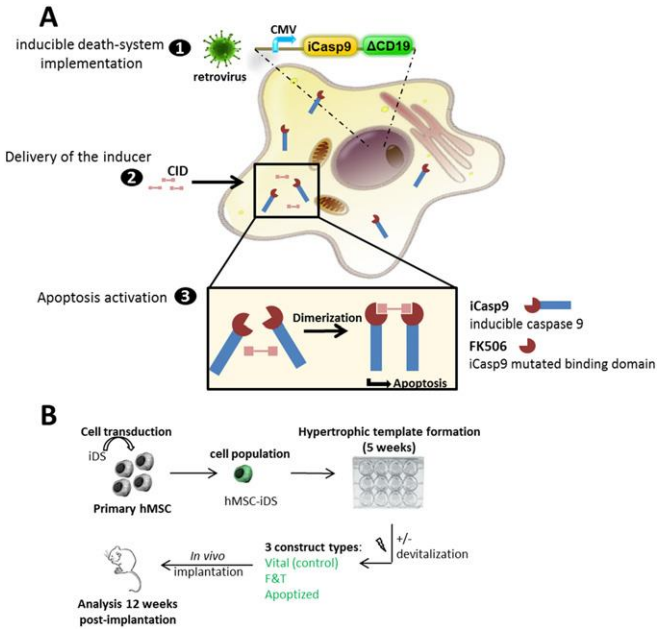

Fig. S2. (*A*) Mode of action of the iDS. The iDS is implemented in the genome of the target cells by the use of a retrovirus (1). Successfully transuded cells constitutively expressed a modified caspase 9 (iCasp9) displaying a mutated binding domain (FK506). The truncated CD19 is used as reporter marker. The delivery of the chemical inducer of dimerization (2) results in the dimerization of the iCasp9 by specific binding. The iCasp9 dimerization leads to the activation of the intrinsic apoptosis pathway (3). (*B*) Experimental set-up to assess the osteoinductive potential of devitalized hypertrophic templates. hMSC-iDS were generated by retroviral transduction. Hypertrophic templates were generated by 5 wk of culture (3 wk chondrogenesis + 2 wk hypertrophy) in the transwell system. Obtained constructs were either nondevitalized (Vital) or devitalized by F&T or apoptosis induction and were subsequently implanted ectopically in nude mice. After 12 wk, samples were retrieved for analysis.

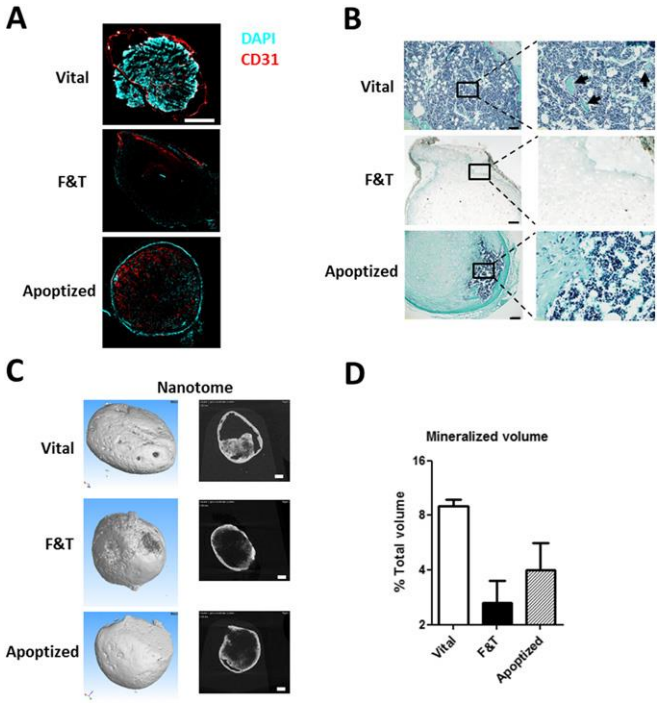

Fig. S3. (*A*) Fluorescence microscopy (DAPI, CD31) of hypertrophic templates retrieved 12 wk after ectopic implantation. F&T samples were characterized by the absence of vessel perfusion and host cell colonization. Apoptized samples were shown to be perfused by vessels although to a lower extent than the Vital constructs. (Scale bar, 0.5 mm.) (*B*) Masson's Trichrome staining revealing the presence of trabecular structure (arrow) only in Vital samples. Despite the presence of perichondral bone and bone marrow, no trabecular bone was found in Apoptized samples. F&T constructs did not show any evidence of frank bone structures. (Scale bar, 0.5 mm.) (*C*) 3D reconstructed microtomographic images of samples cultured for 5 wk in vitro and implanted ectopically in nude mice for 12 wk. (Scale bar, 0.35 mm.) (*D*) Microcomputed tomographic quantification of the mineralized volume in Vital, F&T, and Apoptized samples retrieved 12 wk after in vivo implantation. The measured volume includes both bone and calcified cartilage tissues.

Chapter 4

Interaction of CD14+ monocytes and engineered hypertrophic cartilage during end-stage endochondral ossification

Interaction of CD14+ monocytes and engineered hypertrophic cartilage during end-stage endochondral ossification

Atanas Todorov[1], Celeste Scotti[1,2], Andrea Barbero[1], Arnaud Scherberich[1], Adam Papadimitropoulos[1], Ivan Martin[1]

1 Departments of Surgery and Biomedicine, University Hospital Basel, Hebelstrasse 20, CH-4031 Basel, Switzerland

2 Orthopaedic Institute I.R.C.C.S. Galeazzi, Via R. Galeazzi 4, 20161 Milan, Italy

Abstract

Endochondral ossification of engineered hypertrophic cartilage (HC) is a valuable model for bone growth and regeneration. Factors contained in the hypertrophic matrix such as VEGF or BMP-2 are released by monocyte-/osteoclast-derived MMP-9 and chondrocyte-derived MMP-13. Gently devitalized HC contains similar levels of these factors and is osteoinductive, though less efficient. We hypothesized that additional monocytes and osteoclasts could improve bone formation by digesting HC, releasing factors and attracting osteogenic progenitors. We seeded living or devitalized HC with human blood-derived monocytes and either maintained samples under osteoclastogenic conditions or implanted them in nude mice. Monocytes and osteoclasts invaded HC in vitro and led to the release of proteins. Levels of G-CSF, IL-6, MMP-13, VEGFa and FASL were significantly higher in living compared to devitalized samples. Monocytes, but not MSC or HUVEC, migrated towards the released signals. The addition of monocytes in vivo did not result in more efficient bone formation, yet the bone volume fraction correlated with protein secretion in vitro and the presence of osteoclasts, endothelial cells and macrophages in vivo. In conclusion, seeding of osteoclastogenic monocytes was

not sufficient to improve bone formation of living or devitalized hypertrophic cartilage. While common precursor monocytes could be attracted by devitalized matrix, their survival and differentiation into osteoclasts depended on interactions with hypertrophic chondrocytes. Presence of M2 macrophages was correlated with subsequent vascularization. Our model is consistent in vitro and in vivo and improves the understanding of end-stage endochondral ossification.

Keywords

endochondral ossification, monocytes, osteoclasts, hypertrophic chondrocytes, macrophages, G-CSF, IL-6, MMP-13, VEGFa, FASL

Introduction

Transformation of hypertrophic cartilage into bone tissue is observed during growth and fracture repair of long bones. Remodelling of hypertrophic cartilage can be particularly important in diseases such as juvenile idiopathic arthritis(1, 2), where both growth retardation and growth excess have been described as a result of inflammation. Clinical management of fracture healing through callus formation can equally benefit from an improved understanding of this process. Fractures and the associated morbidity and mortality represent a significant burden(3), resulting in a great need to develop more effective pharmacological treatments and novel bone substitute materials.

Engineered hypertrophic cartilage undergoes endochondral ossification in a process which closely resembles long bone development(4). The transition from hypertrophic matrix to bone is highly dependent on MMP-mediated matrix degradation and attraction of endothelial cells and mesenchymal stromal cells(5-7). Factors such as VEGF or BMP-2 in the hypertrophic matrix are released by monocyte-/osteoclast derived MMP-9 and chondrocyte-derived MMP-13 during remodelling(5) and have an

osteoinductive effect. Gently devitalized hypertrophic matrix contains similar levels of cytokines and growth factors compared to living matrix, but shows a much less efficient bone formation(8). Possibly, the lack of MMP-13 from hypertrophic chondrocytes leads to less cytokine release(5, 9, 10) and therefore less attraction of monocytes and development of osteoclasts(11). In the growth plate of MMP-13 knockout mice upregulation of MMP-9 by monocytes and osteoclasts may however be sufficient for bone formation(10). Although monocytes are attracted to any implanted graft due to an initial immune reaction(12, 13), their number, mode of activation and lack of differentiated osteoclasts may be insufficient for bone formation. However, if monocytes primed to become osteoclasts can be brought into contact with devitalized hypertrophic matrix, they may improve the release of cytokines and growth factors and thus enhance the osteoinductivity.

CD14+ monocytes from peripheral blood are precursors for both osteoclasts and macrophages(14, 15). They can be easily collected, purified and immediately stimulated with RANKL and M-CSF(16) to yield multinucleated osteoclasts, which are fully functional(17, 18).

Our hypothesis in the present study was that primed osteoclastogenic CD14+ monocytes could be seeded on devitalized hypertrophic cartilage, resulting in matrix degradation and release of cytokines, which in turn would attract all necessary progenitor lineages for bone formation and would ultimately lead to increased efficiency of bone formation in vivo. Our aim was to first establish a co-culture system and subsequently identify the most important factors released. In a second step we implanted the seeded matrix to verify bone formation in vivo.

Materials and Methods

Generation of hypertrophic cartilage

Hypertrophic cartilage was generated as described previously(4). Bone marrow mesenchymal stromal cells were extracted from 5 healthy human donors (male, 33.8+-6.8 years) after informed consent (ethical approval at the University Hospital Basel, reference 78/07) and expanded using complete medium (alphaMEM, 10% FBS, 1mM sodium pyruvate, 10mM HEPES, 1% penicillin-streptomycin-glutamine, all from Gibco, Basel, Switzerland) with 5 ng/ml FGF2 (R&D Systems, Wiesbaden, Germany) up to 4 passages. Cells were detached using 0.5 mg/ml trypsin (Gibco), collected and resuspended in chondrogenic medium consisting of serum free medium (DMEM, 1.25 mg/ml human serum albumin, 1 mM sodium pyruvate, 10 mM HEPES, 1% penicillin-streptomycin-glutamine, 1% ITS-1, all from Gibco) together with 10 ng/ml TGFβ1 (R&DSystems), 10^{-7} M dexamethasone and 0.1 mM ascorabic acid 2-phosphate (Sigma Aldrich, Buchs, Switzerland). In the first experiment, a transwell system (0.4 μm membrane pores 24-well-plate, Corning, Root, Switzerland) was used. All subsequent experiments were performed with 1.5 ml screwcap tubes (Sarstedt, Sevelen, Switzerland). 5×10^5 cells were centrifuged at 400g for 5 minutes to form cell aggregates and incubated in a standard incubator at 37°C and 5% CO_2. Medium changes were performed twice per week and chondrogenic medium was used for the first 3 weeks. After this peroid, hypertrophic medium consisting of serum free medium with 0.05μM L-thyroxine, 10^{-6}M dexamethasone, 10 mM β-glycerophosphate and 0.1 mM ascorbic acid 2-phosphate (all from Sigma Aldrich) was used for an additional 2 weeks.

Devitalization of hypertrophic cartilage

Samples were subjected to freeze/thaw devitalization as described previously(8). Briefly, samples were transferred to 15ml plastic tubes and frozen in liquid nitrogen (-

192°C) for 10 minutes, then thawed in a water bath at 37°C for 10 minutes. This cycle was repeated 3 times and the samples finally rinsed with bidistilled water.

Isolation of CD14 positive monocytes

Peripheral blood buffy coats from healthy donors were used and mononuclear cells separated by gradient centrifugation (Ficoll, Histopaque 1077, Sigam-Aldrich) as previously described(19). CD14+ monocytes were sorted using anti-CD14 coated magnetic beads (Miltenyi Biotec, Auburn, CA, USA) according to the manufacturer's instructions.

Co-cultures

CD14+ monocytes were resuspended in co-culture medium (alpha-MEM, 1 mM sodium pyruvate, 10 mM HEPES, 1% penicillin-streptomycin-glutamine, all from Gibco) with 25 ng/ml M-CSF and 50 ng/ml RANK-ligand (R&D systems). As controls, monocytes were seeded on tissue culture plastic to evaluate osteoclast formation. Living or devitalized hypertrophic matrix was incubated with 1-5 million monocytes on an orbital shaker for 24 hours at 37°C. Seeding efficiency was analyzed by incubation with 0.05 mg/ml tetrazolium salt (MTT, Sigma-Aldrich) in phenol-free medium (DMEM, Gibco) for 4 hours at 37°C. MTT was then dissolved with DMSO (Sigma-Aldrich), absorption measured at 575 nm and compared to a monocyte standard curve. After seeding, co-cultures were gently transferred to conical 96-well plates (Corning). Medium changes were performed twice per week and the supernatants frozen at -20°C for later analysis.

Whole mount staining

Samples were fixed in 4% PFA for 15 minutes and incubated with ELF-97 (200 µM ELF-97 from Thermo Fisher Scientific, 0.2 M sodium acetate and 50 mM L(+) tartaric acid from Sigma-Aldrich, pH 5.0) for 15 minutes at 37°C to visualize tartrate resistant

acid phosphatase (TRAP). After washing, samples were incubated with primary antibody for human calcitonin receptor (ab175297, Abcam, UK). Secondary antibody conjugated with AlexaFluor647 (Dako, Baar, Switzerland), FITC conjugated phalloidin and DAPI (Sigma-Aldrich) were added. The samples were analyzed under a Nikon A1 confocal microscope.

Glycosaminoglycan and DNA content

For the measurement of glycosaminoglycans (GAG) and DNA, co-culture samples were digested overnight with Proteinase K solution (1 mg/ml Proteinase K in 50 mM Tris pH 7.6, 1 mM EDTA, 1 mM Iodoacetamide, 10 µg/ml Pepstatin, all from Sigma Aldrich). GAG measurements were performed as described previously(20). Briefly, GAG was precipitated with DMMB, centrifuged and re-dissolved. Absorption was measured at 656 nm and GAG concentrations calculated using a standard curve. DNA measurements were performed with the CyQuant kit (Thermo Fisher Scientific, Zug, Switzerland) according to the manufacturer's protocol.

Migration analysis

Supernatants from co-cultures were diluted 1:2 in fresh co-culture medium and distributed in the bottom chambers of 96-well transwell plates (HTS transwell, 8.0 µm pore size, polyester membrane, Corning) pre-coated with 1% gelatin. 5×10^4 cells in co-culture medium were pipetted in the top chambers. Human MSC of 3 donors were used after 2 passages as described above. HUVEC expanded for 4 passages were kindly provided by Prof. Anna Marsano. CD14+ monocytes were used directly after sorting as described above. Plates were incubated for 24 hours at 37°C, then centrifuged at 400g for 2 minutes and bottom chambers incubated with 1 µM Calcein AM for 15 minutes at 37°C. Fluorescence of the bottom chambers was read at 480 nm excitation and 520 nm emission.

Osteogenic differentiation of MSC

In parallel to the migration analysis, human MSC were resuspended in complete medium and seeded at a density of 5000 cells / cm^2 in 96 well plates. Differentiation was induced by osteogenic medium (complete medium, 10^{-6} M dexamethasone, 10 mM β-glycerophosphate and 0.1 mM ascorbic acid 2-phosphate) with supernatant mixed 4:1. After 3 weeks of differentiation, alkaline phosphatase activity was measured(21). Briefly, 50ul buffer (5 mg/ml p-nitro-phenyl phosphate, 200 mM TRIS, 1 mM MgCl2, pH 9.5) were added to each well and incubated for 30 minutes at 37°C. The reaction was stopped by addition of 50 µl 1 M NaOH, absorption was measured at 405 nm and ALP activity was calculated using a standard curve.

Analysis of GAG and proteins in supernatants

Supernatants were analyzed for GAG as described above, except that no Proteinase K digestion was performed. The content of a panel of growth factors, chemokines, and metalloproteinases was analyzed by multiplex protein assay according to the manufacturer's instructions (Procarta Immunoassay Kit; Panomics).

Implantations

All animal procedures were reviewed and approved by the Swiss Federal Veterinary Office (BS 1797). Female 6-8 week old nude mice were anaesthetized using 2% isoflurane in 1l/min O^2. The skin was disinfected and cut 8mm along the dorsal midline. Subcutaneous pockets were prepared by blunt dissection on both sides. Samples were implanted directly after seeding as mentioned above. The wounds were closed with surgical staples and the animals allowed to recover under red light. Regular checks were performed and staples removed after 7-10 days. Animals were euthanized in a CO^2 chamber after 3 or 8 weeks and samples fixed in 1.5% PFA before further analysis.

Microtomography

Microtomography was performed using a tungsten x-ray source at 70kV and 260 µA with a 0.5 mm aluminium filter (Nanotom M, GE, USA). Transmission images were acquired for 360° with an incremental step size of 0.25°. Volumes were reconstructed using a modified Feldkamp algorithm (software supplied by manufacturer) at a voxel size of 2.5 – 3 µm. Thresholding, segmentation and 3D measurements were performed using the ImageJ(22) software with the BoneJ(23) and 3D Shape(24) additions.

Histology

Samples were embedded in paraffin and sections of 5µm thickness prepared using a microtome. Safranin-O, Masson tri-chrome and tartrate resistant acit phosphatase (TRAP) stainings were performed as published previously (Scotti 2010, Scotti 2014). Primary antibodies for DIPEN (1042002, MDBiosciences, USA), collagen type I (ab6308), collagen type II (ab34712), collagen type X (ab49945), bone sialoprotein (ab52128), MMP-9 (ab38898), MMP-13 (ab39012, Abcam, UK), CD31 (ab28364) and Sca1 (ab51317) were used. After washing and incubation with an appropriate biotinylated secondary antibody (Dako, Denmark), the stainings were developed with the Vectastain ABC kit (Vector Laboratories, USA) according to the manufacturer's protocols.

Fluorescent double staining with conjugated antibodies for F4/80 (MCA497A647, AlexaFluor 647, AbDSerotec, Germany) and CD206 (MCA2235A488, AlexaFluor 488, AbDSerotec) was performed to identify M2 macrophages(25) and DAPI (Sigma Aldrich) added.

Quantifications

Samples were completely sectioned and four to six sections spaced at regular intervals were quantified. For osteoclasts, TRAP positive multinucleated cells were counted. For endothelial cells, CD31 positive cells were counted. For M2 macrophages,

F4/80 and CD206 double positive cells were counted. Only cells inside the implanted matrix or attached to the outer surface were counted and total sample area was considered for counting.

Statistical Analysis

Data was analyzed by t-test, ANOVA and Pearson correlation using the GraphPad Prism v2.2 software. A significance level alpha of 0.05 was set. Average values and standard deviations are reported.

Results

In vitro co-culture of hypetrophic cartilage matrix and CD14+ monocytes

After 5 weeks of in vitro generation, both disks and pellets of hypertrophic cartilaginous matrix (Supplementary Figure 1) showed a typical morphology and presence of molecular markers (collagen I/II/X, BSP) as previously published(4) . Seeing that transwell culture randomly formed disks or pellets, standardized pellet culture was used for 4 out of 5 donors. One million monocytes were used for seeding, since independently from the intial concentration $5.2\pm1.1\times10^5$ cells attached. At day 7, control cultures of monocytes on plastic differentiated into multinucleated TRAP-positive osteoclasts (Supplementary Figure 2). At the same time, whole mount stainings showed monocytes forming actin rings on the surface of devitalized hypertrophic matrix. Multinucleated cells positive for TRAP and human calcitonin receptor were also observed (Figure 1A and B). Histological sections additionally showed TRAP positive monocytes inside the matrix (Figure 1C). Monocytes and multinucleated cells on the living matrix were also positive for TRAP and human calcitonin receptor (Figure 1D), but their actin filaments were organized in long strands.

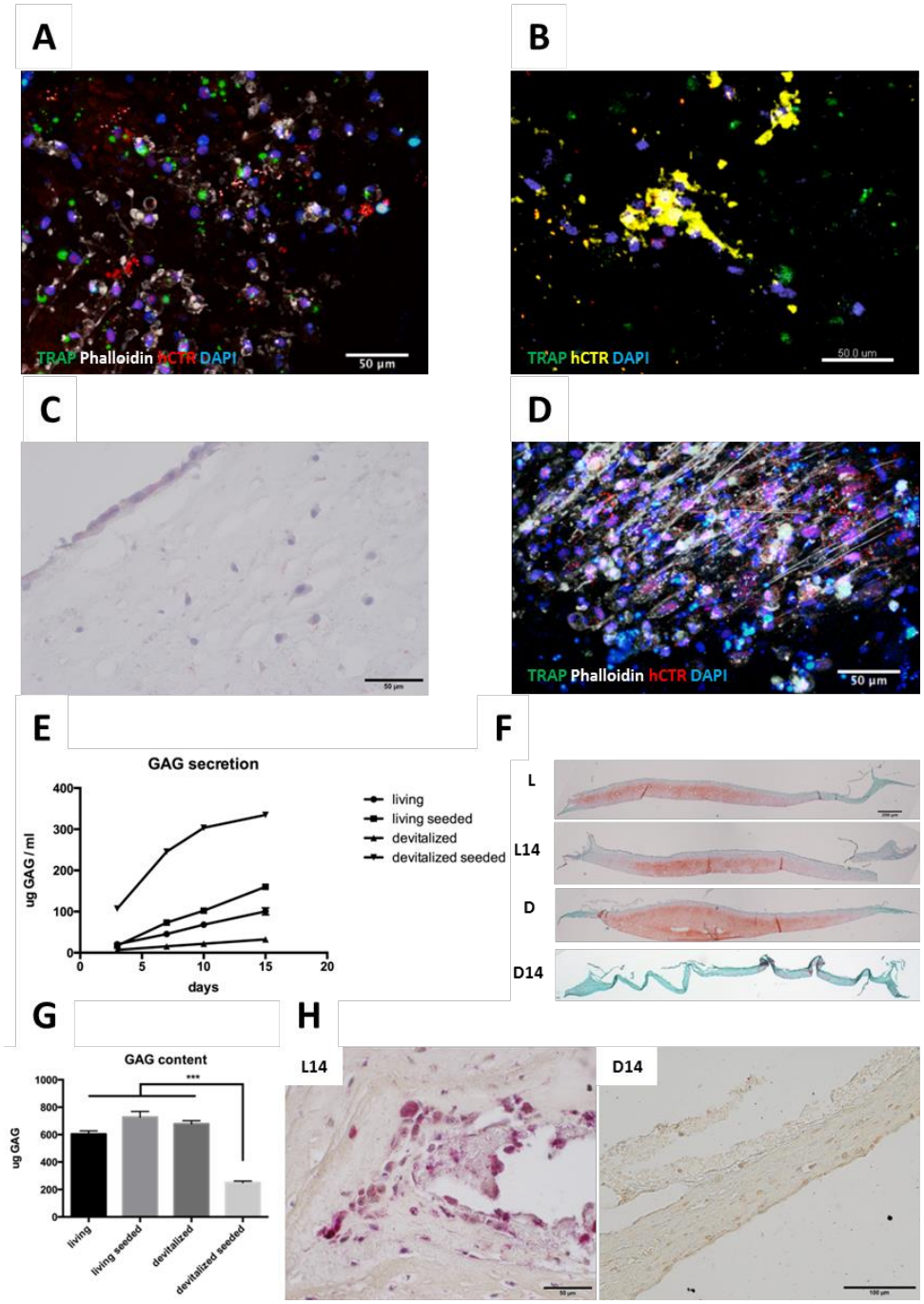

Figure 1: A: 7 days whole-mount staining of devatilzed matrix with tartrate resistant acid phosphatase (TRAP) and human calcitonin receptor (hCTR) positive cells forming actin rings. B: Closeup of TRAP and hCTR positive multinucleated cell on the devitalized matrix. C: TRAP-stained section of devitalized sample shows mononucleated cells invading the matrix. D: Living matrix with TRAP and hCTR positive cells, elongated actin filaments. Bars in A-D represent 50 µm. E: GAG secretion in supernatant over the culture period. Devitalized seeded samples have significantly more GAG in the supernatant at all time points ($P<0.01$). F: Safranin-O staining after 15 days of co-culture. Devitalized seeded show decreased thickness. L = living, L14 = living seeded, D = devitalized, D14= devitalized seeded. Bar in L represents 200 µm. G: GAG content of the matrix after 15 days. GAG is significantly lower in devitalized seeded samples. H: TRAP staining

after 15 days. Living seeded samples display TRAP positive single and multinucleated cells invading the matrix. Bar in L14 represents 50 μm, in D14 100 μm.

In vitro digestion of devitalized hypertrophic cartilage

During the co-culture for up to 15 days, all groups secreted glycosaminoglycans (Figure 1E). Seeded devitalized samples released significantly more GAG than all other groups ($P<0.01$ for all time points and groups). Seeded devitalized matrix showed a reduced volume and loss of Safranin-O positivity (Figure 1F). Significantly less GAG was present in the seeded devitalized matrix (Figure 1G). After 15 days, TRAP positive multinucleated cells were found invading the living matrix, but no cells were found in the devitalized matrix (Figure 1H).

Differences between living and devitalized matrix in co-culture

Using supernatants from the 3rd day of co-culture, migration and alkaline phosphatase activity of human MSC and migration of HUVEC were not affected by any of the groups (Supplementary Figure 3). However, freshly isolated CD14 monocytes showed more migration towards supernatants from seeded living and devitalized samples compared to controls and compared to devitalized matrix only.

Since digestion, monocyte attraction and invasion were observed with seeded living or devitalized matrix and protein secretion was greatest at 3 days, further analysis was performed only on these samples. Supernatants were analyzed for a panel of cytokines, growth factors and metalloproteinases (Table 1). G-CSF was only detected in living samples (Figure 2). IL-6, MMP-13 and VEGFa were significantly higher in living versus devitalized samples. Interestingly, FASL was significantly lower after 3 days, but significantly higher after 7 days in living compared to devitalized samples. All other factors, including the most abundant IL8, did not show significant differences (Supplementary Figure 4). TGFβ1 was not detected in any group.

Protein	Relation to Endochondral Ossification
IL6	cytokine, initiates repair cascade during fracture healing (26)
IL8	cytokine, primes neutrophils during fracture healing (27)
G-CSF	can increase osteoclast number, involved in HSC niche formation by osteoclasts (28)
FASL	mediates apoptosis of leukocytes, important for early bone morphogenesis (29), limited role for apoptosis of osteoblasts and osteoclasts (30) creates immune privilege for engineered cartilage (31)
MCP-1	attracts monocytes (32), implicated in bone remodeling (33)
SCF	chemoattractant, invovled in HSC niche (28), stem cell mobilisation and effect on osteoblasts
SDF-1	chemoattractant, invovled in HSC niche (28), recruitment of MSC to fracture site (34)
VEGFa	Expressed during endochondral ossification, responsible for vascularization (26), can regulate chondrocyte and osteoblast fate (35)
MMP-9	allows remodelling during final stages of endochondral ossification (26)
MMP-13	allows remodelling during final stages of endochondral ossification (26)
OPG	binds to RANKL and regulates osteocalst formation and bone resorption (36), important for resorption of calcificed cartilage
BMP-2	promotes endochondral ossification and bone formation (26), responsible for callus formation
BMP-4	promotes endochondral ossification and bone formation (26)
TGFβ1	promotes various stages of endochondral ossification (26), regulates bone homeostasis (37)

Table 1: Proteins chosen for analysis of supernatants. Dimitriou 2005(26), Bastian 2011(27), Blin-Wakkach 2014(28), Katavic 2003(29), Kovacic 2007(30), Fujihara 2014(31), Deshmane 2009(32), Graves 1999(33), Kitaori 2009(34), Dai 2007(35), Boyce 2008(36), Iqbal 2009(37)

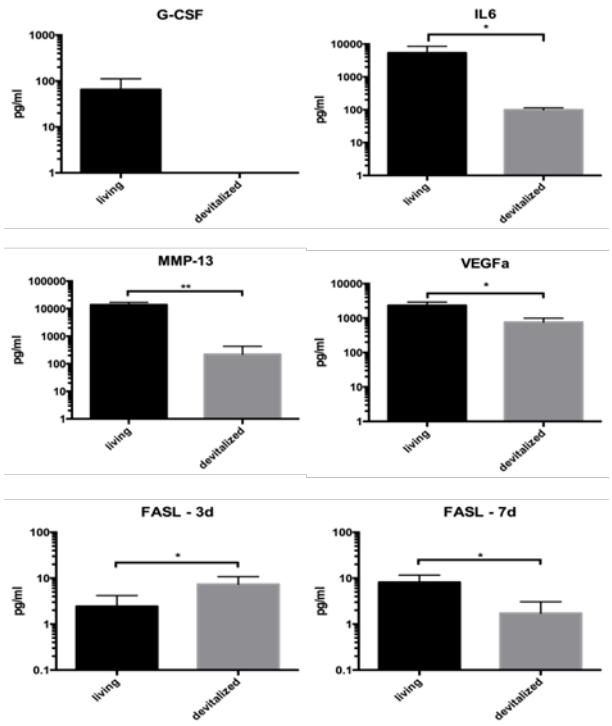

Figure 2: Proteins in supernatants found to be significantly different between living and devitalized seeded groups after 3 days of co-culture. FASL was the only factor found to be significantly lower at 3 days and higher at 7 days in living seeded versus devitalized seeded samples. (*P<0.05;**P<0.01;***P<0.001)

In vivo implantation of co-cultures leads to bone formation in living hypertrophic matrix

Immediately after seeding, samples were implanted in nude mice. After 3 weeks both seeded and unseeded living implants displayed a very slight Safranin-O positivity, suggesting an ongoing loss of GAG (Figure 3A). Devitalized implants appeared devoid of GAG and with a fibrotic internal matrix surrounded by denser tissue. No apparent differences were found between the seeded and unseeded group.

After 8 weeks living implants had formed frank bone tissue with bone marrow and a peripheral bone lamina (Figure 3B). Few remnants of the cartilaginous matrix could be distinguished, along with trabecular structures. Red-stained elastin was present in the osteoid of the seeded living implants, suggesting a more mature bone. Devitalized

implants showed areas of dense matrix containing cells and areas of cell free fibrotic matrix. No differences were observed between seeded and unseeded samples.

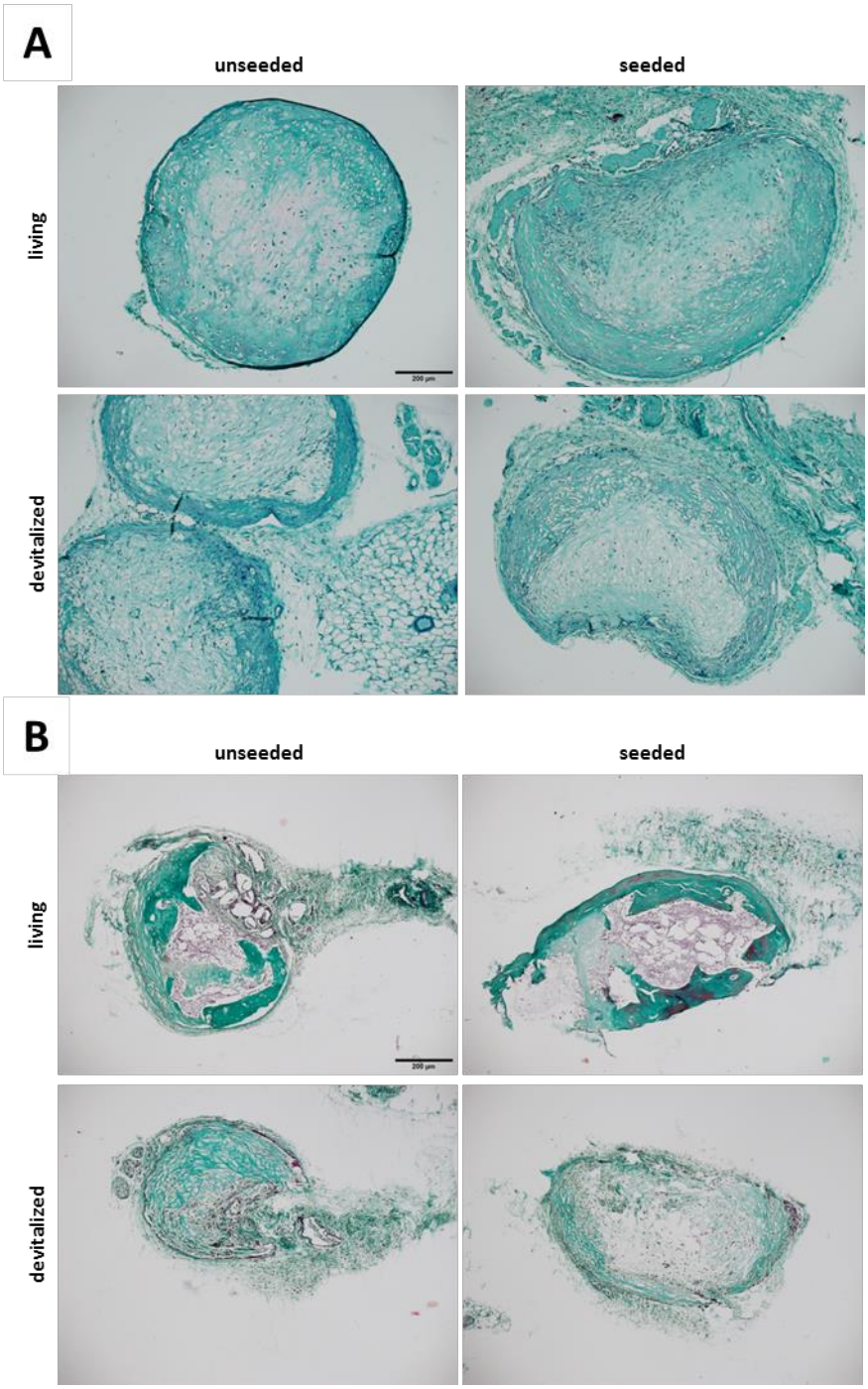

Figure 3: A: Safranin-O staining of representative samples 3 weeks after subcutaneous implantation in nude mice. B: Masson tri-chrome staining of representative samples after 8 weeks in vivo. Bone marrow was observed exclusively in living samples. Red-stained elastin in living seeded implants indicates a more mature osteoid. Devitalized samples display areas of denser matrix and areas of loose fibrotic tissue without a qualitative difference between seeded and unseeded samples. Bars in A and B represent 50 µm.

Bone volume fractions were quantified using a threshold for bone tissue (Figure 4A). All living implants had significantly more bone than devitalized implants. However, seeded implants did not show any significant difference compared to unseeded implants. In seeded living implants versus unseeded living implants there was a trend towards more bone.

In vivo presence of cell types necessary for bone formation

The number of osteoclasts was significantly higher in all living versus devitalized implants (Figure 4B). Seeded implants were not significantly different from unseeded implants. The presence of endothelial cells was highly variable and did not show any significant trend (Figure 4C). There was a tendency towards less endothelial cells in devitalized implants. M2 macrophages were significantly higher in seeded living versus seeded devitalized implants (Figure 4D). No significant difference was found between seeded and unseeded implants. Non-M2 macrophages positive for F4/80 but not for CD206 and Sca1 positive putative MSC were only found sporadically.

Correlation of bone formation with secreted proteins in vitro and attracted cell types in vivo

Bone volume fraction (BV) was significantly correlated with the levels of in vitro secreted proteins. It was also correlated to the presence of osteoclasts and M2 macrophages, but not endothelial cells.

Osteoclasts were only correlated with the secreted proteins, including FASL. M2 macrophages were correlated with G-CSF and IL-6. Endothelial cells only corrleated with the presence of M2 macrophages.

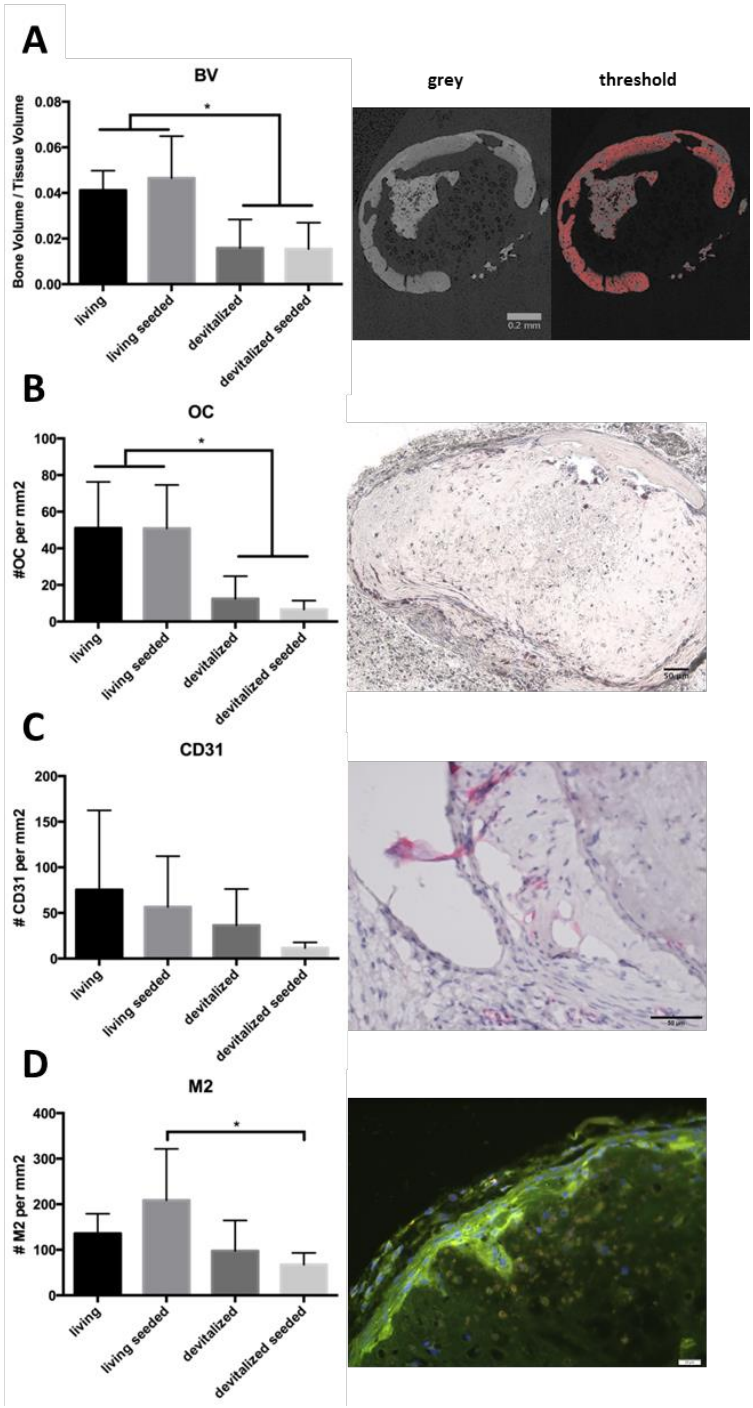

Figure 4: A: Microtomographical quantification of bone and mineralized matrix after 8 weeks in vivo. Living samples had significantly more bone thand devitalized samples. Seeding did not result in significant differences. B: Osteoclast quantification based on TRAP staining after 3 weeks in vivo. Living samples had significantly more osteoclasts than devitalized samples, seeding did not result in significant differences. Black bar is 50 µm. C: Endothelial cell quantification based on CD31 stainings after 3 weeks in vivo. No significant differences. Black bar is 50 µm. D: M2 macrophage quantification based on CD206 and F4/80 co-staining after 3 weeks in vivo. Living seeded samples had significantly more macrophages than devitalized seeded samples. Seeded versus unseeded differences were not significant. White bar is 20 µm. (*P<0.05;**P<0.01;***P<0.001)

		OC	CD31	M2	IL6	MMP13	G-CSF	VEGFa	FASL*	OPG
BV	*rho*	0.90	n.s.	0.84	0.85	0.78	0.83	*(0.72)*	0.81	n.s.
	R2	0.81		0.71	0.72	0.61	0.70	*(0.52)*	0.66	
	P	0.007		0.018	0.017	0.033	0.020	*(0.052)*	0.025	
OC	*rho*		n.s.	n.s.	0.89	0.91	0.85	0.93	0.86	n.s.
	R2				0.79	0.83	0.73	0.86	0.74	
	P				0.018	0.012	0.031	0.008	0.029	
CD31	*rho*			0.83	n.s.	n.s.	n.s.	n.s.	n.s.	n.s.
	R2			0.69						
	P			0.041						
M2	*rho*				*(0.81)*	n.s.	0.82	n.s.	n.s.	n.s.
	R2				*(0.65)*		0.67			
	P				*(0.052)*		0.048			

Table 2: Significant correlations found between bone volume (BV), number of different cell types (OC = osteoclasts, CD31 = endothelial cells, M2 = M2-macrophages) and factors which were differentially expressed during co-cultures. Note: FASL values after 7 days are displayed. FASL values after 3 days were not significant in any correlation.

Discussion

In this present study, monocytes and osteoclasts invaded engineered hypertrophic cartilage in vitro and led to the release of proteins. Levels of G-CSF, IL-6, MMP-13, VEGFa and FASL were significantly higher in living compared to devitalized samples. Monocytes, but not MSC or HUVEC, migrated towards the released signals. The addition of monocytes in vivo did not result in more efficient bone formation, yet the bone volume fraction correlated with protein secretion in vitro and the presence of osteoclasts, endothelial cells and macrophages in vivo.

CD14+ blood derived monocytes are a well described pool of progenitors for osteoclasts(14-18), though monocytes and possibly macrophages are present after differentiation. Mononucleic TRAP positive cells can resorb bone but are less efficient than classical multinucleated osteoclasts(38). Monocytes can also differentiate to inflammatory (M1) or regenerative (M2) macrophages(25). As would be expected during endochondral ossification(39), our co-culture represents a mixture of all these cell types. Further selection of CD14+ monocytes for RANK expression could identify

primed osteoclast progenitors(40), but would decrease the relevance to the physiologic process.

Although cells invaded both living and devitalized samples, digestion in vitro mostly affected devitalized matrix. This was in spite of the fact that MMP-13 was higher in living samples and MMP-9 was not significantly different. One could assume that both the living and devitalized matrix were digested and the living matrix could compensate the loss of protein, yet secretion and final content of glycosaminoglycans suggested that only devitalized samples were significantly affected.

Fuller et al(41) have suggested that MMPs contribute little to bone resorption by osteoclasts, yet in hypertrophic cartilage, MMPs are viewed as crucial(42). MMP-9 knockout mice show a transient increase of the hypertrophic zone as well as a compensatory upregulation of MMP-13(43). MMP-13 knockouts similarly display increased hypertrophic zones, though upregulation of MMP-9 by TRAP positive cells may be sufficient for bone formation(10). However, in our model no compensation between MMP-13 and MMP-9 was present.

Contrary to our expectations, neither MSC nor HUVEC showed any migration, whereas CD14+ monocytes migrated equally toward supernatants from living and devitalized co-cultures. This was paralleled by the absence of MSC after 3 weeks in vivo and by the lack of correlation between endothelial cells and secreted proteins, especially VEGF.

Considering these results, it is likely that the secreted proteins in living co-cultures are part of a regulatory loop between hypertrophic chondrocytes and monocytes. Il-6, VEGF, IL8(41) and G-CSF(44) can attract monocytes and stimulate formation of osteoclasts(35, 45, 46). In our cultures, IL-6, VEGF and G-CSF were significantly different between living and devitalized cultures but IL-8 was similar and most abundant,

suggesting that monocyte migration could be due to the presence of IL-8. VEGF did not elicit endothelial cell migration and correlated with osteoclasts instead of endothelial cells in vivo, suggesting that this potent angiogenic factor(35) more likely regulates osteoclasts during endochondral ossification. IL-6(47) and G-CSF(48, 49) have been shown to differentiate monocytes towards M2 macrophages and could also aid their survival(50), which fits the correlations we observed. On the other hand, FASL secreted by chondrocytes could kill invading monocytes and M1 macrophages and thus protect the matrix, as has been shown in cartilage engineered with normal and FASL deficient chondorcytes(31). Interestingly, FASL has a limited appoptotic effect on osteoclasts(30) and may even aid their differentiation(51), which would explain the observed correlation to osteoclasts in our study.

TGFβ1 is considered an important coupling factor for bone resorption and formation and is stored in osteoid matrix in a latent form(37, 52). However, we did not detect it in our co-cultures. Possibly, it does not play a significant role during matrix remodelling of hypertrophic cartilage.

Surprisingly, endothelial cells correlated only with M2 macrophages, suggesting an interaction between these cell types. Macrophages are essentail for neovascularization during wound repair(53) and resident monocytes and macrophages in the skin are important during subcutaneous implantations(54). Yet, to our knowledge the role of M2 macrophages in vascularization of hypertrophic cartilage has not been described.

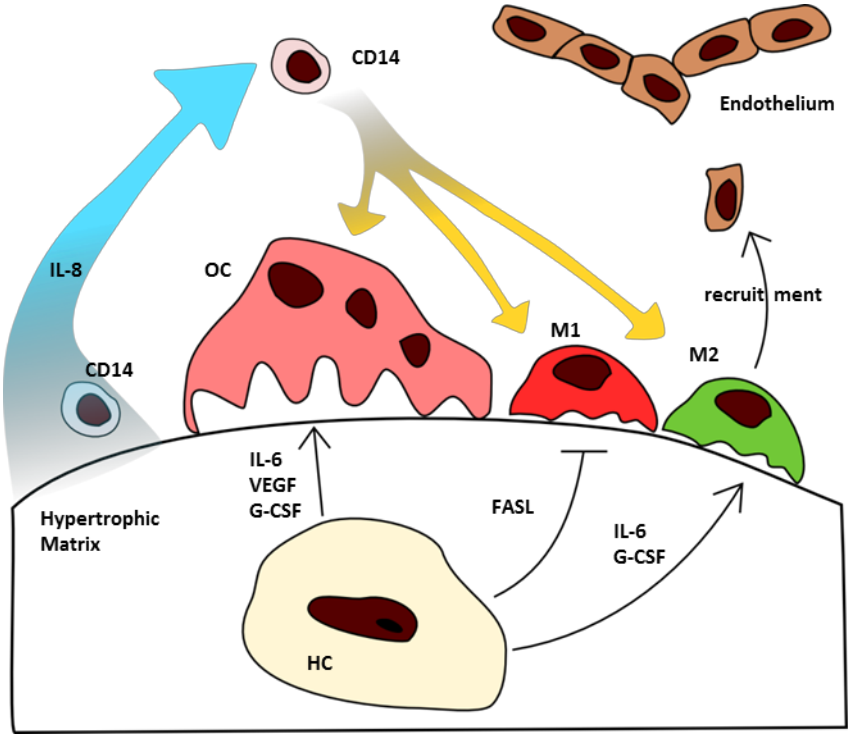

Figure 5: Interactions of monocytes and hypertrophic matrix. CD14 = monocytes, OC = osteoclasts, HC = hypertrophic chondrocytes, M1/M2 = polarized macrophages, IL-6/8 = Interleukin, VEGF = vascular endothelial growth factor, G-CSF = granulocyte colony-stinulating factor, FASL = Fas ligand.

Taken together, our results show that endochondral ossification of engineered hypertrophic cartilage involves crucial interactions with both osteoclasts and macrophages (Figure 5). While common precursor monocytes could be attracted by IL-8, their survival and differentiation into osteoclasts may depend on MMP-13, IL-6, VEGF, G-CSF and FASL. Formation of M2 macrophages could also be dependent on IL-6 and G-CSF signaling and could be crucial for subsequent vascularization. Importantly, devitalized matrices lacking these interactive mechanisms could equally attract monocytes but fail to support differentiation of osteoclasts and M2 macrophages in vivo.

The model system we describe here refines the current understanding of hypertrophic cartilage remodelling and endochondral ossification. Since the basis is engineered hypertrophic matrix, it is possible to modify single matrix components and singaling pathways of hypertrophic chondrocytes(8). It is also possible to control and

analyse monocyte-mediated digestion and signaling. The use of patient derived MSC and CD14+ monocytes opens the possibility to personalize pharmacological screenings and investigate rare disease phenotypes.

In conclusion, seeding of osteoclastogenic monocytes was not sufficient to improve bone formation of living or devitalized hypertrophic cartilage. While common precursor monocytes could be attracted by devitalized matrix, their survival and differentiation into osteoclasts depends on interactions with hypertrophic chondrocytes. Presence of M2 macrophages was correlated with subsequent vascularization. Our consistent in vitro and in vivo model thus improves the understanding of end-stage endochondral ossification.

Acknowledgements

The AO Foundation (AO S-11-13P) and the Swiss National Science Fund (Grant 310030_133110) supported this study. We thank Anna Marsano, Sarah Dimeloe and Marco Fischer for their technical support.

Abbreviations

BMP - bone morphogenic protein
BSP - bone sialoprotein
FASL - Fas ligand
FGF - fibroblast growth factor
G-CSF - granulocyte colony stimulating factor
HUVEC - human umbilical vein endothelial cells
IL- interleukin
MCP – monocyte chemotactic protein
MMP - matrix metalloproteinase
MSC - mesenchymal stromal cells
OPG - osteoprotegerin
SCF – stem cell factor
SDF – stromal cell-derived factor
TGF - transforming growth factor
TRAP - tartrate resistant acid phosphatase
VEGFa - vascular endothelial growth factor a

Supplementary figures

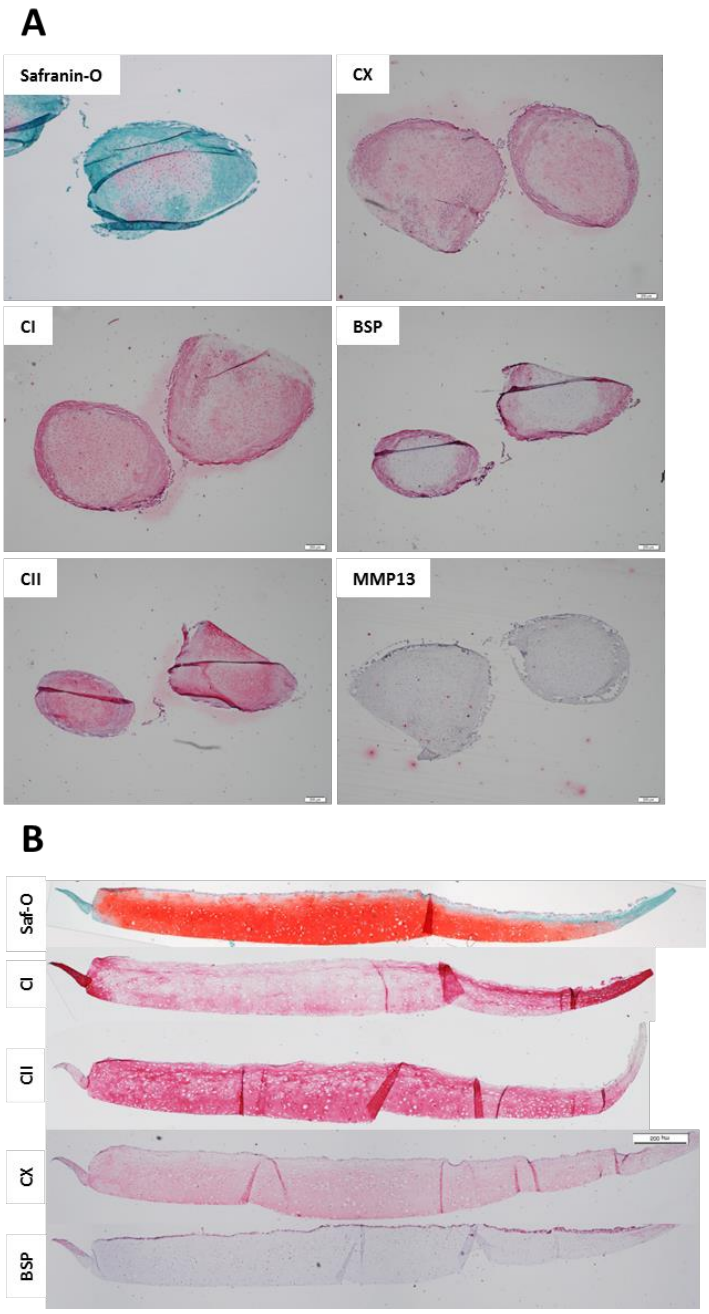

Supplementary Figure 1: Morphological and molecular appearance of hypertrophic matrix after 5 weeks of in vivo culture. A: Pellet culture in polypropylene tubes. CI = collagen type I, CII = collagen type II, CX = collagen type X, BSP = bone sialoprotein, MMP13 = matrix metalloproteinase 13. Scale bar is 200 um. B: Transwell culture. Scale bar is 500um

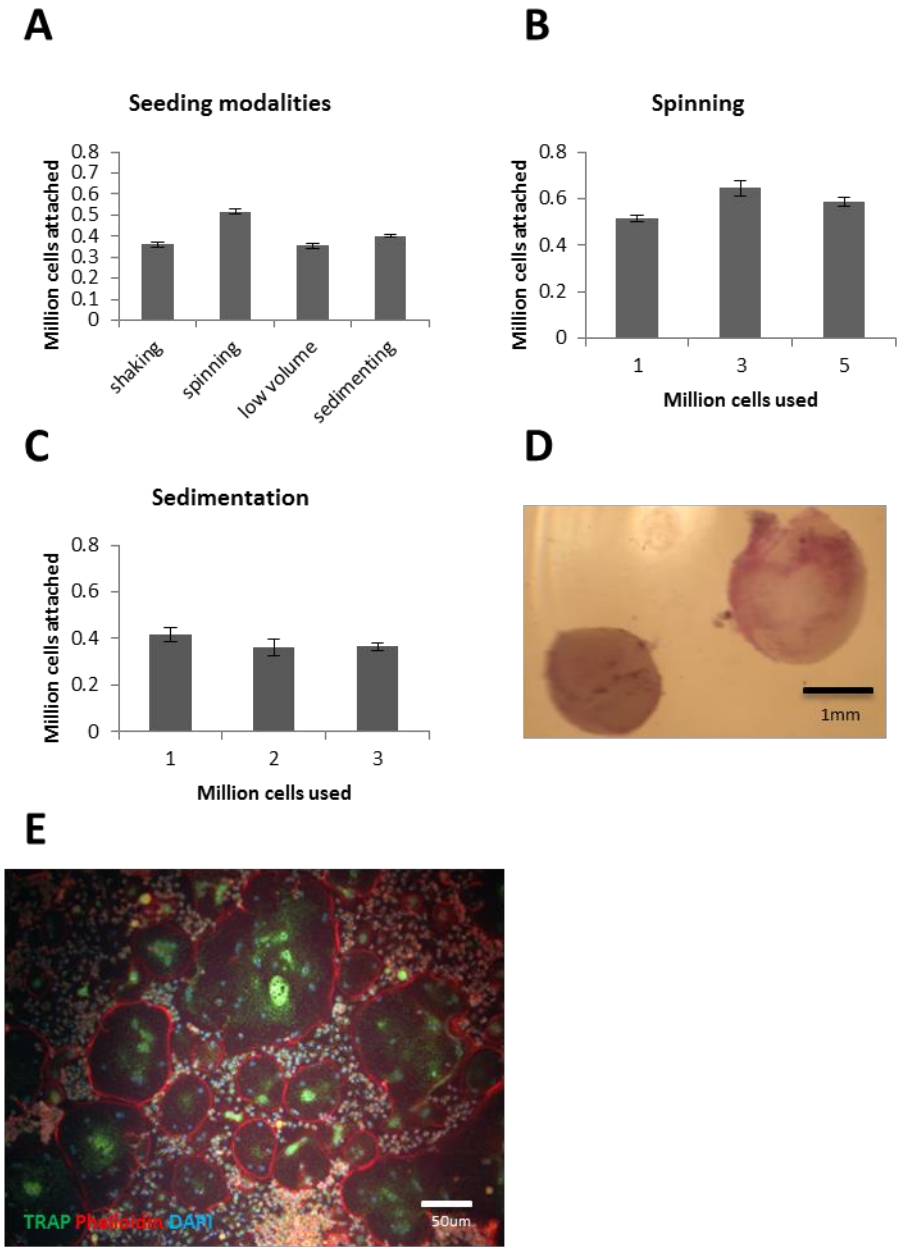

Supplementary Figure 2: Seeding of CD14 monocytes and development of osteoclasts. Living monocytes were seeded onto deviatlized hypertrophic matrix. 24h later the number of attached cells was calculated with the use of MTT. Different seeding modalities (A) with variable monocyte numbers (B and C) were used. Regardless of modality or cell concentration, an average of 520'000 cells attached in aggregates (D). After 1 week of culture on plastic large multinucleated TRAP positive cells with actin rings had formed (E).

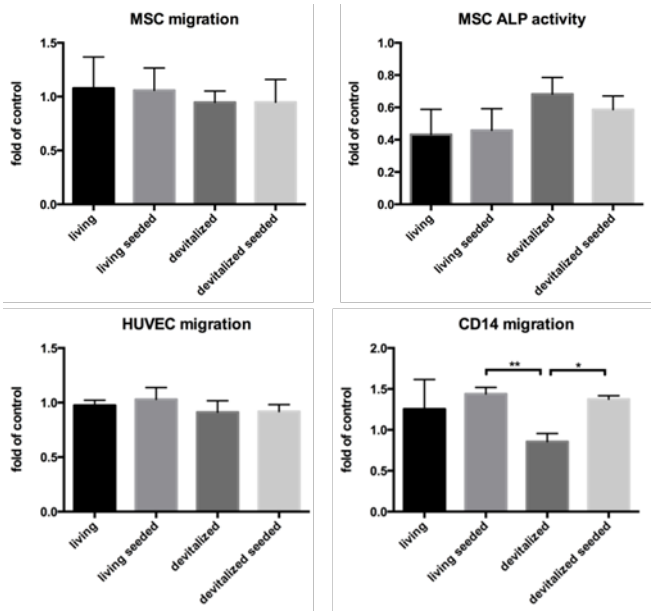

Supplementary Figure 3: Migration and differentiation studies using supernatants from the co-culture. Human MSC do not show any migration differences or difference in alkaline phosphatase activity between groups. HUVEC do not show any difference in migration between groups. Human CD14 migration is significantly higher in living seeded and devitalized seeded samples compared to devitalized samples.

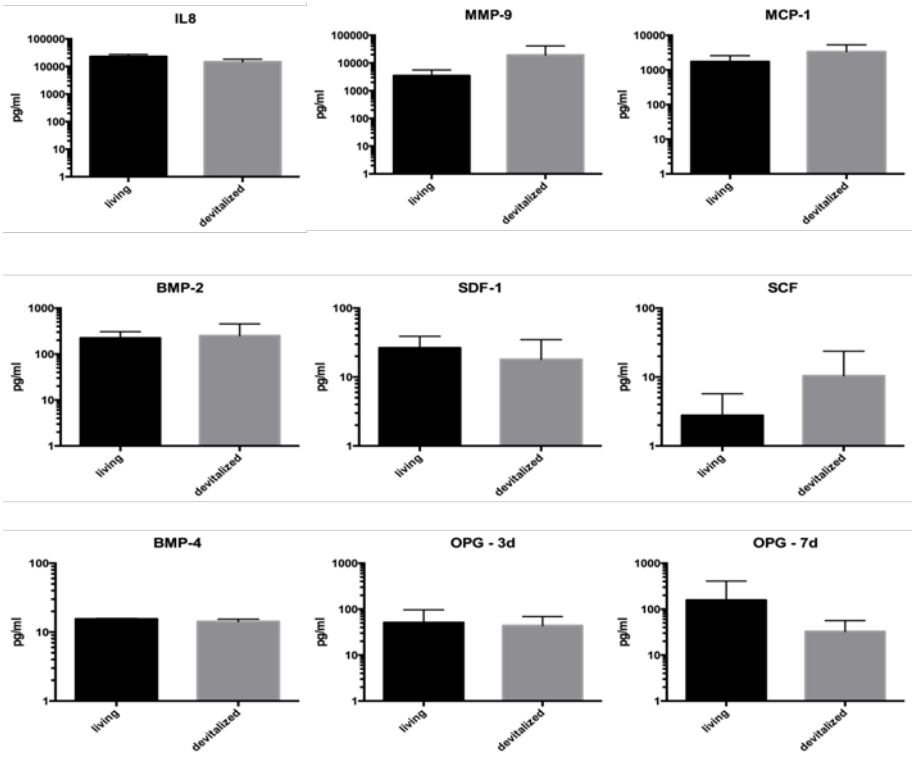

Supplementary Figure 4: Proteins which were not significantly different in living and devitalized seeded groups. No TGFb was found in any of the supernatants.

References

1. MacRae VE, Farquharson C, & Ahmed SF (2006) The pathophysiology of the growth plate in juvenile idiopathic arthritis. *Rheumatology* 45(1):11-19.
2. Michigami T (2013) Regulatory mechanisms for the development of growth plate cartilage. *Cellular and molecular life sciences : CMLS* 70(22):4213-4221.
3. Fox C, Edwards MH, Dennison EM, & Cooper C (2015) Personal and Societal Burden of Osteoporotic Fractures. *Clinic Rev Bone Miner Metab* 13(2):53-60.
4. Scotti C*, et al.* (2010) Recapitulation of endochondral bone formation using human adult mesenchymal stem cells as a paradigm for developmental engineering. *Proceedings of the National Academy of Sciences of the United States of America* 107(16):7251-7256.
5. Ortega N, Behonick D, Stickens D, & Werb Z (2003) How proteases regulate bone morphogenesis. *Annals of the New York Academy of Sciences* 995:109-116.
6. Mackie EJ, Ahmed YA, Tatarczuch L, Chen KS, & Mirams M (2008) Endochondral ossification: how cartilage is converted into bone in the developing skeleton. *The international journal of biochemistry & cell biology* 40(1):46-62.
7. Mackie EJ, Tatarczuch L, & Mirams M (2011) The skeleton: a multi-functional complex organ: the growth plate chondrocyte and endochondral ossification. *The Journal of endocrinology* 211(2):109-121.
8. Bourgine PE*, et al.* (2014) Osteoinductivity of engineered cartilaginous templates devitalized by inducible apoptosis. *Proceedings of the National Academy of Sciences of the United States of America* 111(49):17426-17431.
9. Ortega N, Wang K, Ferrara N, Werb Z, & Vu TH (2010) Complementary interplay between matrix metalloproteinase-9, vascular endothelial growth factor and osteoclast function drives endochondral bone formation. *Disease models & mechanisms* 3(3-4):224-235.
10. Inada M*, et al.* (2004) Critical roles for collagenase-3 (Mmp13) in development of growth plate cartilage and in endochondral ossification. *Proceedings of the National Academy of Sciences of the United States of America* 101(49):17192-17197.
11. Gerber HP*, et al.* (1999) VEGF couples hypertrophic cartilage remodeling, ossification and angiogenesis during endochondral bone formation. *Nature medicine* 5(6):623-628.
12. Wong KL*, et al.* (2012) The three human monocyte subsets: implications for health and disease. *Immunologic research* 53(1-3):41-57.
13. Thomas G, Tacke R, Hedrick CC, & Hanna RN (2015) Nonclassical patrolling monocyte function in the vasculature. *Arteriosclerosis, thrombosis, and vascular biology* 35(6):1306-1316.
14. Teitelbaum SL & Ross FP (2003) Genetic regulation of osteoclast development and function. *Nature reviews. Genetics* 4(8):638-649.
15. Sorensen MG*, et al.* (2007) Characterization of osteoclasts derived from CD14+ monocytes isolated from peripheral blood. *Journal of bone and mineral metabolism* 25(1):36-45.
16. Quinn JM, Elliott J, Gillespie MT, & Martin TJ (1998) A combination of osteoclast differentiation factor and macrophage-colony stimulating factor is sufficient for both human and mouse osteoclast formation in vitro. *Endocrinology* 139(10):4424-4427.
17. Seta N, Okazaki Y, & Kuwana M (2008) Human circulating monocytes can express receptor activator of nuclear factor-kappaB ligand and differentiate into functional osteoclasts without exogenous stimulation. *Immunology and cell biology* 86(5):453-459.

18. Hemingway F, *et al.* (2011) In vitro generation of mature human osteoclasts. *Calcified tissue international* 89(5):389-395.
19. Papadimitropoulos A, *et al.* (2011) A 3D in vitro bone organ model using human progenitor cells. *European cells & materials* 21:445-458; discussion 458.
20. Barbosa I, *et al.* (2003) Improved and simple micro assay for sulfated glycosaminoglycans quantification in biological extracts and its use in skin and muscle tissue studies. *Glycobiology* 13(9):647-653.
21. Burstone MS (1958) Histochemical demonstration of acid phosphatases with naphthol AS-phosphates. *Journal of the National Cancer Institute* 21(3):523-539.
22. Schneider CA, Rasband WS, & Eliceiri KW (2012) NIH Image to ImageJ: 25 years of image analysis. *Nature methods* 9(7):671-675.
23. Doube M, *et al.* (2010) BoneJ: Free and extensible bone image analysis in ImageJ. *Bone* 47(6):1076-1079.
24. Sheets KG, *et al.* (2013) Microglial ramification and redistribution concomitant with the attenuation of choroidal neovascularization by neuroprotectin D1. *Molecular vision* 19:1747-1759.
25. Mantovani A, *et al.* (2004) The chemokine system in diverse forms of macrophage activation and polarization. *Trends in immunology* 25(12):677-686.
26. Dimitriou R, Tsiridis E, & Giannoudis PV (2005) Current concepts of molecular aspects of bone healing. *Injury* 36(12):1392-1404.
27. Bastian O, *et al.* (2011) Systemic inflammation and fracture healing. *Journal of leukocyte biology* 89(5):669-673.
28. Blin-Wakkach C, Rouleau M, & Wakkach A (2014) Roles of osteoclasts in the control of medullary hematopoietic niches. *Archives of biochemistry and biophysics* 561:29-37.
29. Katavic V, *et al.* (2003) Non-functional Fas ligand increases the formation of cartilage early in the endochondral bone induction by rhBMP-2. *Life Sci* 74(1):13-28.
30. Kovacic N, *et al.* (2007) The Fas/Fas ligand system inhibits differentiation of murine osteoblasts but has a limited role in osteoblast and osteoclast apoptosis. *Journal of immunology* 178(6):3379-3389.
31. Fujihara Y, Takato T, & Hoshi K (2014) Macrophage-inducing FasL on chondrocytes forms immune privilege in cartilage tissue engineering, enhancing in vivo regeneration. *Stem cells* 32(5):1208-1219.
32. Deshmane SL, Kremlev S, Amini S, & Sawaya BE (2009) Monocyte chemoattractant protein-1 (MCP-1): an overview. *Journal of interferon & cytokine research : the official journal of the International Society for Interferon and Cytokine Research* 29(6):313-326.
33. Graves DT, Jiang Y, & Valente AJ (1999) The expression of monocyte chemoattractant protein-1 and other chemokines by osteoblasts. *Frontiers in bioscience : a journal and virtual library* 4:D571-580.
34. Kitaori T, *et al.* (2009) Stromal cell-derived factor 1/CXCR4 signaling is critical for the recruitment of mesenchymal stem cells to the fracture site during skeletal repair in a mouse model. *Arthritis and rheumatism* 60(3):813-823.
35. Dai J & Rabie AB (2007) VEGF: an essential mediator of both angiogenesis and endochondral ossification. *Journal of dental research* 86(10):937-950.
36. Boyce BF & Xing L (2008) Functions of RANKL/RANK/OPG in bone modeling and remodeling. *Archives of biochemistry and biophysics* 473(2):139-146.
37. Iqbal J, Sun L, & Zaidi M (2009) Coupling bone degradation to formation. *Nature medicine* 15(7):729-731.
38. Yagi M, *et al.* (2005) DC-STAMP is essential for cell-cell fusion in osteoclasts and foreign body giant cells. *The Journal of experimental medicine* 202(3):345-351.
39. Blumer MJ, Longato S, & Fritsch H (2008) Localization of tartrate-resistant acid phosphatase (TRAP), membrane type-1 matrix metalloproteinases (MT1-MMP)

and macrophages during early endochondral bone formation. *Journal of anatomy* 213(4):431-441.
40. Atkins GJ, *et al.* (2006) RANK Expression as a cell surface marker of human osteoclast precursors in peripheral blood, bone marrow, and giant cell tumors of bone. *Journal of bone and mineral research : the official journal of the American Society for Bone and Mineral Research* 21(9):1339-1349.
41. Fuller K, Kirstein B, & Chambers TJ (2007) Regulation and enzymatic basis of bone resorption by human osteoclasts. *Clinical science* 112(11):567-575.
42. Alvarez J, Costales L, Serra R, Balbin M, & Lopez JM (2005) Expression patterns of matrix metalloproteinases and vascular endothelial growth factor during epiphyseal ossification. *Journal of bone and mineral research : the official journal of the American Society for Bone and Mineral Research* 20(6):1011-1021.
43. Kojima T, *et al.* (2013) Histochemical aspects of the vascular invasion at the erosion zone of the epiphyseal cartilage in MMP-9-deficient mice. *Biomedical research* 34(3):119-128.
44. Knudsen E, *et al.* (2011) G-CSF enhances the proliferation and mobilization, but not the maturation rate, of murine myeloid cells. *European journal of haematology* 87(4):302-311.
45. Souza PP & Lerner UH (2013) The role of cytokines in inflammatory bone loss. *Immunological investigations* 42(7):555-622.
46. Li S, *et al.* (2015) Granulocyte Colony-Stimulating Factor Induces Osteoblast Inhibition by B Lymphocytes and Osteoclast Activation by T Lymphocytes during Hematopoietic Stem/Progenitor Cell Mobilization. *Biology of blood and marrow transplantation : journal of the American Society for Blood and Marrow Transplantation* 21(8):1384-1391.
47. Roca H, *et al.* (2009) CCL2 and interleukin-6 promote survival of human CD11b+ peripheral blood mononuclear cells and induce M2-type macrophage polarization. *J Biol Chem* 284(49):34342-34354.
48. Yamaguchi T, *et al.* (2012) Preventive effect of G-CSF on acute lung injury via alveolar macrophage regulation. *The Journal of surgical research* 178(1):378-384.
49. D'Aveni M, *et al.* (2015) G-CSF mobilizes CD34+ regulatory monocytes that inhibit graft-versus-host disease. *Science translational medicine* 7(281):281ra242.
50. Lieschke GJ, *et al.* (1994) Mice lacking granulocyte colony-stimulating factor have chronic neutropenia, granulocyte and macrophage progenitor cell deficiency, and impaired neutrophil mobilization. *Blood* 84(6):1737-1746.
51. Park H, *et al.* (2005) Interaction of Fas ligand and Fas expressed on osteoclast precursors increases osteoclastogenesis. *Journal of immunology* 175(11):7193-7201.
52. Tang Y, *et al.* (2009) TGF-beta1-induced migration of bone mesenchymal stem cells couples bone resorption with formation. *Nature medicine* 15(7):757-765.
53. Brancato SK & Albina JE (2011) Wound macrophages as key regulators of repair: origin, phenotype, and function. *The American journal of pathology* 178(1):19-25.
54. Summerfield A, Meurens F, & Ricklin ME (2015) The immunology of the porcine skin and its value as a model for human skin. *Molecular immunology* 66(1):14-21.

Chapter 5

Fat-derived stromal vascular fraction cells enhance the bone forming capacity of devitalized engineered hypertrophic cartilage matrix

Manuscript submitted to Annals of Surgery

Fat-derived stromal vascular fraction cells enhance the bone forming capacity of devitalized engineered hypertrophic cartilage matrix

Matthias Kreutz[1,2,3°] & Atanas Todorov[1,2,°], Alexander Haumer[1,2], Celeste Scotti[4], Andrea Barbero[1], Paul E. Bourgine[1,§], Arnaud Scherberich[1], Claude Jaquiery[2,3], Ivan Martin[1,2]

[1] Department of Biomedicine, University of Basel, Switzerland; [2] Department of Surgery, University Hospital Basel, Switzerland, [3] Clinic for Oral and Maxillofacial Surgery University Hospital Basel, Switzerland and [4] I.R.C.C.S. Istituto Ortopedico Galeazzi, Milano, Italy

° Matthias Kreutz and Atanas Todorov contributed equally to this article.

§ Current affiliation: Department of Biosystems Science and Engineering (D-BSSE), ETH Zurich, 4058 Basel, Switzerland

Corresponding authors: Ivan Martin (ivan.martin@usb.ch) and Claude Jaquiery (claude.jaquiery@usb.ch), University Hospital Basel, Hebelstrasse 20, 4031 Basel, Switzerland

Running headline: Reactivation of devitalized engineered hypertrophic cartilage

Abstract

Engineered and devitalized hypertrophic cartilage (HC) has been proposed as an off-the-shelf bone substitute material potentially combining the features of osteoinductivity, resistance to hypoxia, capacity to attract blood vessels and potential to be customized for specific indications. However, as compared to the vital tissues, devitalized HC grafts have reduced efficiency of bone formation and longer remodeling times. In order to address these limitations, here we tested the possibility to activate devitalized HC by stromal vascular fraction (SVF) cells from human adipose tissue, which include mesenchymal, endothelial and osteoclastic progenitors. HC pellets generated by human stromal cells from bone marrow were devitalized by freeze/thaw and implanted ectopically in nude mice or in calvarial defects in nude rats, after embedding in fibrin gel with or without different amounts of SVF cells. Ectopically, SVF cells added to devitalized HC increased the amount of bone formation in a cell-number-dependent fashion and directly contributed to endothelial, osteoblastic and osteoclastic populations. Bone volume correlated with the number of implanted CD31+CD34+CD146+ endothelial progenitors. Also in the calvarial model, SVF activation of HC strongly enhanced bone tissue formation. Our findings outline a bone augmentation strategy based on devitalized allogeneic HC, intraoperatively activated with autologous SVF cells.

Keywords: bone, stromal vascular fraction, endochondral ossification, endothelial progenitors, orthotopic defect

Introduction

Clinical treatment of challenging bone defects often requires a suitable bone graft, yet extensive donor site morbidity and complication rates around 60%(1) pose significant problems to the use of autologous bone. Commercially available bone substitute materials typically lack intrinsic osteoinductive potential and the long-term integration into bone defects is not always warranted(2).

The use of engineered hypertrophic cartilage is receiving an increasing consideration as a possible bone substitute, due to many inherent advantages. As a bradytroph and hypoxia-resistant tissue(3), it does not require immediate vascularization. Moreover, it has some initial mechanical stability and it embeds the biological signals for the remodelling into a complete bone organ, resembling the processes of embryonic bone development (4). Although the bone forming capacity of engineered hypertrophic cartilage has been demonstrated in stringent ectopic implantation models as well as in an orthotopic non-union model (5-9), clinical translation can be hampered by the required use of autologous cells, their known and unpredictable variability across different donors, and the long times for in vitro construct generation.

Devitalization and off-the-shelf storage of engineered, allogeneic hypertrophic cartilage could offer an attractive bone substitute material, based on the assumption that the deposited extracellular matrix (ECM) would physiologically deliver a suitable combination of cytokines and morphogens to recruit and instruct endogenous osteoprogenitors at the repair site(10). Previous work has shown that the signals necessary for osteoinduction can be preserved in the ECM, provided a mild but effective devitalisation strategy(11). Yet, the efficiency of bone formation remains reduced as compared to the vital tissue. Moreover, this difference is expected to become increasingly relevant along with the graft size, due to the time required by host cells to penetrate and reactivate the matrix, a pre-requisite for tissue remodelling into bone(12).

Inspired by the "developmental engineering" concept of modularity, whereby "the interfaces between developing entities are initially uncoupled"(13), here we investigated the possibility of using multiple small organoids of engineered and devitalized hypertrophic cartilage to generate a larger bone volume. The strategy is based on the rationale that each construct would efficiently develop into bone tissue as an independent module, due to the large surface area to volume ratio, and the tissues would then fuse into a monolithic trabecular structure.

In order to enhance the reactivation and remodelling of the devitalized ECM, we further introduced the use of stromal vascular fraction (SVF) cells, freshly harvested from human adipose tissue and embedded within a gel along with the devitalized cartilage matrix. The rationale was based on the fact that SVF cells contain endothelial progenitors, monocytes and mesenchymal stromal cells(14), with the respective capacity to potentially enhance tissue vascularization, osteoclast-mediated remodelling and bone formation.

The goal of the present study was thus to test the hypothesis that the supplementation of human SVF cells to multiple pellets of engineered & devitalized hypertrophic cartilage leads to a composite construct with enhanced capacity to form de novo bone tissue, both ectopically (i.e., subcutaneously in nude mice) and orthotopically (i.e., in a calvarial defect model in nude rats).

Materials and Methods

All human samples were collected with informed patient consent and after approval by the local ethical committee, in accordance to Swiss law. Animal procedures were approved by the Swiss Federal Veterinary Office (Kantonal permit BS-2590).

Preparation of devitalized hypertrophic constructs

Human bone marrow stromal cells from 5 donors (35.4 ± 11.3 years, all male) were expanded for 2 passages in complete medium (alpha-MEM, 10% fetal bovine serum, 10 mM HEPES, 1 mM sodium pyruvate, 100 U/mL penicillin, 100 μg/mL streptomycin, 0.29 mg/mL

glutamate, all from Invitrogen) containing FGF-2 (5 ng/mL, R&D systems, USA), as previously described(15). Pellets were prepared by centrifuging $0.5x10^6$ cells in 1.5 mL screw cap Eppendorf tubes at 300 g for 5 minutes and cultured in serum free medium (DMEM, 1.25 mg/mL human serum albumin, 10 mM HEPES, 1 mM sodium pyruvate, 100 U/mL penicillin, 100 µg/mL streptomycin, 0.29 mg/mL glutamate and ITS-A [10 µg/mL insulin, 5.5 µg/mL transferrin, 5 ng/mL selenium, 0.5 mg/mL bovine serum albumin] from Invitrogen) supplemented with 10 ng/mL TGF-β1 (R&D Systems), 10^{-7}M dexamethasone and 0.1 mM ascorbic acid 2-phospahte (Sigma-Aldrich) (chondrogenic medium). After 3 weeks, resulting cartilaginous pellets were further cultured in hypertrophic medium (serum free medium with 50 nM thyroxine, 10 mM β-glycerophosphate, 10^{-8} M dexamethasone, 0.1 mM ascorbic acid 2-phosphate and 50 pg/mL IL-1β, Sigma-Aldrich) for 2 weeks, as previously described(15, 16). The generated hypertrophic pellets were devitalized using 3 cycles of freezing (-196°C for 10 minutes) and thawing (37°C for 10 minutes) and a final wash with deionized water. Pellets were stored at -80°C until further use.

Isolation of SVF cells

SVF cells from liposuctions or excision fat were isolated from 12 donors (33.7 ± 7.7 years, 2 males and 10 females) as described previously(17, 18). Briefly, minced fat tissue was incubated for 60 minutes in 0.15% collagenase type 2 solution, centrifuged and supernatants discarded. Cells were resuspended, filtered through 100 µm mesh filters and counted in a Neubauer counting chamber using crystal violet. FACS analysis for CD31, CD34, CD146, CD90, CD105 and CD15 (AbD Serotec, USA) was performed as previously described(17). Cells were frozen in fetal bovine serum and 10% DMSO and kept in the gaseous phase of liquid nitrogen until further use.

Preparation of grafts

SVF cells were thawed, counted and the appropriate amount resuspended in 40 µL fibrinogen (100 mg/mL, Tisseel, Baxter USA). Control samples contained no SVF cells. Multiple devitalized hypertrophic pellets (12 to 24, depending on the experiment, but constant for all

groups in one experiment) were mixed with this solution and 40 µL of thrombin (400 units/mL with 40 µM $CaCl_2$, Tisseel, Baxter USA) were added. Polymerization was allowed to occur for 30 minutes at 37°C, followed by immediate implantation.

Ectopic and orthotopic implantation

For ectopic implantations, grafts were inserted into subcutaneous pouches of nude mice (CD-1 nude/nude, Charles River Laboratories) at 4 pouches per mouse, with duplicate grafts per donor and experimental group. The operation was performed with Isoflurane (Attane Isoflurane, Provet AG, Switzerland) anaesthesia and Buprenorphine (Temgesic, Reckitt Benckiser AG) analgesia and animals were checked periodically. After 12 weeks, mice were euthanized with CO_2 and explants were assessed as described below.

For orthotopic implantations, nude rats (RNU, Charls River Laboratories) were anesthetized using Isoflurane and the calvaria were exposed by dissection of the subcutaneous tissue and periosteum. Bilateral 4 mm defects were created in the central area of each parietal bone using a saline-cooled trephine bur. The defect was refined using a piezoelectric knife in order not to injure the dura mater. The sites were constantly irrigated with sterile NaCl 0.9% to prevent overheating of the bone margins and to remove the bone debris. Grafts were moulded into the defect using a small spoon and spatula. Incisions were closed in double layer by sutures and clamps, which were removed after 10 days. Animals were carefully monitored for behavioural abnormalities after the operation. After 4 weeks, the rats were euthanized with CO_2 followed by decapitation and the calvaria were stored and assessed as described below.

Microtomography

After explantation, samples were fixed in 4% paraformaldehyde overnight and then transferred to PBS. Microtomography was performed using a tungsten x-ray source at 70 kV and 260 µA with an aluminium filter of 0.5 mm (Nanotome, GE, USA). Transmission images were acquired for 360° with an incremental step size of 0.25°. Volumes were reconstructed using a

modified Feldkamp algorithm (software supplied by manufacturer) at a voxel size of 2.5 – 15 μm. Thresholding, segmentation and 3D measurements were performed using the ImageJ(19) software with the BoneJ(20) and 3DShape(21) additions.

Histology

Samples were decalcified using a 7% EDTA 30% sucrose solution (Sigma-Aldrich, USA) and either embedded in paraffin for histological stainings or frozen in OCT for immunofluorescence. Sections (5-10 μm thick) were stained with haematoxylin and eosin (HE), Masson trichrome or Safranin-O. HE stained sections were used for the histological quantification of bone as described previously(22). In situ hybridization for human ALU sequences was performed as described previously(11) (PNAS 2014) to detect the presence of human cells. Immunohistochemistry and immunofluorescence were performed using primary antibodies for DIPEN (1042002, MDBiosciences, USA), type X collagen (ab49945), type II collagen (ab34712), MMP13 (ab39012), MMP9 (ab38898), CD31 (ab28364), human calcitonin receptor (ab175297, all from Abcam, UK) and human CD34 (CBL496, Dako, Denmark). Secondary antibodies labelled with Alexa Fluor 488, Alexa Fluor 546 or Alexa Fluor 647 (Invitrogen, USA) were used and DAPI (Sigma-Aldrich, USA) was used to stain nuclei in fluorescence images. Immunohistochemistry was done with biotinylated secondary antibodies (Dako, Denmark) and the Vectastain ABC kit (Vector Laboratories, USA). The Olympus BX61, BX63, Zeiss LSM 710 and Nikon A1R microscopes were used to acquire images.

Statistical analysis

The data was visualized and analysed using the GraphPad Prism v. 6 software. Parametric ANOVA with the appropriate post-hoc tests as well as linear regressions were performed. P-values below 0.05 were considered to indicate statistically significant differences.

Results

Devitalized hypertrophic constructs activated with SVF cells form ectopic bone

Hypertrophic cartilage pellets engineered from human bone marrow-derived mesenchymal stromal cells (between 300 to 800 pellets for each of the five donors used) had an approximate diameter of 1-2 mm. Positive staining for glycosaminoglycans, type II and type X collagen (Figure 1A) were consistent with previously reported morphological and molecular features(15). After freeze/thaw devitalization, 12 pellets were suspended in a fibrin gel with or without the addition of human SVF cells (6 million cells/ml gel) and implanted into nude mice (Figure 1B).

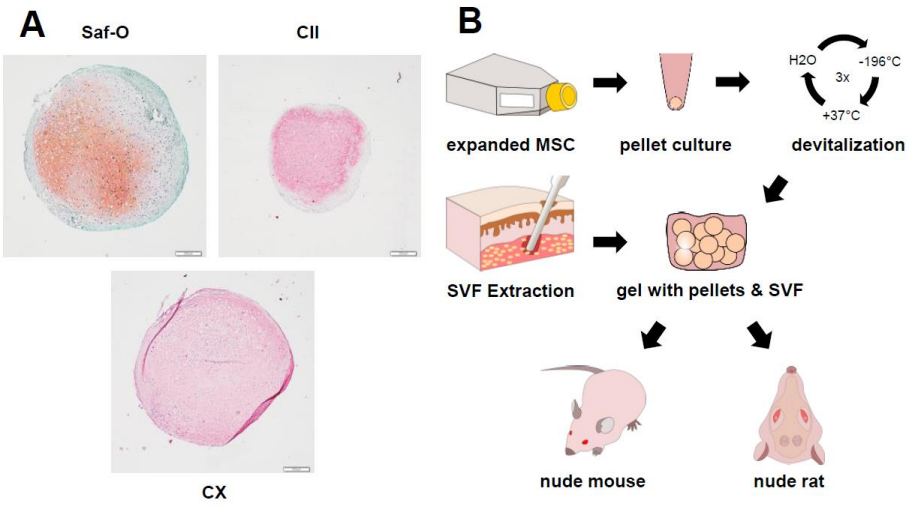

Figure 1. **A**: Representative staining of devitalized hypertrophic cartilage pellets. Saf-O = Safranin-O, CII = type II collagen, CX = type X collagen. Bars = 200um. **B**: Experimental setup for the generation of grafts, ultimately tested by implantation subcutaneously (nude mouse, ectopic model) or in calvarial defects (nude rat, orthotopic model).

After 12 weeks, control grafts in cell-free fibrin gel displayed depletion of glycosaminoglycans and only limited, scattered areas of remodelling into bone tissue (Figure 2A). Instead, SVF-activated grafts contained abundant osteoid matrix, embedding large areas occupied by bone marrow. In situ hybridization for human ALU sequences indicated that the SVF-activated grafts still contained human cells after 12 weeks in vivo, in contrast to the non-activated, devitalized grafts (Figure 2A). A closer immunohistochemical analysis showed that both the activated and non-activated grafts were undergoing MMP-driven degradation of cartilage matrix leading to aggrecan cleavage, as signalled by detection of the major MMP

cleavage site DIPEN (Figure 2B). Thus, aggrecan depletion did not appear to be directly related with the efficiency of bone and bone marrow development, which occurred to a markedly higher extent following SVF cell-based activation.

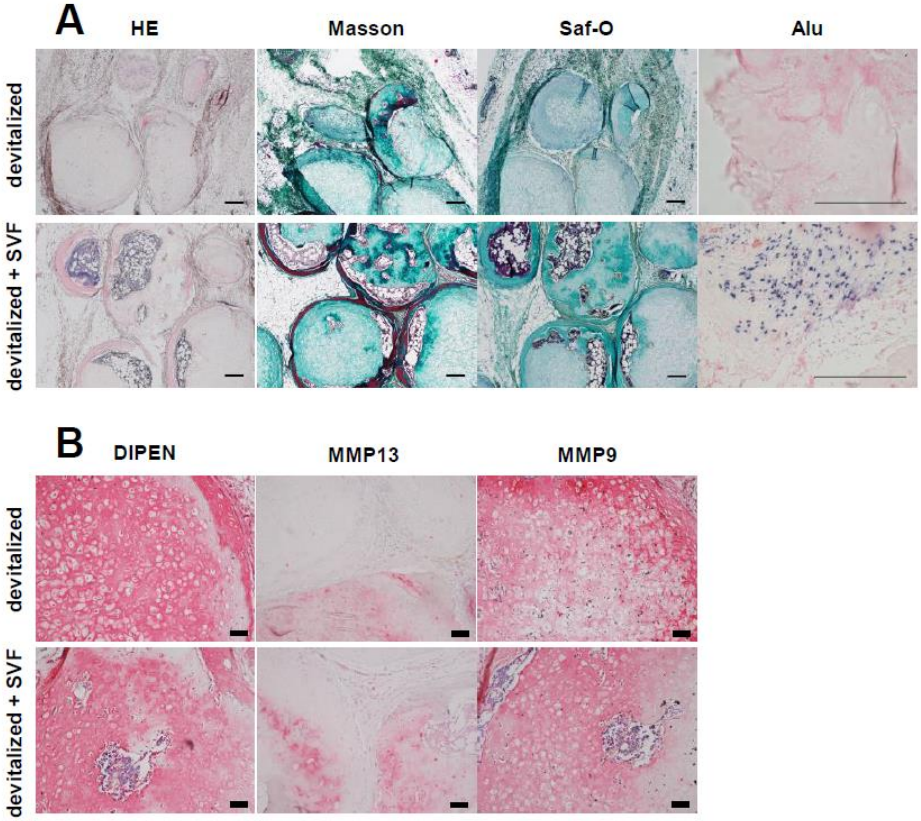

Figure 2. Ectopic bone formation of grafts based on devitalized hypertrophic cartilage pellets, embedded in fibrin gel without or with (+SVF) stromal vascular fraction cells from adipose tissue. **A**: Representative Hematoxilin and Eosin (HE), Masson-Tri-Chrome (Masson), Safranin-O (Saf-O) stainings and in situ hybridization for human ALU-sequences after 12 weeks in vivo. Bars = 200 μm. **B**: Stainings for metalloproteinase (MMP)13 and MMP9, as well as for the N-terminal neoepitope at the major MMP cleavage site (DIPEN) after 12 weeks in vivo. Bars = 50 μm.

The number of SVF cells correlates with ectopic bone quantity

We then assessed a possible dose-response in the effect of SVF cells. Up to 12 million cells/mL gel we identified a clear correlation between the number of SVF cells at implantation and the resulting amount of mineralized tissue, measured by microtomography (R^2 = 0.347; P = 0.01; Figure 3A), or of bone matrix, quantified in histological sections (R^2 = 0.546; P = 0.0025; Figure 3B). It should be highlighted that quantification of the total space covered by bone structures, including bone marrow cavities embedded within the osteoid trabeculae (Figure 3C), would lead to even more marked differences in the effect of SVF cells. The amount of bone

formation was similar or even reduced by graft activation with more than 12 million SVF cells/mL gel.

SVF cells contribute to osteoclast-mediated matrix resorption

The number of implanted SVF cells correlated significantly with the density of TRAP positive osteoclasts, histologically quantified after 12 weeks in vivo ($R^2 = 0.31$, $P = 0.03$; Figure 3D&E). Immunofluorescence staining for the human isoform of calcitonin receptor identified some multinucleated positive cells in the vicinity of the osteoid matrix even after 12 weeks in vivo (Figure 3F), especially in the conditions when a high number of SVF cells was used at implantation. These data suggest that activation of devitalized hypertrophic cartilage by SVF cells may enhance its resorption and that SVF cells could not only attract resident osteoclasts, but also offer a source for those.

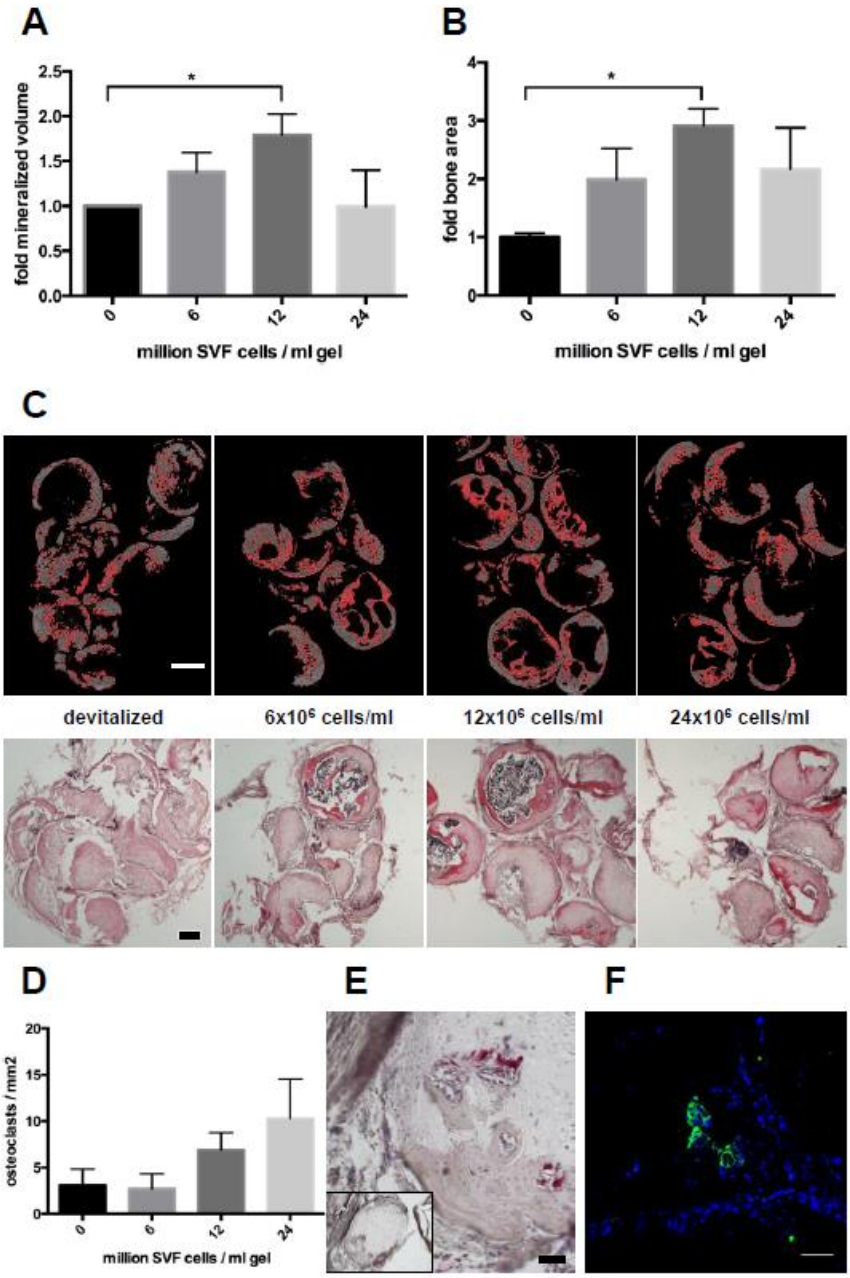

Figure 3. Following ectopic implantation, the amount of mineralized bone volume, quantified by microtomography (**A**) or the area covered by bone tissue, assessed in histological slides stained by Hematoxilin&Eosin (HE) (**B**), was expressed as fold difference of the non-activated grafts and plotted vs the number of embedded SVF cells (n = 5-6 grafts assessed / group; * = P < 0.05). **C**: Representative microtomography sections, with pixels marked in red if beyond the selected density threshold (top line) and HE-stained sections (bottom line) used to generate the data displayed in A and B. Bars = 500 μm. **D**: The density of osteoclasts, assessed by tartrate resistant acid phosphatase staining (TRAP), was plotted vs the number of embedded SVF cells (n = 3 grafts assessed per group). **E**: Representative TRAP staining. Bar = 50 μm or 300 μm (inset). **F**: Staining for human calcitonin receptor (hCTR, green fluorescence), indicating the direct contribution of SVF cells to osteoclast formation. Bar = 50 μm.

Specific SVF sub-populations of endothelial lineage correlate with total bone quantity

Considering the phenotypic heterogeneity of freshly isolated SVF cells, we addressed whether the amount of mineralized tissue could be correlated with the delivered dose of specific

SVF sub-populations. Therefore, we analyzed data generated from graft activation by different SVF preparations (n = 9 donors) against cytofluorimetric analysis of their phenotype, performed in parallel using the markers CD31, CD34, CD146, CD90, CD105 and CD15. The ratio of mineralized volume to total volume correlated most strongly with the number of implanted CD31 CD34 CD146 triple positive cells (R^2= 0.4756; P = 0.013; Figure 4A), which identify endothelial cells. No correlation was found with CD90 (R^2= 0.0226; P = 0.608; Figure 4B), CD105 (R^2 = 0.0450; P = 0.467) or CD15 (R^2 = 0.0616; P = 0.392) positive cells. Staining for DAPI, type X collagen and CD31 indicated that the activated grafts displayed a more advanced colonization of the hypertrophic matrix and a more uniformly organized vascular network than the non-activated grafts after 12 weeks in vivo (Figure 4C&D). Immunohistochemistry and immunofluorescence staining for the human isoform of CD34 indicated that some of the endothelial cells lining the vessels were of human origin (Figure 4E).

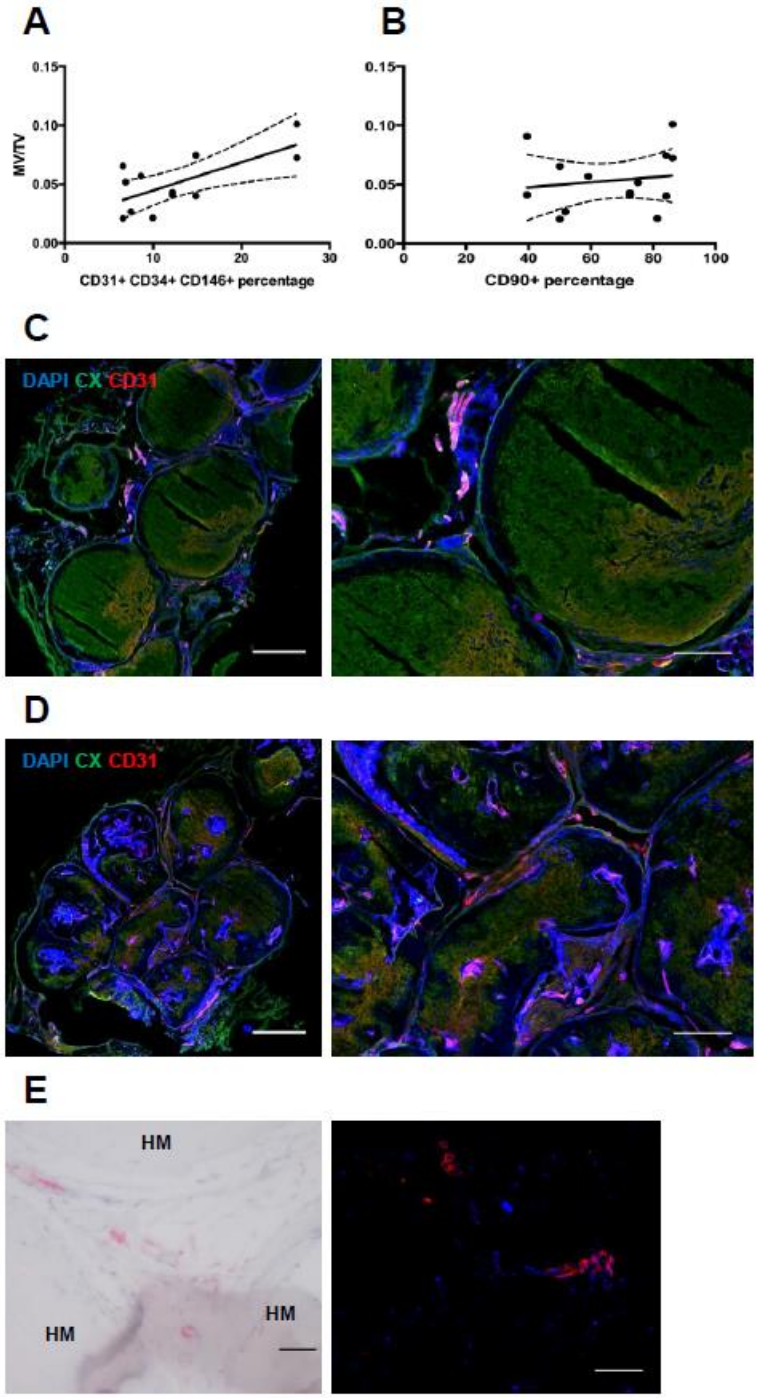

Figure 4. Plots of mineralized tissue volume (MV) / total tissue volume (TV) vs the percentage of embedded CD31+CD34+CD146+ (R2= 0.4756; P = 0.013) (**A**) or CD90+ SVF cells (R2= 0.0226; P = 0.608) (**B**). Dots represent single grafts. **C&D**: Representative immunofluorescence stainings for type X collagen (CX), CD31 and DAPI of devitalized samples without (**C**) or with SVF activation (**D**) after 12 weeks in vivo. Bars = 500 µm for left images and 200 µm for right images. **E**: Immunohistochemistry and immunofluorescence stainings for human CD3, identifying positive cells between remnants of hypertrophic matrix (HM). Bars = 50 µm.

SVF-activated constructs enhance early orthotopic bone formation and bridging to host bone

To evaluate the orthotopic bone regenerative capacity of SVF activated grafts, we implanted devitalized hypertrophic cartilage pellets with or without (control) additional SVF cells (12 million/ml fibrin) into 4 mm rat calvarial defects (Figure 1B). After 4 weeks, calcified volume inside the defects was nearly identical (Figure 5A). However, more rigorous histological analysis revealed that the percentage of defect area filled by bone matrix was up to 7-fold larger in the SVF activated than in the non-activated grafts ($P < 0.0001$; Figure 5B), with osteoid formation also reaching the center of the defect (Figure 5C,D). Higher magnification assessments indicated that bone formation in the SVF-activated group was developing by (i) remodelling of the pellets into trabecular bone organoids and (ii) merging of those modular structures with each other and with the rat calvarium surrounding the defect (Figure 5E). Both processes could not be recognized in the non-activated grafts, also due to the minimal amounts of bone formed at the time point of observation. In some areas of implants activated by SVF cells, human origin cells could be observed inside the osteoid matrix, including the areas corresponding to newly formed bone marrow sinusoids (Figure 5F).

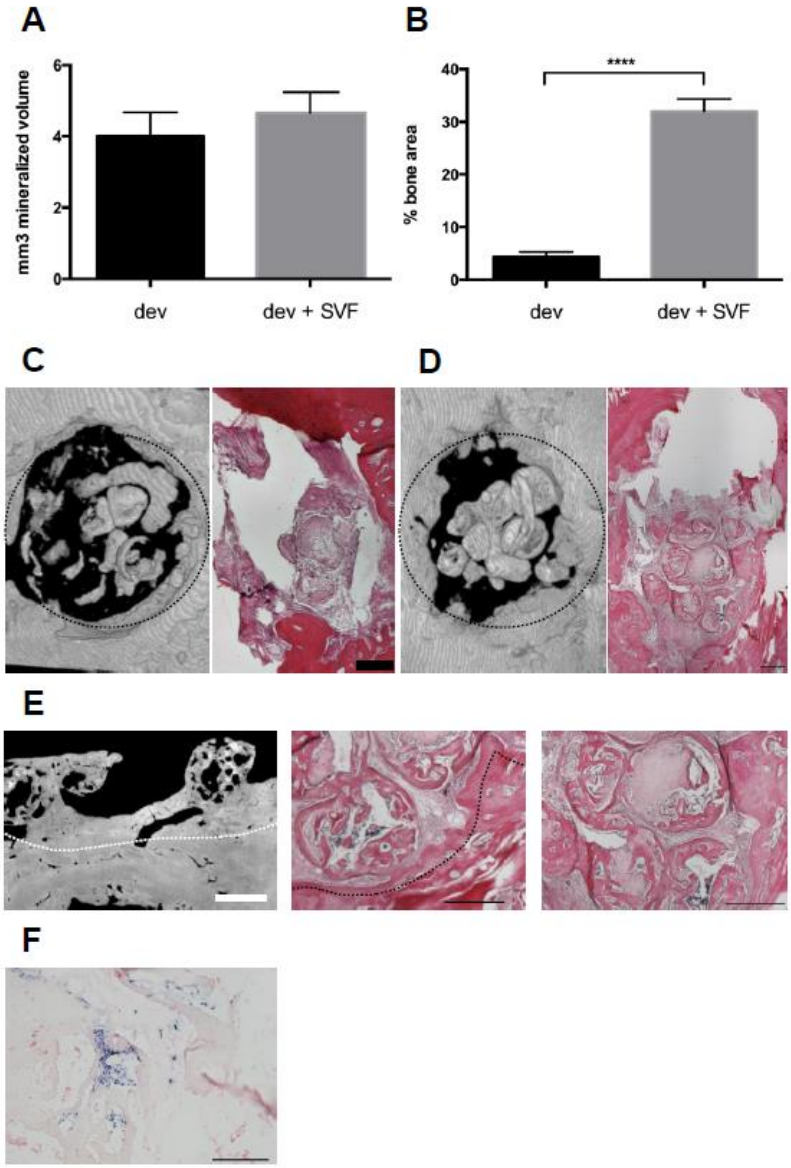

Figure 5. Bone repair capacity of devitalized hypertrophic cartilage pellets, embedded in fibrin gel without (dev) or with (dev+SVF) stromal vascular fraction (SVF) cells from adipose tissue, following implantation in rat calvarial defects. **A**: Mineralized volume quantified by microtomography (n = 9 grafts assessed / group). **B**: Bone area assessed in histological sections, expressed as percentage of total defect area (n = at least 24 sections assessed / group). **** = P < 0.0001. **C&D**: Representative 3D microtomography reconstructions (left) and Hematoxili/Eosin (HE) stainings (right) of the calvarial defects filled with devitalized grafts, implanted without (**C**) or with (**D**) activation by SVF cells after 4 weeks. Dotted circles indicate the defect borders (4mm diameter). Bars = 500 µm. **E**: Microtmography (left) and HE staining (middle & right) displaying the bridging between hypertrophic matrix and bone of the calvarium, or the fusion of single pellets (right). White bar = 850 µm. Black bars = 500 µm. Dotted lines indicate the edge of the calvarium. **F**: In situ hybridization for ALU sequences showing the presence of human cells in the explants. Bar = 200 µm.

Discussion

In this study we investigated the bone forming capacity of constructs generated by the combination of devitalized engineered hypertrophic cartilage pellets with freshly isolated SVF

cells from human adipose tissue. SVF activation of the hypertrophic cartilage strongly enhanced its bone formation efficiency, tested in subcutaneous ectopic implantation and calvarial defect models. In particular, the density of SVF cells was correlated with that of osteoclasts in the grafts, and the percentage of SVF-derived endothelial lineage cells was correlated with the amount of deposited mineralized matrix.

The concept of using multiple pellets formed by chondrogenic differentiation of human MSC for the engineering of bone substitute materials has been previously proposed for the treatment of segmental bone defects in immunodeficient mice(7) or rats(5). In both studies, the cartilage grafts resulted in the generation of vascularized bone tissue, thereby supporting that recapitulation of endochondral ossification is a valid strategy for bone repair at orthotopic sites. However, despite the overall good performance, limited integration across the implanted pellets was observed(7), indicating that scaling up bone graft materials by the principle of bringing together smaller modules may require further improvement. Moreover, the implantation of living tissues required the use of autologous cells, with associated cost and logistics issues.

In this context, the here described possibility of using engineered and then devitalized hypertrophic cartilage pellets would offer the distinct advantage of having 'off the shelf' units, possibly engineered by allogeneic cells. Our results indicate that the MSC-deposited, cell-free extracellular matrix does contain the cues to trigger bone and bone marrow formation, and that its effect is strongly potentiated by the activation through living progenitors derived from fat tissue. Interestingly, we observed highly efficient integration among the different pellets and with the surrounding bone areas. This could be due to the presence of a gel embedding the pellets, which would allow the ingrowing cells or the seeded SVF cells to interconnect the structures during the remodelling process.

One relevant contribution of SVF cells was demonstrated to be related to the endothelial subpopulation that they include. In fact, SVF-activated grafts qualitatively displayed a more uniformly organized vascular network and the presence even 12 weeks after implantation of

human endothelial cells, both within and around the implanted pellets. Moreover, a quantitative correlation could be established between the amount of mineralized matrix formed and the density of delivered endothelial cells, phenotypically identified as expressing CD31, CD34 and CD146(23-25). Our data are consistent with the previously recognized role of SVF cells in enhancing and directly contributing to vascularization of engineered tissues(18, 26) or even of avital cortical bone(27).

An increasing number of delivered SVF cells was associated with a higher density of chondroclasts/osteoclasts in the grafts. These cells were in part of human origin, thus derived from the monocytic population of the SVF, and in part from the host, likely recruited thanks to the enhanced blood vessel invasion. A moderate increase in the density of osteoclasts from baseline values, achieved by the delivery of 12 million SVF cells / mL gel, could have been pivotal in enhancing the efficiency of bone formation. In fact, osteoclasts would mediate release of cytokines and morphogens contained in the devitalized hypertrophic cartilage, in turn activating resident osteoprogenitor cells. On the other hand, a larger increase in the density of osteoclasts, corresponding to the delivery of 24 million SVF cells / mL gel, was associated with a reduced bone formation. It is possible that excessive graft colonization by osteoclasts at early time points, as previously observed upon delivery of VEGF(28), would disrupt bone homeostasis towards excessive degradation, ultimately resulting in more limited net amounts of bone matrix.

Although SVF cells contain progenitors for osteoblasts, their direct contribution to the osteoid formation appeared to be rather marginal. The fact that SVF cell delivery strongly enhanced the total density of osteoblastic cells ultimately forming abundant bone matrix suggests their role in recruiting local osteoprogenitors through the paracrine effect of trophic factors. An analogue mode of action was recently proposed for Wharton Jelly-derived mesenchymal progenitors, upon implantation in a calvarial defect(29). Importantly, ectopic implantation of freshly harvested SVF cells in combination with calcium phosphate-based materials was previously reported to yield dense connective tissue but no bone formation(30),

unless BMP-2 was additionally delivered(31). These findings underline the strong regulatory/inductive role of the devitalized hypertrophic extracellular matrix as compared to ceramic materials in the process of ossification.

In our study, hypertrophic cartilage matrix was engineered starting from bone marrow-derived MSC and subsequently devitalized. Gawlitta et al. previously proposed the use of decellularized xenogenic cartilage-derived matrix particles, also incorporated within a gel material in combination with MSC(32), and found that it induced no increase in bone tissue formation. The difference from our findings may be related to the use of articular as opposed to hypertrophic cartilage, whereby the former is phenotypically stable and developmentally not competent to support bone formation. The general approach of using engineered instead of native tissue as a source of devitalized extracellular matrix could be associated with additional advantages. In fact, an engineered matrix may be customized and enriched in defined factors (e.g., osteoinductive, angiogenic or chemotactic cues) by using (i) specific culture medium supplements, (ii) cells transduced to undergo apoptosis upon exposure to chemical agents, thereby achieving a devitalization with better preservation of the matrix(11) and/or (iii) customized cells lines engineered to express larger amounts of the target factors(10). Finally, it would be tempting to speculate that a devitalized extracellular matrix can be most effective in instructing formation of bone if it does not derive from the fully developed tissue, but rather from the earlier stages of its development, as it is the case for hypertrophic cartilage(33).

Conclusions

Our findings support a novel strategy for bone repair or augmentation, whereby allogeneic hypertrophic cartilage is engineered, devitalized, and then clinically used as an off-the-shelf material in combination with autologous SVF cells, intraoperatively derived from a lipoaspirate. Manufacturing of hypertrophic cartilage could take place within bioreactor systems, whereby biological processes could be monitored, controlled, automated and standardized(34). Towards

clinical fruition, further studies are necessary in more relevant animal models, which should include the critical factors of immunocompetence and mechanical loading.

Acknowledgments

This work was supported by the Swiss National Science Foundation (SNF NMS1725), the AO Foundation (AO S-11-13P), the Osteology Foundation (13-059) and the European Union (Eurostars E!7865 Endomatrix).

References

1. Li P, Fang Q, Qi J, Luo R, & Sun C (2015) Risk Factors for Early and Late Donor-Site Morbidity After Free Fibula Flap Harvest. *Journal of oral and maxillofacial surgery : official journal of the American Association of Oral and Maxillofacial Surgeons* 73(8):1637-1640.
2. Kneser U, Schaefer DJ, Polykandriotis E, & Horch RE (2006) Tissue engineering of bone: the reconstructive surgeon's point of view. *Journal of cellular and molecular medicine* 10(1):7-19.
3. Grimshaw MJ & Mason RM (2000) Bovine articular chondrocyte function in vitro depends upon oxygen tension. *Osteoarthritis and cartilage / OARS, Osteoarthritis Research Society* 8(5):386-392.
4. Scotti C*, et al.* (2013) Engineering of a functional bone organ through endochondral ossification. *Proceedings of the National Academy of Sciences of the United States of America* 110(10):3997-4002.
5. van der Stok J*, et al.* (2014) Chondrogenically differentiated mesenchymal stromal cell pellets stimulate endochondral bone regeneration in critical-sized bone defects. *European cells & materials* 27:137-148; discussion 148.
6. Kuhn LT*, et al.* (2014) Developmental-like bone regeneration by human embryonic stem cell-derived mesenchymal cells. *Tissue engineering. Part A* 20(1-2):365-377.
7. Bahney CS*, et al.* (2014) Stem cell-derived endochondral cartilage stimulates bone healing by tissue transformation. *Journal of bone and mineral research : the official journal of the American Society for Bone and Mineral Research* 29(5):1269-1282.
8. Harada N*, et al.* (2014) Bone regeneration in a massive rat femur defect through endochondral ossification achieved with chondrogenically differentiated MSCs in a degradable scaffold. *Biomaterials* 35(27):7800-7810.
9. Yang W, Yang F, Wang Y, Both SK, & Jansen JA (2013) In vivo bone generation via the endochondral pathway on three-dimensional electrospun fibers. *Acta biomaterialia* 9(1):4505-4512.
10. Papadimitropoulos A, Scotti C, Bourgine P, Scherberich A, & Martin I (2015) Engineered decellularized matrices to instruct bone regeneration processes. *Bone* 70:66-72.
11. Bourgine PE*, et al.* (2014) Osteoinductivity of engineered cartilaginous templates devitalized by inducible apoptosis. *Proceedings of the National Academy of Sciences of the United States of America* 111(49):17426-17431.
12. Kojima T*, et al.* (2013) Histochemical aspects of the vascular invasion at the erosion zone of the epiphyseal cartilage in MMP-9-deficient mice. *Biomedical research* 34(3):119-128.

13. Lenas P, Moos M, & Luyten FP (2009) Developmental engineering: a new paradigm for the design and manufacturing of cell-based products. Part I: from three-dimensional cell growth to biomimetics of in vivo development. *Tissue Eng Part B Rev* 15(4):381-394.
14. Riordan NH, *et al.* (2009) Non-expanded adipose stromal vascular fraction cell therapy for multiple sclerosis. *Journal of translational medicine* 7:29.
15. Scotti C, *et al.* (2010) Recapitulation of endochondral bone formation using human adult mesenchymal stem cells as a paradigm for developmental engineering. *Proceedings of the National Academy of Sciences of the United States of America* 107(16):7251-7256.
16. Mumme M, *et al.* (2012) Interleukin-1beta modulates endochondral ossification by human adult bone marrow stromal cells. *European cells & materials* 24:224-236.
17. Guven S, *et al.* (2012) Validation of an automated procedure to isolate human adipose tissue-derived cells by using the Sepax(R) technology. *Tissue engineering. Part C, Methods* 18(8):575-582.
18. Guven S, *et al.* (2011) Engineering of large osteogenic grafts with rapid engraftment capacity using mesenchymal and endothelial progenitors from human adipose tissue. *Biomaterials* 32(25):5801-5809.
19. Schneider CA, Rasband WS, & Eliceiri KW (2012) NIH Image to ImageJ: 25 years of image analysis. *Nature methods* 9(7):671-675.
20. Doube M, *et al.* (2010) BoneJ: Free and extensible bone image analysis in ImageJ. *Bone* 47(6):1076-1079.
21. Sheets KG, *et al.* (2013) Microglial ramification and redistribution concomitant with the attenuation of choroidal neovascularization by neuroprotectin D1. *Molecular vision* 19:1747-1759.
22. Martin I, *et al.* (2002) Fluorescence microscopy imaging of bone for automated histomorphometry. *Tissue engineering* 8(5):847-852.
23. Ingram DA, *et al.* (2004) Identification of a novel hierarchy of endothelial progenitor cells using human peripheral and umbilical cord blood. *Blood* 104(9):2752-2760.
24. Rohde E, *et al.* (2007) Immune cells mimic the morphology of endothelial progenitor colonies in vitro. *Stem cells* 25(7):1746-1752.
25. Yoder MC, *et al.* (2007) Redefining endothelial progenitor cells via clonal analysis and hematopoietic stem/progenitor cell principals. *Blood* 109(5):1801-1809.
26. Klar AS, *et al.* (2014) Tissue-engineered dermo-epidermal skin grafts prevascularized with adipose-derived cells. *Biomaterials* 35(19):5065-5078.
27. Kloeters O, *et al.* (2011) Revitalization of cortical bone allograft by application of vascularized scaffolds seeded with osteogenic induced adipose tissue derived stem cells in a rabbit model. *Arch Orthop Trauma Surg* 131(10):1459-1466.
28. Helmrich U, *et al.* (2013) Osteogenic graft vascularization and bone resorption by VEGF-expressing human mesenchymal progenitors. *Biomaterials* 34(21):5025-5035.
29. Todeschi MR, *et al.* (2015) Transplanted Umbilical Cord Mesenchymal Stem Cells Modify the In Vivo Microenvironment Enhancing Angiogenesis and Leading to Bone Regeneration. *Stem cells and development* 24(13):1570-1581.
30. Muller AM, *et al.* (2010) Towards an intraoperative engineering of osteogenic and vasculogenic grafts from the stromal vascular fraction of human adipose tissue. *European cells & materials* 19:127-135.
31. Mehrkens A, *et al.* (2012) Intraoperative engineering of osteogenic grafts combining freshly harvested, human adipose-derived cells and physiological doses of bone morphogenetic protein-2. *European cells & materials* 24:308-319.
32. Gawlitta D, *et al.* (2015) Decellularized cartilage-derived matrix as substrate for endochondral bone regeneration. *Tissue engineering. Part A* 21(3-4):694-703.
33. Martin I (2014) Engineered tissues as customized organ germs. *Tissue engineering. Part A* 20(7-8):1132-1133.
34. Martin I, *et al.* (2014) The survey on cellular and engineered tissue therapies in Europe in 2011. *Tissue engineering. Part A* 20(3-4):842-853.

Chapter 6

Conclusion and Perspective

Conclusion and Perspective

The aim of my thesis was to validate the use of in vitro engineered hypertrophic cartilage as a bone substitute. I explored two available options for a rapid clinical translation. First, I engineered hypertrophic cartilage from bone marrow derived mesenchymal stromal cells for autologous use. I identified a suitable production method for the generation of large grafts and a way of monitoring and assuring the quality of the resulting grafts. Second, I produced allogeneic hypertrophic grafts, devitalized them and seeded them with different cell types to enhance their osteoinductive properties.

Hypertrophic cartilage was generated in a perfusion bioreactor system with rabbit bone marrow derived mesenchymal stem cells and in vivo bone formation was tested in order to generate protocols and guidelines for a future pre-clinical trial in a rabbit orthotopic model. Glycosaminoglycan and alkaline phosphatase content in culture supernatants were monitored to collect information on tissue integrity and maturity. The monitored parameters correlated with tissue quality and in vivo bone formation. This correlation might be used to maximize the efficiency, reproducibility and most importantly quality of the manufacturing process.

A major difficulty of autologous use was the variability of cartilage formation with different rabbit donors, which is in line with reports in human MSCs. To address this issue, pre-production of allogeneic devitalized tissue was considered. Engineered hypertrophic matrix subjected to different modes of devitalization was characterized for preservation of growth factors and components of the extracellular matrix and in vivo bone formation. It was demonstrated that suitably devitalized matrix, could deliver the set of factors necessary to induce formation of bone and bone marrow. The findings outlined a paradigm relying on the engineering of cell-based but cell-free niches, which could recruit and instruct endogenous cells to form predetermined tissues.

Devitalized constructs remained inferior to vital ones, which could be due to a deficient remodelling by host cells. To actively stimulate tissue degradation, thus releasing chemoattractant factors and ultimately improving bone formation, osteoclastogenic monocytes were seeded on both living and devitalized matrix. In vitro, the formation of osteoclasts, the secretion of factors in supernatants, the attraction of monocytes, endothelial cells or mesenchymal stem cells and the differentiation of mesenchymal stem cells in the presence of secreted factors were analyzed. In vivo, the presence of osteoclasts, macrophages, endothelial cells and mesenchymal stem cells was described at an early time point, as well as the bone formation at a late time point. In vitro and in vivo the observations were consistent. No improvement of bone formation was observed in living or devitalized grafts. MSC were not attracted and vascularization was only correlated with the presence of recruited M2 macrophages. While monocytes could be attracted by devitalized matrix, their survival and differentiation into osteoclasts strongly depended on interactions with hypertrophic chondrocytes.

As a way to provide multiple progenitor lineages and enhance bone formation, stromal vascular fraction (SVF) cells from human adipose tissue were used. Multiple pellets of devitalized matrix were combined together with different amounts of SVF and implanted subcutaneously. The contribution of SVF to the bone formation, vascularization and bone resorption was analyzed. SVF activation of the hypertrophic cartilage strongly enhanced the bone formation efficiency, both in subcutaneous ectopic implantation and calvarial defect models. In particular, the density of SVF cells was correlated with that of osteoclasts in the grafts, and the percentage of SVF-derived endothelial lineage cells was correlated with the amount of deposited mineralized matrix. These findings support a novel strategy for bone repair or augmentation, whereby allogeneic engineered and devitalized hypertrophic cartilage is clinically used as an off-the-shelf material in combination with autologous SVF cells.

Taken together, the results of my thesis provide a stepping stone for the use of hypertrophic cartilage as a tool for bone regeneration. The presented manufacturing process using monitored

bioreactor systems allows a controlled and standardized production of hypertrophic cartilage. The resulting tissue could be used as is, cut to a specific shape or minced to provide a bone-filling granulate. However, to satisfy clinical demand an up-scaled bioreactor-based production system using human MSC will have to be developed. The proposed monitoring parameters could then be used to establish suitable product quality and release criteria. The described variability in cartilage formation will need to be better understood and addressed with appropriate changes to the culture protocol.

The collected insights in the process of remodelling could guide the engineering of hypertrophic matrix to further enhance osteoinductivity. Yet, the limited understanding of cellular and molecular mechanisms regulating efficient endochondral bone formation still needs to be expanded. For example, neutrophils present during fracture and wound healing may have a significant effect on the implanted hypertrophic cartilage. The role of macrophages polarized towards a regenerative phenotype (M2) needs to be further characterized. Pivotal to tissue engraftment, the kinetics and regulation of vascularization appear to be significantly different in implanted hypertrophic cartilage compared to other grafts and require further studies. The attraction of mesenchymal stromal cells and their interaction with osteoclasts and macrophages is not well understood in endochondral ossification and could be crucially influenced by signals from the hypertrophic matrix. During long-term remodelling, immunoregulatory mechanisms absent from the nude mouse/rat model, such as T-regulatory cells or antibodies, could have a significant impact on bone formation. The effect of mechanical stress on remodelling, e.g. in a load-bearing orthotopic site, also remains to be elucidated.

The large volume of bone marrow resulting from the remodelling of hypertrophic cartilage has been shown to harbour haematopoietic stem cells(2). This opens the possibility to engineer the signals provided by the hypertrophic cartilage and thus carefully dissect the formation of the physiological or pathological haematopoietic niche. Intriguingly, a better understanding of the

remodelling process could lead to in vitro controlled bone marrow formation and haematopoiesis using the 3D culture system presented here (3).

Finally, a cell-line with reproducible behaviour could be generated for superior biological performance and customization of the matrix to actively drive tissue repair (1).

In order to develop a commercial osteoinductive off-the-shelf material, devitalized tissue using the proposed soft devitalization method would have to be extensively tested to ensure that no safety concerns remain regarding the host immune reaction, transmission of diseases and tumor formation. On the other hand, the use of freeze/thaw devitalized hypertrophic cartilage with autologous SVF could be a faster alternative, since no genetic manipulation of cells and therefore less extensive testing is required. Indeed, a recent clinical trial of the feasibility and safety of intraoperative SVF application in humeral fractures (ClinicalTrials.gov: NCT01532076) used a silicated calcium phosphate carrier material and showed de novo ossicle formation. To use freeze/thaw devitalized hypertrophic cartilage as carrier material instead, it would be required to test the immunological reaction in immunocompetent animals and to guarantee a safe and regulatory compliant production.

In conclusion, although further in-depth studies in more relevant animal models are necessary, clinical application of the herein explored strategies may be within reach during the current decade.

References

1. Papadimitropoulos A, Scotti C, Bourgine P, Scherberich A, & Martin I (2015) Engineered decellularized matrices to instruct bone regeneration processes. Bone 70:66-72.
2. Scotti C, et al. (2013) Engineering of a functional bone organ through endochondral ossification. Proceedings of the National Academy of Sciences of the United States of America 110(10):3997-4002.
3. Di Maggio N, et al. (2011) Toward modeling the bone marrow niche using scaffold-based 3D culture systems. Biomaterials 32(2):321-329.